POLITECNICO
MILANO 1863

SCUOLA DI ARCHITETTURA URBANISTICA
INGEGNERIA DELLE COSTRUZIONI

Dynamic tests' plastic strains estimation through thermal imaging measurement

TESI DI LAUREA MAGISTRALE IN
AERONAUTICAL ENGINEERING - INGEGNERIA AERONAUTICA

Author: Formaggia Luca

ID studente: 965932
Advisor: Prof. Marco Anghileri
Co-Advisor: Ing. Ivan Colamartino
Anno accademico: 2022-23

Abstract

In this work, the possibility of using temperature measurements via thermal imaging to estimate plastic deformation during dynamic tests was investigated.
First the mechanical proprieties of the material ear fuond to define the hardening rule. Aluminum specimens were tested in the range between 1 mm/min and 5 m/s, and strains were derived through DIC analysis, showing the material's independence of strain rate.
Once the material was characterized, tests with the thermal imaging camera, with velocities between 50 mm/s and 3 m/s, are carried out.
Through a time integration scheme, the energy equation was integrated with the deformation as integration variable and, by comparing them with the DIC, we ascertained the validity of the results.
Once the strains were derived and related to the respective temperature changes, a polynomial regression was performed on the data to derive a characterization curve that could be used for subsequent tests.
The characterization curve was then tested on dynamic compression tests of circular cylinders demonstrating the ability of the method to show the deformations distribution.

Key words: Thermal imaging, Plastic strains, Dynamic tests, No contact measurements

Abstract in italiano

In questo lavoro è stata studiata la possibilità di utilizzare le misure di temperatura attraverso termocamera per stimare le deformazioni plastiche durante prove dinamiche. Per prima cosa sono state analizzate le proprietà meccaniche del materiale per definire la regola di indurimento.
I campioni di alluminio sono stati testati in un intervallo compreso tra 1 mm/min e 5 m/s e le deformazioni sono state ricavate attraverso l'analisi DIC, dimostrando l'indipendenza del materiale dalla velocità di deformazione.
Una volta caratterizzato il materiale, sono state eseguite prove con la termocamera, con velocità comprese tra 50 mm/s e 3 m/s.
Attraverso uno schema di integrazione temporale, l'equazione dell'energia è stata integrata con la deformazione come variabile di integrazione e, confrontandola con il DIC, si è accertata la validità dei risultati.
Una volta ricavate le deformazioni e messe in relazione con le rispettive variazioni di temperatura, è stata eseguita una regressione polinomiale sui dati per ricavare una curva di caratterizzazione da poter utilizzare durante le prove dinamiche.
La curva di caratterizzazione è stata poi testata su prove dinamiche di compressione di cilindri circolari dimostrando la capacità del metodo di mostrare la distribuzione delle deformazioni.

Parole chiave: Termografia, Deformazioni plastiche, Prove dinamiche, Misure senza contatto

Contents

Introduction

Over time, new measurement methods for calculating strains have always been sought, each with its own merits and shortcomings. Among these methods, noncontact measurement methods are popular. These methods have the advantage of not interfering with the measured event and have a lower probability of failure with possible loss of data. At the same time they require special conditions to be accurate.
For the past few years, the evolution of technologies underlying thermal imaging cameras has made it possible to obtain reliable results at high resolution and high recording rates while reducing costs and complexity of use.

The main objective of this work is to produce a methodology for the estimation of the plastic deformations produced during dynamic events by exploitingits link with the temperature.
During dynamic events, bodies are deformed considerably, many times creating folds whose exact position is difficult to predict since it is closely related to the material, geometry and variability within the test.
Because of these aspects, the measurement methods normally used can run into problems of no small consequence as they can easily run into problems including:

- Sensor breakage
- Going ouside the operating parameters
- Placement in uninteresting areas
- Loss of traceability

The first issue is related practically only to contact measurement methods among them the classical electrical, optical or mechanical strain gauges since they are in direct contact with the body to be measured and therefore subject to the dynamics of the body itself that can put the sensor in the condition to break.
The second issue is more relevant during dynamic tests since the large deformations involved can heavily modify the measurement conditions.
One examples in this regard are the resistive strain gauges, such as rosettes, suitable for measuring locally plane states of deformation. Consequently their measurement will not be reliable if they come to a pronounced bend like on top of a fold.
Another example is measurement by laser, which measures the distance between the point of emission and the first body it encounters. The nature of the measurement allows its use for dynamic testing only in very rare cases since it cannot be guaranteed that the laser beam always points to the same point, thereby we wouldn’t know exactly what it measured.
The third issue is present for local measurement methods. In methods that measure strain only locally, sensor placement is critical, and it can easily happen that they are in uninteresting positions due to the variability of dynamic tests.

The fourth issue is related to the most widely used non-contact measurement methodology: DIC analysis.
As previously explained, DIC traces during the test a stochastic pattern applied on the body to be deformed by calculating its displacements and deformations.
The feature of tracking through the pattern is probably the greatest advantage of DIC, as it allows the entire range of deformations to be obtained, but at the same time it turns out to be also the weak point.
During a test with measurement through DIC, the stochastic pattern must meet certain characteristics to allow accurate measurements, some of which cannot always be assured during dynamic tests.
Measurement by DIC requires that the surface involved in the measurement must be as flat as possible and always facing the direction of the camera. This can be partially circumvented by using multiple cameras relying, therefore, on a three-dimensional DIC analysis increasing the complexity of the measurement.
Moer importantly, the stochastic pattern must always be able to be visible and recognizable throughout the entire deformation history. Unfortunately, during dynamic tests the pattern may no longer be clearly visible or even parts of it may be occluded from view due to folds and large deformations generated during the test.
Measurement through temperature measurement with the thermal imaging camera offers the advantage of being able to assess deformation at all visible points in the video without having to resort to a pattern even though a coating is needed to increase emissivity.
The ability to produce results even in the presence of large deformation and folds therefore could makes it more suitable for measurement during dynamic testing.

1 The conversion of plastic work into heat

The link between temperature change and deformation is found in the energy balance equation.

$$\rho C_p \dot{T} - K\nabla^2 T = \beta \sigma_{ij} \dot{\varepsilon}_{ij}^{p} - \alpha \frac{E}{1-2\nu} T \dot{\varepsilon}_{kk}^{e} - \frac{A_s}{V}(h(T - T_\infty) + \hat{\sigma}\tilde{\varepsilon}(T^4 - T_\infty^4))$$

The terms that appear in the equation are, respectively, thermal storage, conduction, plastic work, thermoelastic work, convection and radiation.
The presence of so many terms results in considerable complexity of the problem from the experimental point of view. Fortunately, experimental conditions and practical knowledge can be exploited to simplify the expression.

1.1 Convection and radiation

Convection and radiation represent the heat exchange of material with the environment.
Convection is the exchange of energy between the surface of a body and the moving fluid surrounding it.
Convection can be a natural type, thus due to temperature and density gradients of the fluid caused by heat exchange, or it can be a forced type if the fluid motion is caused by other means.
The amount of energy exchanged with the fluid depends on the surface area exposed to the fluid, the temperature of the fluid and the body, and the convection coefficient. The latter is a coefficient that depends on many variables, including the physical condition of the fluid, the geometry of the body-fluid interface and the relative velocity.

Radiation is a transfer of energy through electromagnetic waves emitted by bodies due to their temperature.
Atoms, excited by thermal agitation, de-excite and emit photons with a frequency dependent on the temperature of the body.
Radiation, besides being proportional to the fourth power of temperature, is proportional to the emissivity of the body. Emissivity depends on the material and surface area and represents the fraction of energy emitted relative to a black body under the same conditions.

From a purely theoretical point of view there would be no problem in their inclusion given the sole dependence of temperature, the data being measured.
From a practical point of view, a controlled measurement environment and knowledge of the heat transfer coefficients related to the environment itself are required, greatly complicating a methodology designed to simplify measurement.

In order to ignore convection and radiation, the strain time must be much lower than the time characteristic of heat transfer of this type.
In the literature it can be found that already at strain rates of 0.1 s^{-1} convection and radiation can be ignored.

1.2 Conduction

Conduction is a mechanism of contact heat transfer.
It can occur between two bodies in contact with different temperatures or in the single body in the presence of thermal gradients.
In the higher temperature zones, atoms oscillate with more velocity, bumping into neighboring atoms transferring momentum that is visible at macroscopic scales in the form of heat energy exchange.
Conduction is a diffusive effect, consequently the time evolution of the phenomenon leads to homogenization of the temperature field.
In the conduction phenomenon there is no transport of matter but only of momentum.
In the case of testing at high strain rates, conduction does not produce noticeable effects, consequently, one can decide to apply the adiabatic strain condition thus eliminating the thermal conduction term.
In the case otf thermal imaging the entire temperature field is available making the calculation of the diffusion term relatively simple.
Consequently, it was decided to keep this term within the equation for the integration process.

1.3 Thermoelastic work

Thermoelastic work takes into account the deformation undergone by the body due to temperature change. This component represents the energy component generated by mechanical stresses working for thermal deformations.
This term is generally ignored since it is much smaller than all the other terms in the equation.

1.4 The plastic work

Plastic work is the focal point of the entire study and is the term from which the strains will be derived.
Fundamental is the characterization of the material in its plastic section; specifically, it is necessary to derive an analytical law to express stress as a function of strain.
The law must be sufficient to adequately describe the behavior of the material, but an overly complicated law is not recommended given the need to also know the derivatives with respect to strain and strain rate.

1.5 The Taylor-Quinney's coefficient

The Taylor-Quinney coefficient, generally expressed as β, represents the fraction of plastic work that is converted to heat energy.
During plastic deformation most of the energy is converted to heat, the remainder is stored within the material in its new equilibrium configuration.
In this new configuration, the dislocations, moved and generated during plastic deformation, distort the crystal structure by storing a certain amount of elastic energy, which is called cold working energy.
The Taylor-Quinney coefficient was introduced to simplify the energy equation and allow the cold working energy, the calculation of which is particularly complicated, to be disregarded.
In the literature it is generally considered constant although more recent studies have shown a link to strain.
There are currently two models formulated by Zehder and Aravas developed for an isotropic hardening law.
Unfortunately, the two models show discordant trends and the applicability of one or the other depends on the material under consideration.
As for this study, the Taylor-Quinney coefficient will be considered constant.

2 Digital Image correlation Basics

DIC uses the analysis of a sequence of images to calculate the displacement field by following the stochastic patterns present on the specimen surface.
The stochastic pattern must meet three conditions to ensure the accuracy of the method:

- the pattern must not repeat
- speckles must have high density and small size
- the contrast must be high

The first condition allows the software to recognize and follow the subsets as they are unique.
The second is related to the size of the subsets. The finer the pattern the smaller the subsets can be thus having a more accurate result.
This condition, however must be balanced with the capabilities of the camera, which must have enough resolution to distinguish speckles and not lose them during the test.
The third condition allows more effective detection of speckles by reducing the risk of losing track of them during deformation.

2.1 Stochastic pattern preparation

In most cases, the natural surface of the specimen is not the best pattern that can be obtained. There are many ways to apply artificial patterns, and the main techniques are listed below.

2.1.1 Paint

Painted patterns are popular because the paint is relatively compatible with most technical materials, and high-quality patterns can be applied quickly with spray paint.
Because paint colors other than black and white will inherently have less contrast, the use of black and white paint is recommended.
If it is expected that the specimen will undergo large deformations and/or high strain rates, it is recommended to perform the experiment within 24-48 hours after painting. As the paint dries and hardens, it loses its ability to deform with the sample.
For this work, it was decided to use a black background with white speckles.

2.1.2 Inks and dyes

For hyperelastic materials (including many elastomers, polymers and biomaterials), the paint is not elastic enough to follow the sample in its deformation.
Inks and dyes that permeate the sample material may be viable options.
Molding, masking, spraying and stenciling can be used to apply the ink or dye. For example, biological soft tissues can be stained with methylene blue and then sprayed with white paint to get the speckles.
Some DIC operators also use permanent markers.

2.1.3 Powder

For wet or sticky materials, such as silicone-based rubbers, powder particles may adhere better than paint.
Graphite powder is popular for dark specks. Alumina, talc, or magnesium oxide can be used for a white base.
Another option for using powder designs is to get smaller speckles than can be achieved with paint. Using a combination of filters and compressed air, powder particles smaller than 10 microns can be deposited on a smooth/glossy sample to form a speckled pattern.

2.1.4 Laser Incision

In some cases, the surface of the specimen can be etched with a laser cutter. This method provides patterns that can remain intact during high-temperature testing.

2.1.5 Nanoparticles

To obtain even smaller grains than powders (about 20 to 100 nanometers, for digital image correlation in scanning electron microscopy), self-assembled nanoparticles can be used.

2.1.6 Lithographed patterns

Lithography is another method for obtaining smaller speckles, with the advantage of a greater degree of control than most other microscale patterning methods.

1 EXAMPLE OF PAINTED SPECIMEN

2 DETAIL OF DIC PATTERN

2.2 Computation of displacements and deformations

The basic operation of DIC is to track a pattern in a sequence of images. The process of a DIC experiment can be divided into three stages:

1. Obtain a pattern on the sample for tracking
2. Acquire images of the sample during movement/deformation
3. Analyze the images to calculate the displacements of the sample surface

The first image in the sequence is defined as the reference image, the baseline against which the other images are compared with.
The DIC program compares the pattern between the reference image and the deformed image; then, it calculates the pattern displacements between the reference image and the deformed image.
In the case of large deformations, it is advisable to update the reference image to reduce errors.

A simplification of a DIC analysis process is shown below.

a) The reference image has a recognizable pattern of points that will be plotted.
b) A part of the pattern, called a subset, is selected for tracking.
c) The center of the subset (the red point, which is not part of the pattern) is the point on the reference image from which the displacement will be calculated.
d) After the material has been deformed from the initial position of the reference image, the subset of the deformed image is matched with the subset of the reference image.
e) Once the subset has been matched, the relative displacement of the center of the subset between the reference image and the deformed image is calculated. The displacement in this case is the difference between the blue and red points.

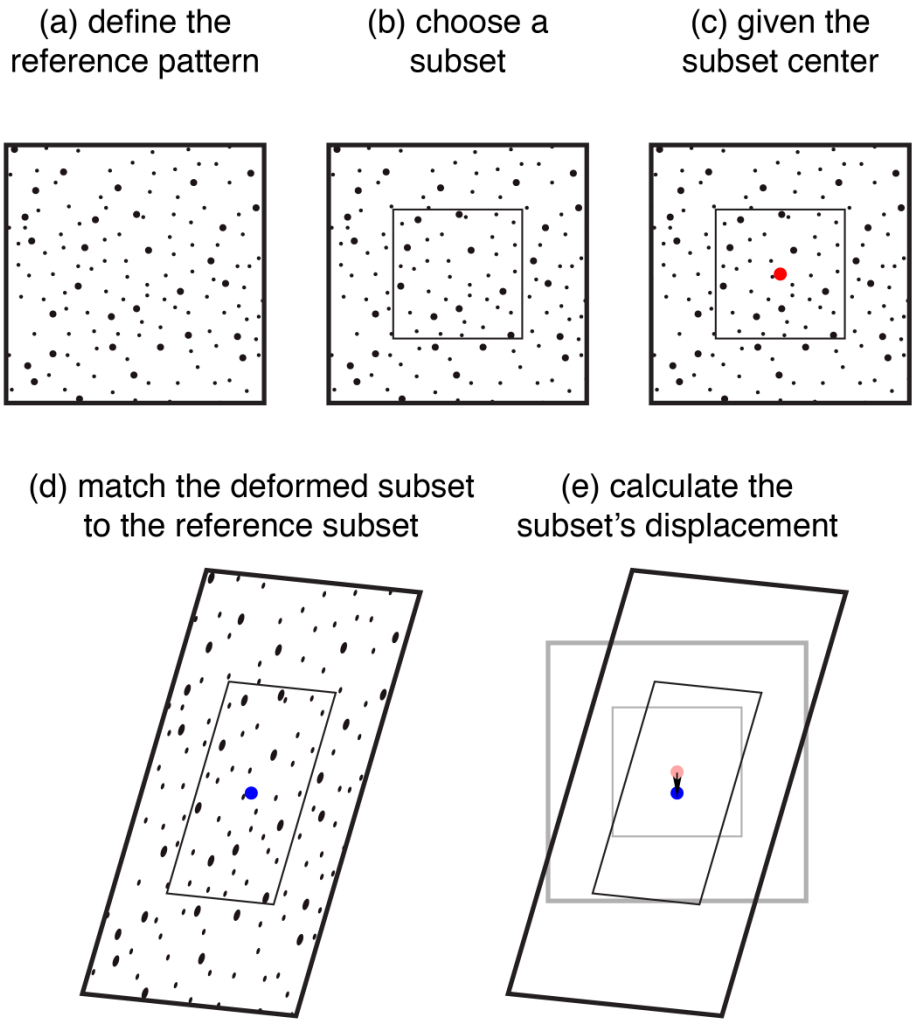

3 EXAMPLE OF DIC CALCULATION

The previous example computed displacements from a single subset, but DIC computes a range of displacements by plotting multiple subsets.
The same procedure is repeated, but this time with four subsets of equal size in a two-by-two grid. This yields four more points with displacement information, for a total of five points.

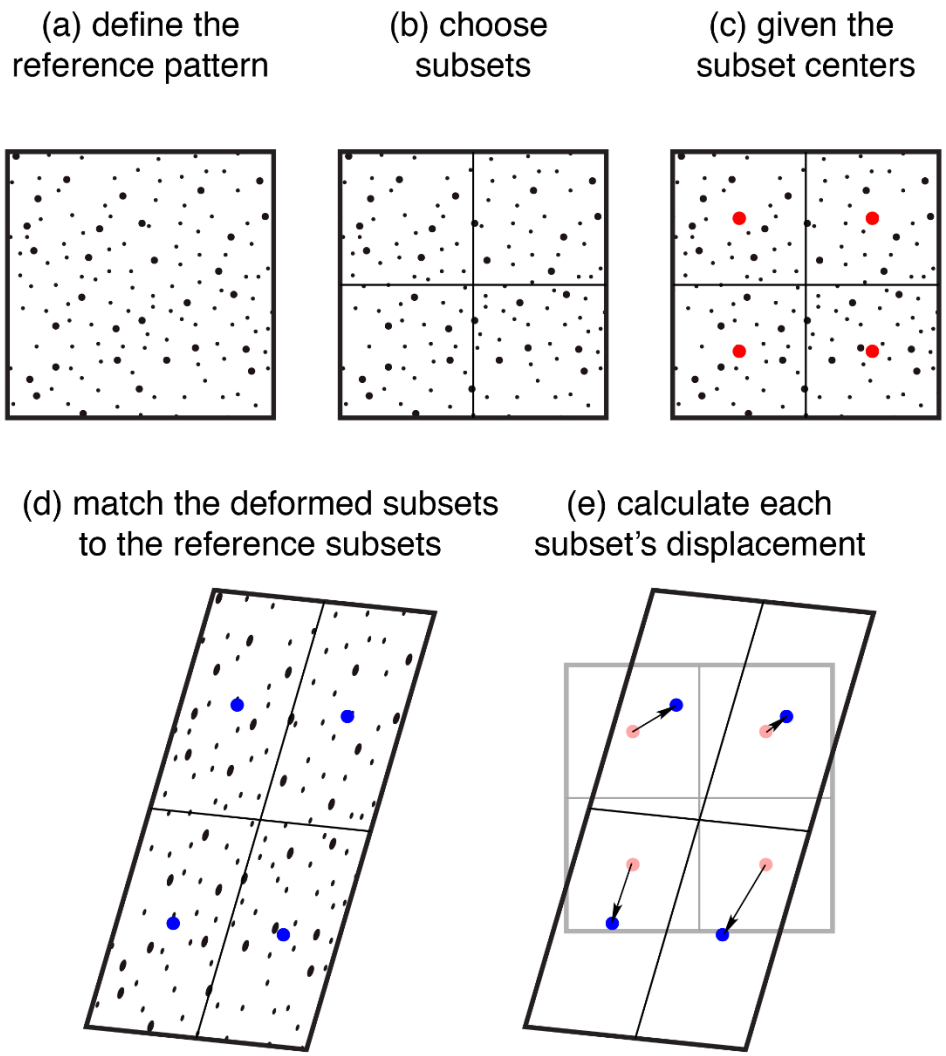

4 DIC OPERATION WITH MULTIPLE SUBSETS

From the five subsets, five total points are obtained for which displacements can be calculated. Each of these points can be called a DIC point.
The displacement at each DIC point is a vector, so the components of the vector can be decomposed. For two displacement dimensions, the components can be written in a Cartesian coordinate system as horizontal and vertical displacement.
Once the displacement field has been calculated, the strain field can be calculated.

2.3 Subsets and step dimensions

Two important dimensions in the DIC calculation are the subset size and the step size. The subset dimension is the width and height of the square of the subset in the reference image.
The step size is the distance between the centers of the subset. Both subset size and step size are measured in units of pixels.
The most important factor in determining the subset size is that each subset must contain at least three speckles.
A secondary factor in the choice of subset size is the competition between better pattern matching for larger subsets, with greater uniqueness, and better spatial resolution for smaller subsets, with less spatial attenuation/filtering of image data.

A third factor is that larger subsets require more computational time. Step size has a much stronger effect on spatial resolution than subset size. Smaller step sizes produce more DIC data points and thus higher spatial resolution. The diagram below shows a range of step sizes for the same field of view and subset size.

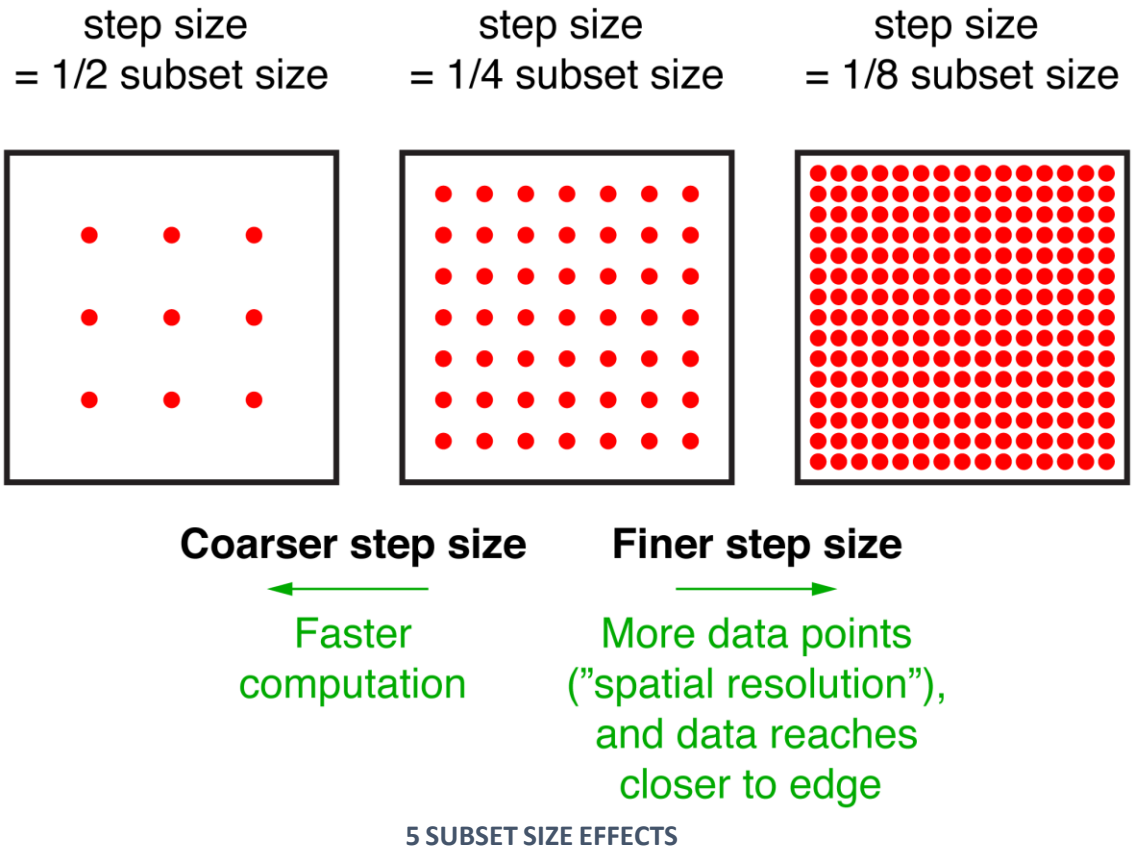

5 SUBSET SIZE EFFECTS

2.4 Strain calculation

For deformations, the size of the subset from which the program will take displacement results for strain calculation must be chosen. The choice is made by taking the smallest possible radius that is not affected by noise. In addition, using smaller sizes improves the accuracy of the results. Depending on the software used, the choice of the size is facilitated by a graphical representation. The subset size is appropriate when the displacement points are on the plane.

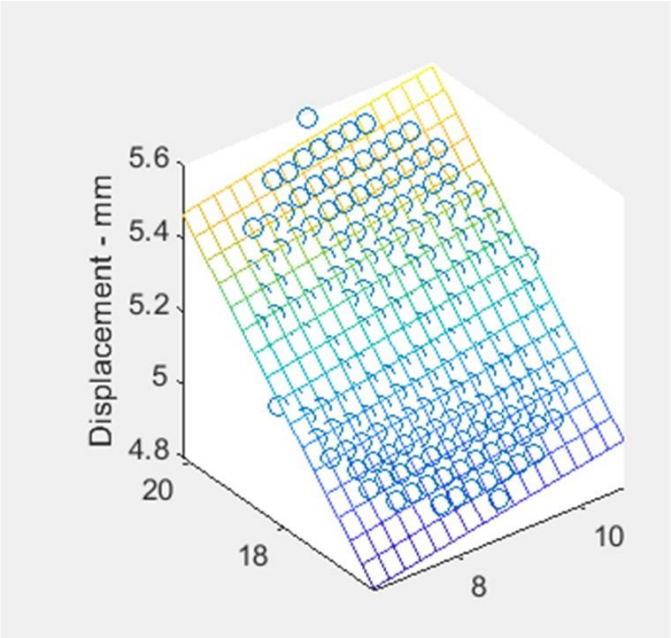

6 DIC POINT DISPLACEMENTS RESPECT TO THE PLANE

2.5 Data elaboration

One of the advantages of DIC is being able to obtain the entire strain range thus obtaining a large amount of data.
There are various formulations for strain, each with its own uses and advantages.
Almansi strains, referring to the deformed geometry, provide an excellent visual representation of the deformations allowing simplified identification of the deformation mechanisms at work.
Green-Lagrange strains, referred to the reference geometry, are particularly useful in data processing when the deformation history of a point is to be obtained.
Normally, the strain values for each stage are exported to a matrix that, in the case of Lagrangian formulation, turns out to have constant dimensions for all stages considered. This feature makes it possible to eliminate the tracking stage of the points since they are always represented at the same position in the matrix.

Since the DIC is based on physical experiments there is a need to filter the data. The temporal filter used here is a butterworth applied forward and backward to eliminate phase shifting.
The deformations are derived from spatial data, so it is a good idea to average the values of the single point with those in its vicinity.
An easy way to do this is by exploiting the matrix form of the data through a convolution. Using for convolution a kernel with odd dimensions and with values whose sum is equal to 1, it's possible to apply a two-dimensional moving average on the original matrix in which the points are weighted by the corresponding kernel elements.
In the case where all elements of the kernel have the same value, all points have the same weight, but it is not uncommon to use a higher weight on the central element and a lower weight the further towards the edges one goes.
In this example, it can be seen that, during the test, the deformation is uniform in the central area of the specimen, while toward the end there is a concentration of localized deformation in the necking area as was expected.

7 SPECIMEN AT FRAME 60

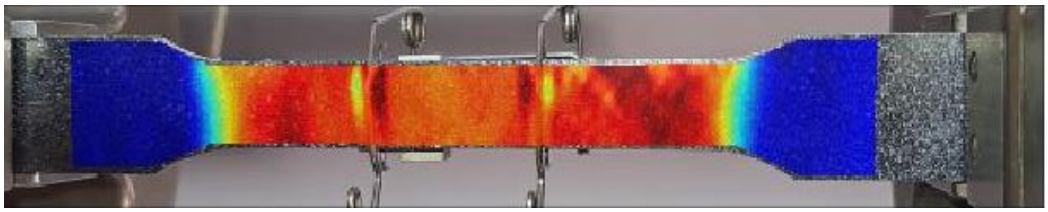

8 DIC RESULT AT FRAME 60

8 SPECIMEN AT FRAME 90

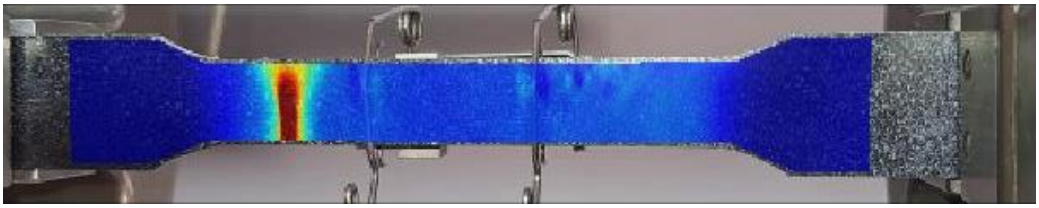

10 DIC RESULT AT FRAME 90

3 Thermal camera

A thermal imaging camera is an instrument for measuring temperature through video. Operation is based on the detection of infrared radiation emitted by any body with temperature greater than absolute zero.
The detection is implemented through a sensor consisting of a grid of pixels sensitive to infrared radiation.
Depending on the incident radiation, the sensor generates an electrical signal that is sent to a processor where it is converted into a temperature measurement.
Thermal sensors are mainly based on two technologies:

- Microbolometers
- Pyroelectric materials

3.1 Microbolometers

The microbolometer is a radiation-sensitive device.
Any radiation directly striking the absorbing element of a microbolometer causes a corresponding increase in temperature; the greater the absorbed energy, the higher the temperature becomes.
This temperature change can be measured directly with a resistive thermometer and then processed.
In essence, a microbolometer consists of a thin layer of metal that is connected directly to a thermal reservoir (at a constant temperature) via a thermal link.
The sensor array houses thousands of detector pixels arranged in a grid. Each pixel in the array reacts to infrared radiation directly striking it by producing a resistance that can be translated into an electronic signal. The signal from each pixel is processed by applying a mathematical formula that forms the basis of the color map of the object's captured temperature.
Microbolometer-based thermal imaging cameras are also called uncooled thermal imaging cameras because there is no need for a separate cooling mechanism to operate the microbolometer sensors. The immediate advantage is that these cameras are much lighter than conventional cooled models.

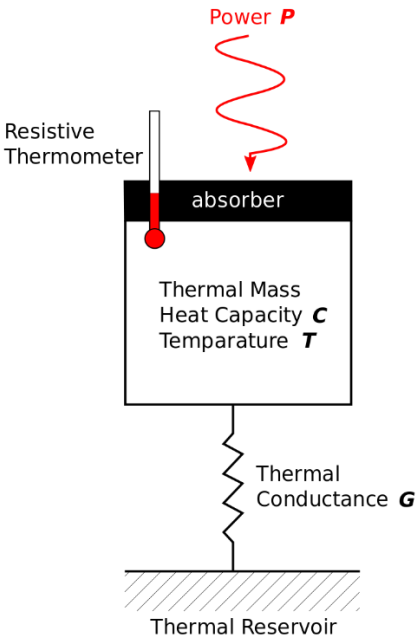

9 SCHEME OF OPERATION OF A BOLOMETER

3.2 Pyroelectric materials

Thermal imaging cameras based on pyroelectric materials use a cooled sensor detector. An example is lithium tantalate.
The material generates a small electrical voltage in response to temperature changes. In this sense, it directly detects infrared photons. This is a photovoltaic system, unlike thermal imaging cameras based on uncooled microbolometers that use photoconductivity.
Although they offer a number of advantages, such as long-distance infrared detection and more refined temperature difference results, cooled thermal cameras are gradually losing ground to uncooled devices. This is mainly due to their higher price and bulky nature.

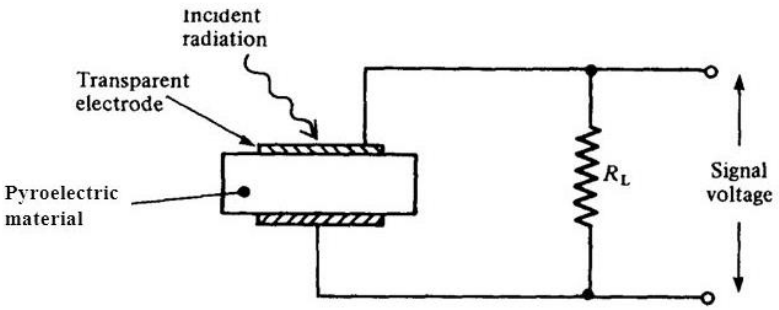

10 SENSOR OPERATION BASED ON PYROELECTRIC MATERIALS

4 Integration of ordinary differential equations

Given a system of differential equations, in explicit or implicit form, and initial conditions, the process of calculating the solution of the equation is called integration. Except for simple cases, the solution can only be found numerically, thus an approximate representation of the true solution. The quality of the solution will depend on the characteristics of the method and the problem.
Integration methods can be classified as

- Single step vs. Multistep
- Implicit vs explicit
- Single stage or Multistage

The two most important features are the accuracy and stability of the algorithm.

4.1 General linear multistep methods

The general form of the linear multistep method is of the form

$$Y_k = \sum_{i=1}^{n} a_i Y_{k-i} + h b_0 \dot{Y}_k + h \sum_{i=1}^{n} b_i \dot{Y}_{k-i}$$

Where h is the time step and ai and bj are the coefficients specific to each method.

In the case where n=1 we speak of single-step methods. These methods are commonly chosen for two reasons:

- They require only the initial conditions at time t0 and not those at earlier times.
- They generally produce better results in the presence of discontinuities because they reduce the regularization caused by dependence on previous steps.

A method is said to be implicit when the solution yk at time tk depends on the derivative at time yk otherwise the method turns out to be explicit, thus a function only of the previous time values. In other words, a method is said to be explicit when b0=0.

4.2 Accuracy

Accuracy refers to the ability of a numerical integration scheme to integrate a polynomial of a certain order. A method of order n can exactly integrate a polynomial of order n.
To determine accuracy, the solution is defined as $y(t) = \sum_{i=0}^{n} t^i$, replace it in the integration scheme and check the minor power remaining after the elimination process.
The accuracy trend can be evaluated using the error through the formula

$$n = \lim_{h \to 0} \log_2 \left(\frac{E(2h)}{E(h)} \right)$$

4.3 Stability

Stability is an extremely important property. The term refers to the stability of the numerical process that estimates the solution. A method that is not algorithmically stable could result in a divergent solution when in fact the physical problem being solved would result in a non divergent solution. In other words, it would produce a false positive.
There is no guarantee for the opposite case: a method that is algorithmically stable may provide a nondivergent solution when the physical problem is actually unstable. In other words, algorithmic stability may result in a false negative
Stability can be conditional or unconditional. Conditional stability occurs when it is verified only for an interval of time steps extending from zero to a boundary value. This is the case for explicit integration schemes. When stability is only conditional, the time-step size is limited by stability considerations independent of any accuracy considerations, since algorithmic stability is mandatory for successful integration. Implicit integration schemes, in contrast, can have unconditional stability. When stability is unconditional, the time step size can be chosen based on accuracy considerations, since algorithmic stability is always guaranteed.
In considering stability, the value of the time step has, in truth, small significance. What is really important is the ratio between the time step and the characteristic time of the problem.

4.3.1 Zero Stability

Zero stability occurs when the numerical method, applied to a stable problem, is non divergent for h → 0. This means that stability must exist for an interval of time steps h that includes h = 0.
Zero stability formalizes the notion of conditional stability.

4.3.2 A Stability

A stability occurs when the numerical method, applied to a stable problem, is zero stable and non divergent regardless of the value of h.
A stability formalizes the notion of unconditional stability.
An example of a A stable method is the Crank-Nicolson method used in this work.

4.3.3 L Stability

L-stability occurs when the numerical method, applied to a stable problem, is A-stable and guarantees that the larger the time step, the faster any perturbation vanishes.
L stability is due to an intrinsic dampening factor in the integration scheme that lead to the attenuation of high frequency dynamics. A L stable scheme can be useful in the presence of high frequency noise that would pollute the solution at the price of less accuracy.

5 Specimen informations

The geometry of the test piece is one of the most important features affecting the strain distribution during the event. For this reason, in an attempt to characterize the material, we chose to work with a classical tensile test specimen.
The dimensions are in accordance with ISO 6892 concerning tensile tests for metallic materials, specifically Annex B.3 is referred to.
The material chosen for characterization is an aluminum whose mechanical properties were obtained through tensile testing.
Since heat production is mainly a local effect a good characterization of the material behavior is necessary.
Therefore, the use of Digital Image Correlation turns out to be an excellent option being a noninvasive technique capable of returning the entire strain field.
For simplicity it was decided to use the same geometry for the material characterization tests and the thermal camera tests.
The specimens are painted with a DIC pattern for the material characterisation tests, meanwhile for the tests with the thermal camera they are anodised to improve the emissivity.

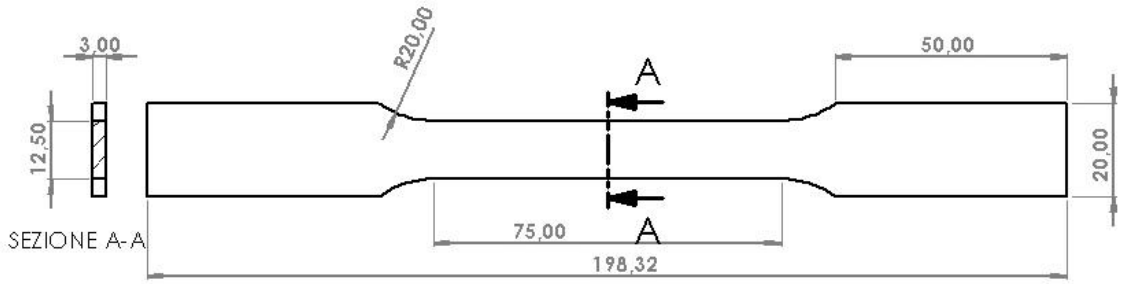

11 SPECIMEN DIMENSIONS

6 Experimental data elaboration

6.1 Material informations

First of all, it is necessary to define the material data.

- The Taylor-Quinney coefficient
- The density
- The specific thermal capacity
- The conduction coefficient

The function describing the plastic work and its derivatives with respect to strain and strain rate must also be specified. The latter are necessary in order to apply the iterative method for integration.

6.2 Temperature measurements

Extracted temperature measurements from the thermal camera must be saved in a format suitable for processing.
Generally, each frame is represented by a matrix whose indices identify the position of the pixels and the arguments the relative measured temperature.
Matrices can be saved, for convenience, by various methods depending on the capabilities of the programming language used.
Whichever method is chosen, it is preferable to have the ability to isolate individual matrices and the ability to create a vector composed of the temperature data from an assigned location.
Since the method used in this work is written as a Matlab script, the choice was made to use three-dimensional matrices.
Although it is relatively slow computationally and heavier in terms of memory than its two-dimensional counterpart, it allows for easy and intuitive use.
In the process of creating the 3-D matrix, each frame goes through a smooting process, applying a convolution between the original matrix and a 3X3 kernel matrix with equal values, thus applying a moving average to the data.

6.3 Thermal history of a point

Once the 3-D matrix is set up, it is possible to isolate the temporal temperature data of a point of choice, through which the program will calculate the deformation of that specific point.
Since the diffusion term also needs to be calculated, not only will the time history of the point of interest need to be extracted, but also those nearby to allow the Laplacian to be calculated.
The data are then filtered with a low-pass filter to remove any fluctuations due to the experimental data.
It was decided to use a first-order butterworth filter applied back and forth to eliminate phase shifting effects.

6.4 Numerical calculation of derivatives

In the energy equation, temperature does not appear as an absolute value, but its importance lies in its temporal and spatial variation.
In particular, it is necessary to calculate the time first derivative and the Laplacian.
The first derivative in time is calculated by the method of central differences for all instants of time except for extremes for which the method of forward and backward differences will be used.

$$\dot{Y}_i^{central} = \frac{Y_{i+1} - Y_{i-1}}{2h}$$

$$\dot{Y}_i^{forward} = \frac{-3Y_i + 4Y_{i+1} - Y_{i+2}}{2h}$$

$$\dot{Y}_i^{backward} = \frac{3Y_i - 4Y_{i-1} + Y_{i-2}}{2h}$$

The second derivative for the Laplacian is calculated by the method at central differences for second derivatives.

$$Y_{/xx} = \frac{T_{x+1} - 2T_x + T_{x-1}}{dx^2}$$

7 Iterative integration method

7.1 Integration of a function

Extrapolation of strain is derived from time integration of the energy equation with ε as the integration variable.

$$\rho C_p \dot{T} - K\nabla^2 T = \beta \sigma_{(\varepsilon)} \dot{\varepsilon^p} = g(\varepsilon, \dot{\varepsilon})$$

This equation can be rewritten in a more useful version as

$$F_{(\varepsilon,\dot{\varepsilon})} = \beta \sigma_{(\varepsilon)} \dot{\varepsilon^p} - \rho C_p \dot{T} + K\nabla^2 T = g(\varepsilon, \dot{\varepsilon}) - C_{(T)} = 0$$

At each step, the program finds the value of ε such that the function |F| is minimized through an iterative process based on the Newton-Rhaphson method.
At the beginning of the step, the integration variable is estimated through the chosen integration method.

$$Y_k = \sum_{i=1}^{n} a_i Y_{k-i} + h b_0 \dot{Y}_k + h \sum_{i=1}^{n} b_i \dot{Y}_{k-i}$$

In the case of this paper, it was decided to use the Crank-Nicolson method, whose coefficients are a_1=1, b_0=b_1=0.5.
To use the Newton-Rhaphson method both the function to be integrated and the approximation for the integration variable must be linearized.
For step k at iteration j we have:

$$\begin{cases} F_{\left(Y_k^{(j)}, \dot{Y}_k^{(j)}\right)} = F_{\left(Y_k^{(j-1)}, \dot{Y}_k^{(j-1)}\right)} + \dfrac{\partial F}{\partial \dot{Y}} \Delta \dot{Y} + \dfrac{\partial F}{\partial Y} \Delta Y = 0 \\ \Delta Y = h b_0 \Delta \dot{Y} \end{cases}$$

By substituting the second equation into the first, a linear equation can be derived for $\Delta\dot{Y}$.

$$\left(\frac{\partial F}{\partial \dot{Y}} + \frac{\partial F}{\partial Y} h b_0\right) \Delta\dot{Y} = -F_{\left(Y_k^{(j-1)}, \dot{Y}_k^{(j-1)}\right)}$$

Once $\Delta\dot{Y}$ has been found, the values for the current iteration can be easily found

$$\begin{cases} \dot{Y}_k^{(j)} = \dot{Y}_k^{(j-1)} + \Delta\dot{Y} \\ Y_k^{(j)} = Y_k^{(j-1)} + h b_0 \Delta\dot{Y} \end{cases}$$

Iterations continue as long as the value of the function to be minimized exceeds a user-defined tolerance.
In the traditional Newton-Rhaphson method the derivatives are evaluated at each iteration. This aspect can generate slowdowns if the number of iterations is high so one can think of simplifying the method by evaluating the derivatives only at the initial point. This saves time by not calculating the derivatives at the cost of slower convergence of the solution.
In this case the form of the function to be integrated allows convergence of the solution to be achieved with only a few iterations so the traditional form of the method is adequate.

A simplified version of the method is shown in the figure. For ease of visualization the thermal energy terms C and that of plastic work g have been separated. The strain value for the current step corresponds to the point where the curves meet.

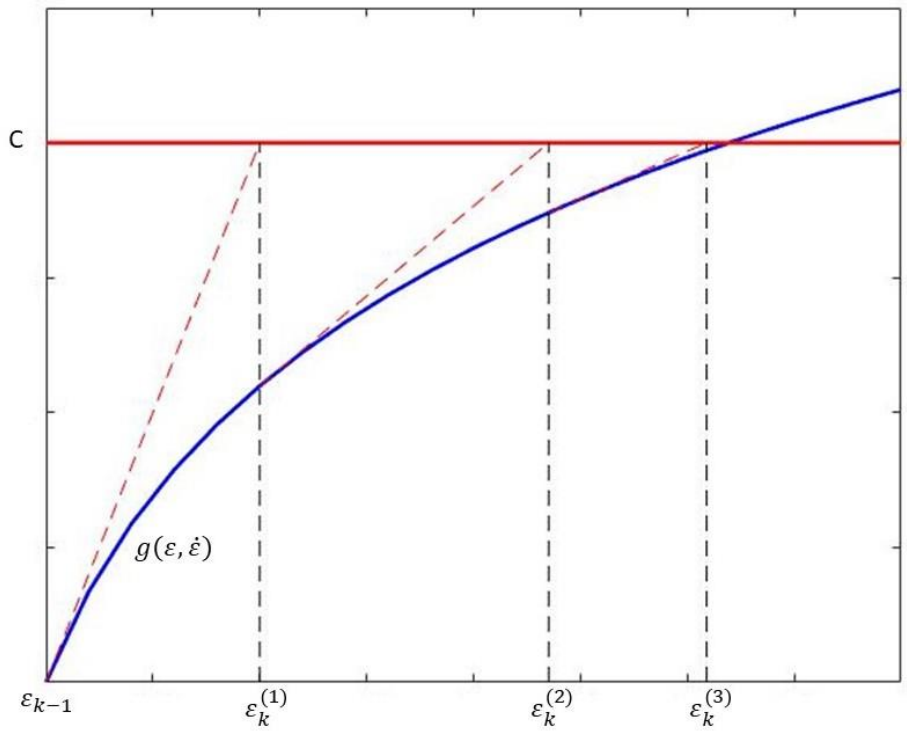

12 ITERATIVE INTEGRATION PROCESS

7.2 Integration of a piecewise function

Modeling of the plastic region of the material can be done using various models, some of which can be formulated with a function defined at the discontinuity point.
The integration process must then take into account the variation of the function at the point of discontinuity.
In this case, the plastic work can be expressed as.

$$\begin{cases} g_1(y, \dot{y}) & y \leq \bar{y} \\ g_2(y, \dot{y}) & y > \bar{y} \end{cases}$$

At each step the program starts by minimizing the function $f_1(y, \dot{y}) = g_1(y, \dot{y}) - C$.
The result is compared with the discontinuity point. If it is smaller, the result can be accepted and the program can move on to the next step.
In the case where it is greater, it means that the discontinuity point has been passed and the solution found is invalid.
In this case, a new iterative process must be performed to correct the solution.
First of all, the starting point of the iterative process is placed on the discontinuity point.
As can be easily seen from the graph the remaining section to reach the goal is
$C - g_1(\bar{y}, \dot{\bar{y}}) = -f_1(\bar{y}, \dot{\bar{y}}) = C_d$
Consequently, the function to be minimized in this section becomes $f_d = g_2(y, \dot{y}) - C_d$
The program will then try to find the strain required to generate the heat not produced by the first portion of the plastic work function.

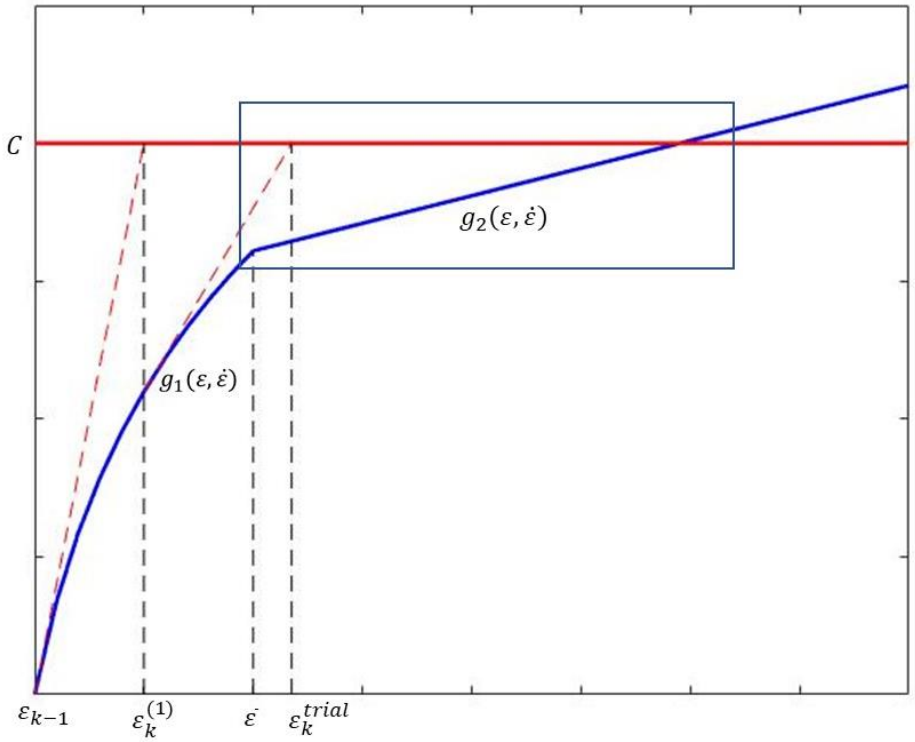

13 ITERATIVE PROCESS FOR PIECEWISE FUNCTION

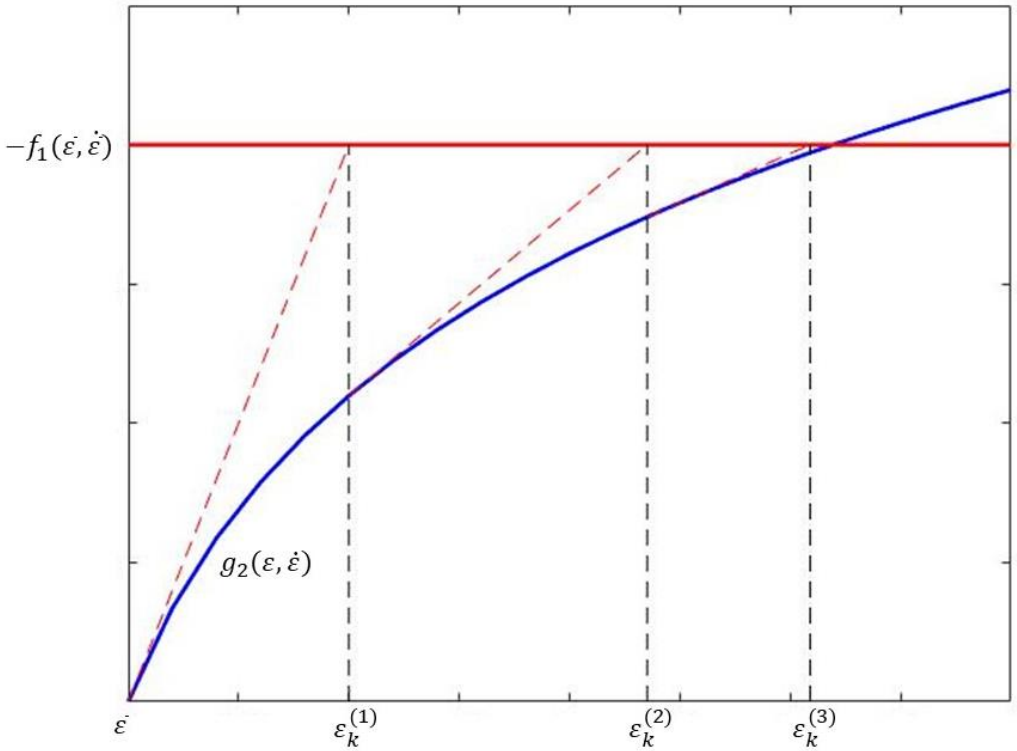

14 CLOSE UP THE ITERATIVE PROCESS IN THE DISCONTINUITY

Once the discontinuity has been handled, the program can move on to the next step using the new function to be minimized $f_2(y, \dot{y}) = g_2(y, \dot{y}) - C$.
The nature of the function defined in strokes creates a condition on the accuracy of the integration.
To ensure correct integration, one or more solutions must fall within the first interval. In other words, the event must be slow enough to record the first strain interval without jumping directly to the second interval.
Considering a constant strain rate

$$\dot{\varepsilon} < \frac{n \cdot \bar{\varepsilon}}{t_{end} \cdot m}$$

$\bar{\varepsilon}$: dicontinuity point

n: number of integration steps

m: number of solution points required in the first interval

t_{end}: total time of the event

In case this condition cannot be met, integration through a single function is preferred.

8 Mechanical characterization of the material

8.1 Static tests setup

15 TRACTION TEST MACHINE

Static tests were performed at speeds of 1 mm/s and 3 mm/s. A strain gauge is placed as a backup strain measurement.
Since, during the test, the breaking point resulted outside the measuring area of the strain gauge, its data cannot be used to characterize the material at the breaking point. However, they can be exploited to validate the result of the DIC analysis and the strain extrapolation method.
The video was recorded at 30 frames per second at high resolution using a cellphone. The device was attached to a stand to prevent movement throughout the test.
The cellphone was used instead of a traditional camera, as it allowed for closer positioning to the specimen, enabling more detailed images of the surface of interest to be recorded.
The scene was also illuminated by a spotlight to promote contrast between the specimen's black background and its white DIC pattern.

16 SPECIMEN AT THE BEGINNING OF THE TEST

17 SPECIMEN AT THE END OF THE TEST

Because the test is performed under quasi-static conditions, the resulting video, recorded at 30 frames per second, contains thousands of frames. Most of these frames are not useful for DIC analysis, so a reduced sampling rate was used during the extraction of frames from the video.

8.2 High speed tests setup

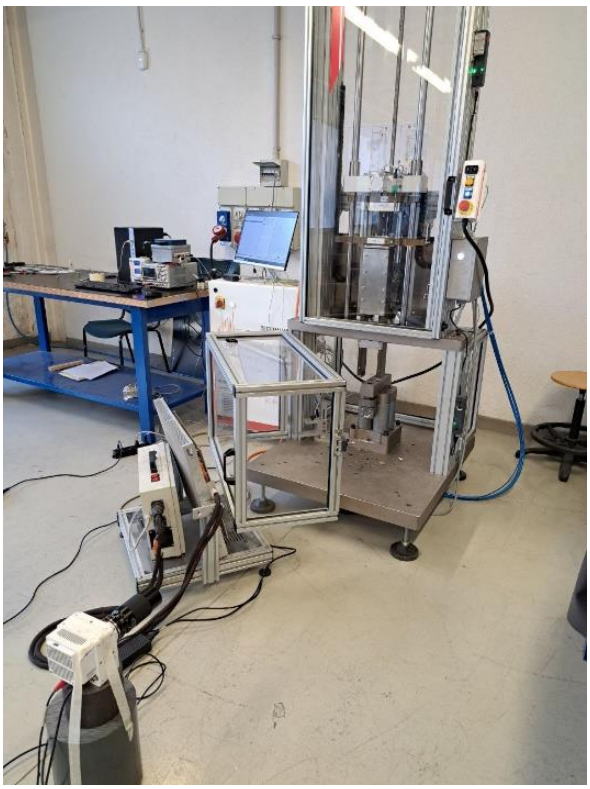

18 DROP TOWER TEST SETUP

High-speed tests were performed using a drop tower.
Videos were recorded with a high-speed camera that allowed an adequate number of frames to be recorded for DIC analysis.
To increase the frequency of video frames, only a portion of the specimen was framed and the point of failure was called in that region, creating a thin cut.

8.3 Results

provino	Velocità [m/s]	Strain Rate [s^{-1}]	Recording speed [frame/s]
S1	$1.67*10^{-5}$	$1.7*10^{-4}$	30
S2	$1.67*10^{-5}$	$1.7*10^{-4}$	30
S3	$5*10^{-5}$	$5.1*10^{-4}$	30
TV1	3.05	31.1	24000
TV2	3.63	37	15000
TV3	4.04	41.2	15000
TV4	5.06	51.6	15000

TABLE 1 TRACTION TESTS

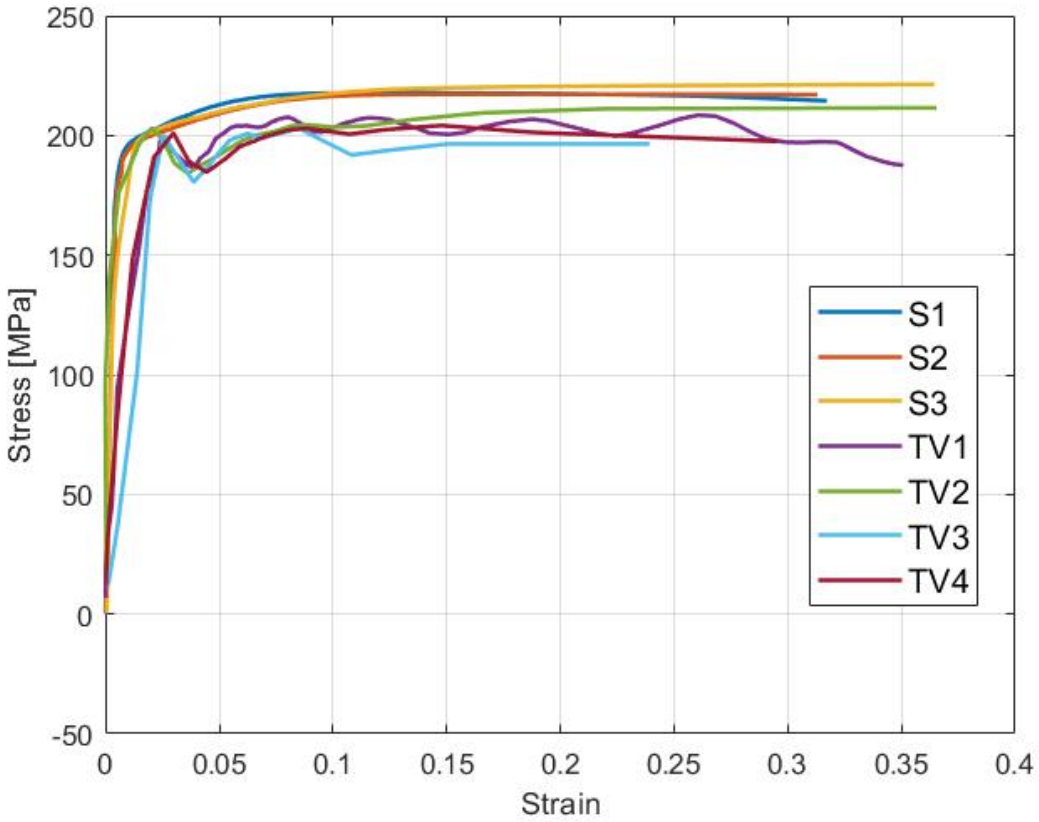

19 MATERIAL CHARACTERISATION RESULTS

The tests show that the material is independent of strain rate.
A simplified Jhonson-Cook model was chosen as hardening law.

$$\sigma = A + B\varepsilon^{N}$$

A=172 Yield stress
B=71 Hardening module
N= 0.2049 Hardening coefficient

9 Tests with the thermocamera

9.1 Specimen preparation and setup

The specimen cannot be left as pure aluminum because this would create two problems:

- The emissivity of aluminum, being very low, reduces the accuracy of thermal data
- The surface easily reflects the thermal image of its surroundings creating inaccuracies in the measurement

To avoid this, the specimen was anodized, creating a black surface.
Since anodizing is only a surface treatment, special care must be taken when interpreting the results. When the specimen starts to break, the internal reflective surface starts to show, invalidating the data at those points.
As before, the breaking point of the sample was defined with a slight cut.

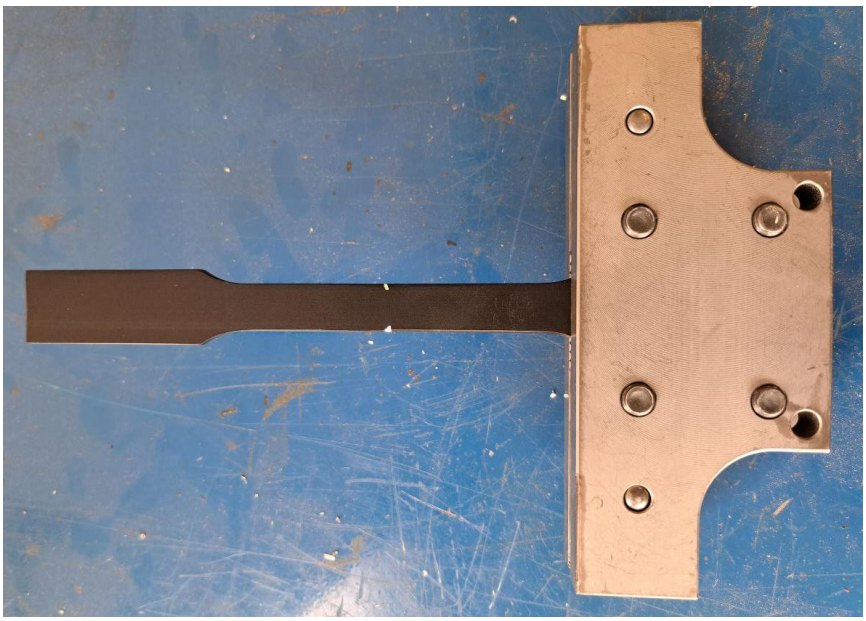

22 ANODISED CUTTED SPECIMEN

The tests were performed using the same machines as the material characterization tests.
In this case, however, a background screen was used to eliminate possible interferences, such as reflective or emitting surfaces.

9.2 Integration results

The reported results refer to two separate points on the specimen. Point A is taken at the point of rupture. Point B is taken at a point on the midsection away from the point of rupture.
The former point can be compared with the DIC results, while the latter can be compared with the results of both the DIC and the strain gauge.

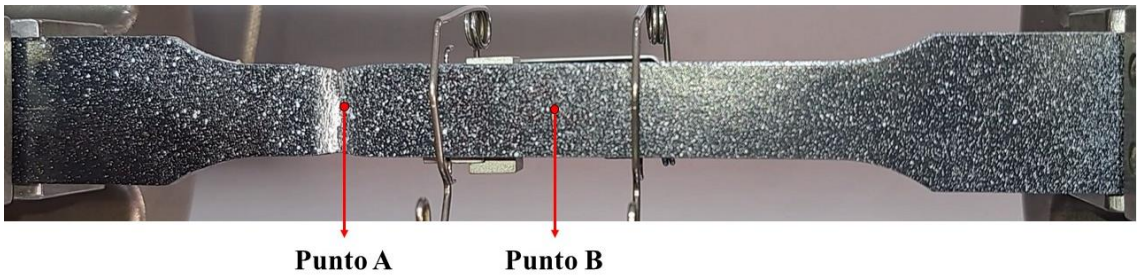

203-POSITION OF CHOOSEN POINTS

Specimen	Speed [m/s]	Strain rate [1/s]	Recording speed [frame/s]
A	0.2	2.04	300
B	0.2	2.04	300
H	0.4	4.08	300
F	0.05	0.51	300
D	3.6	36.7	1400
E	3	30.6	1700

TABLE 2 THERMAL CAMERA TESTS

9.2.1 Specimen A

Point A

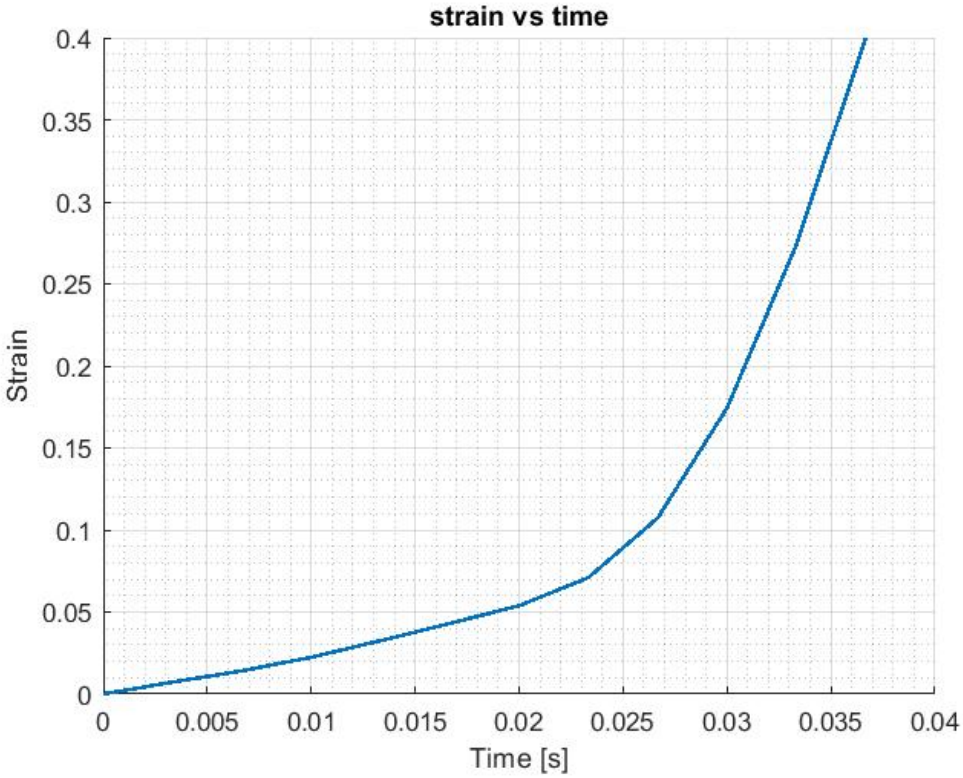

21 STRAIN SPECIMEN A POINT A

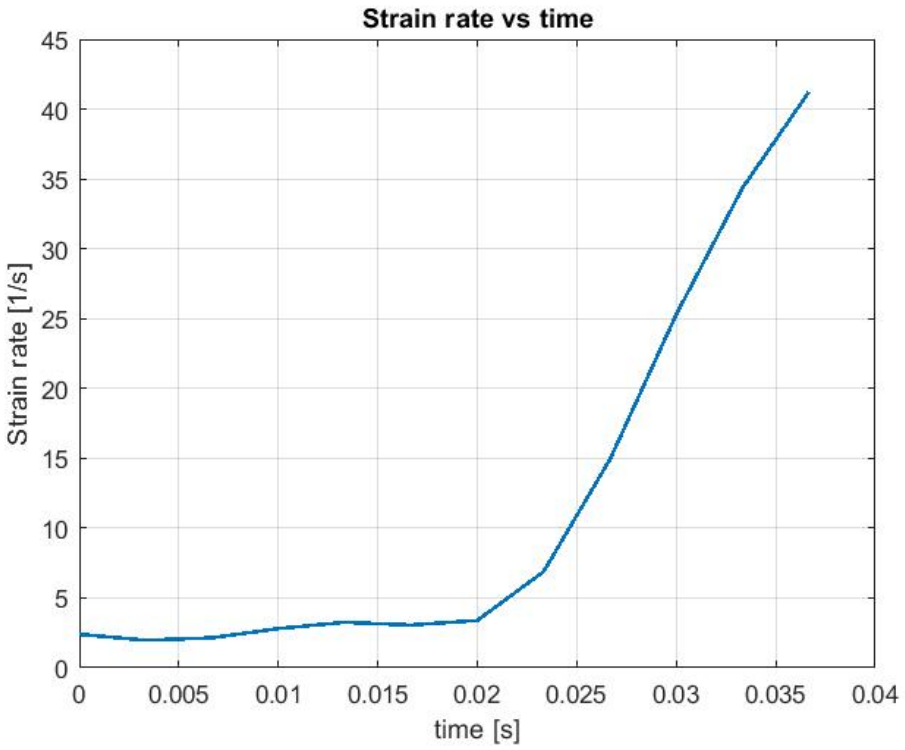

22 STRAIN RATE SPECIMEN A POINT A

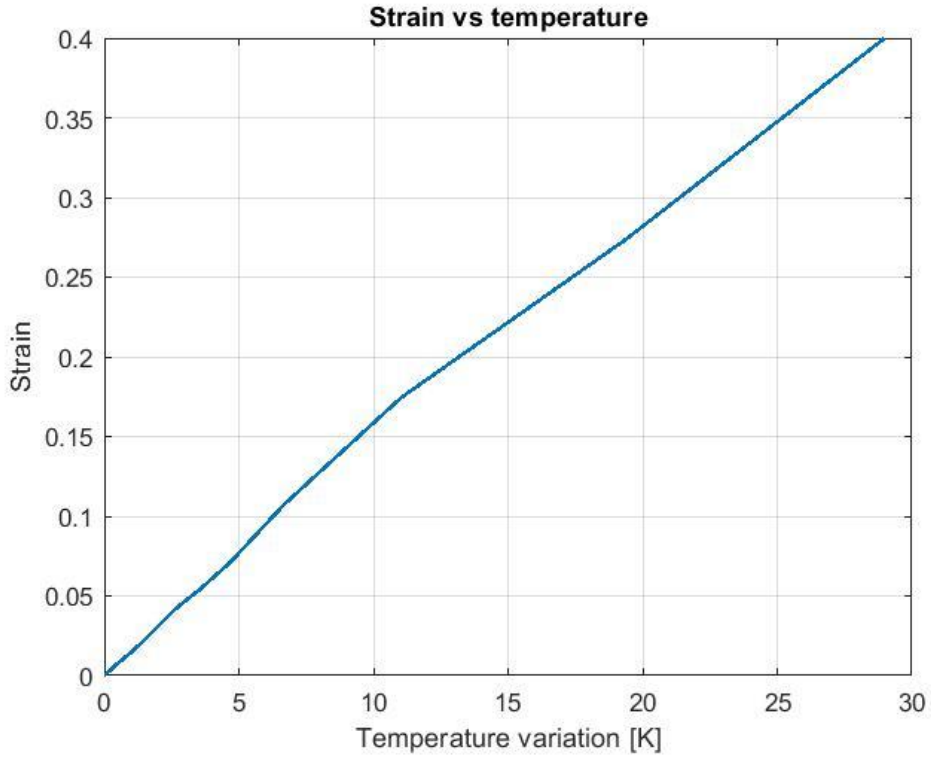

23 STRAIN VS ΔT SPECIMEN A POINT A

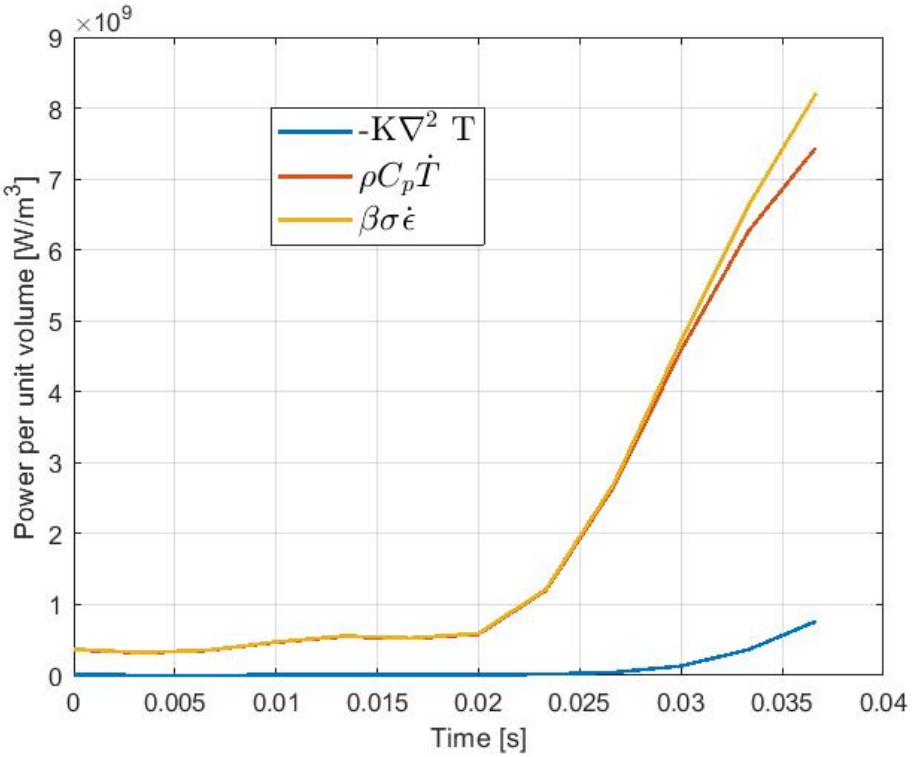

24 POWER COMPONENT SPECIMEN A POINT A

Point B

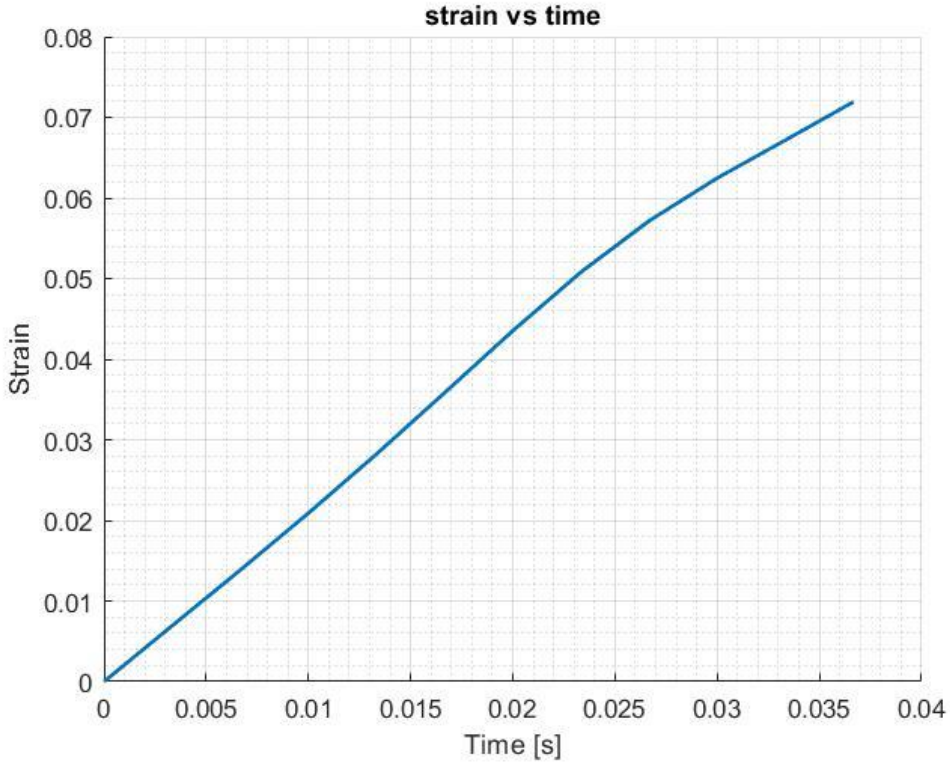

25 STRAIN SPECIMEN A POINT B

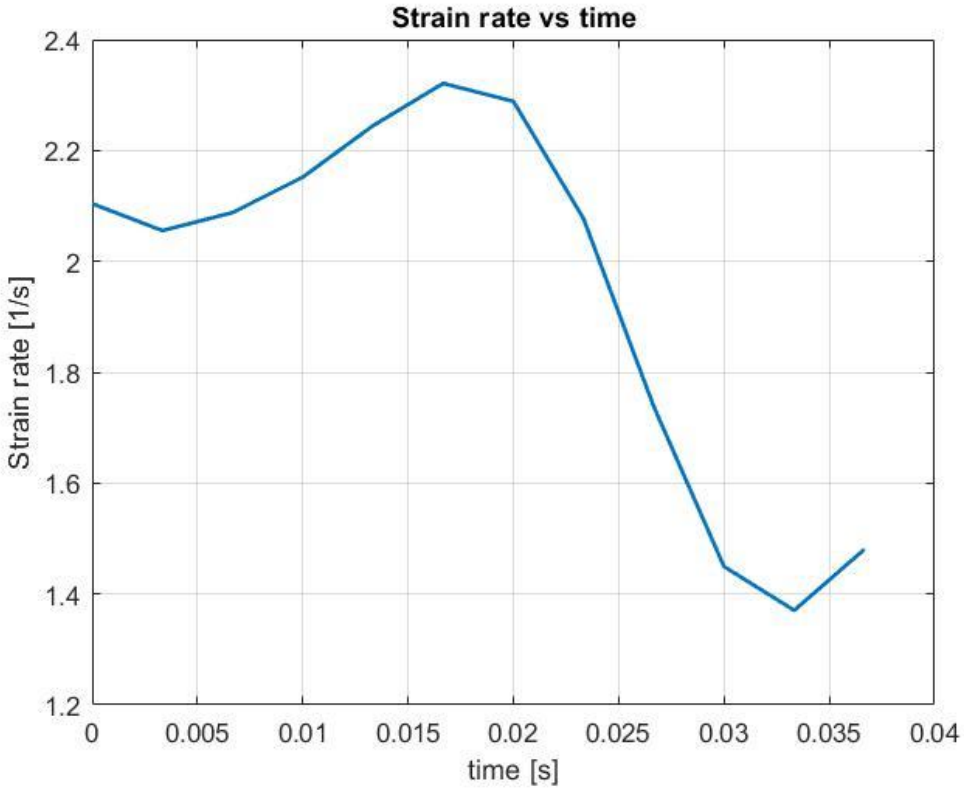

26 STRAIN RATE SPECIMEN A POINT B

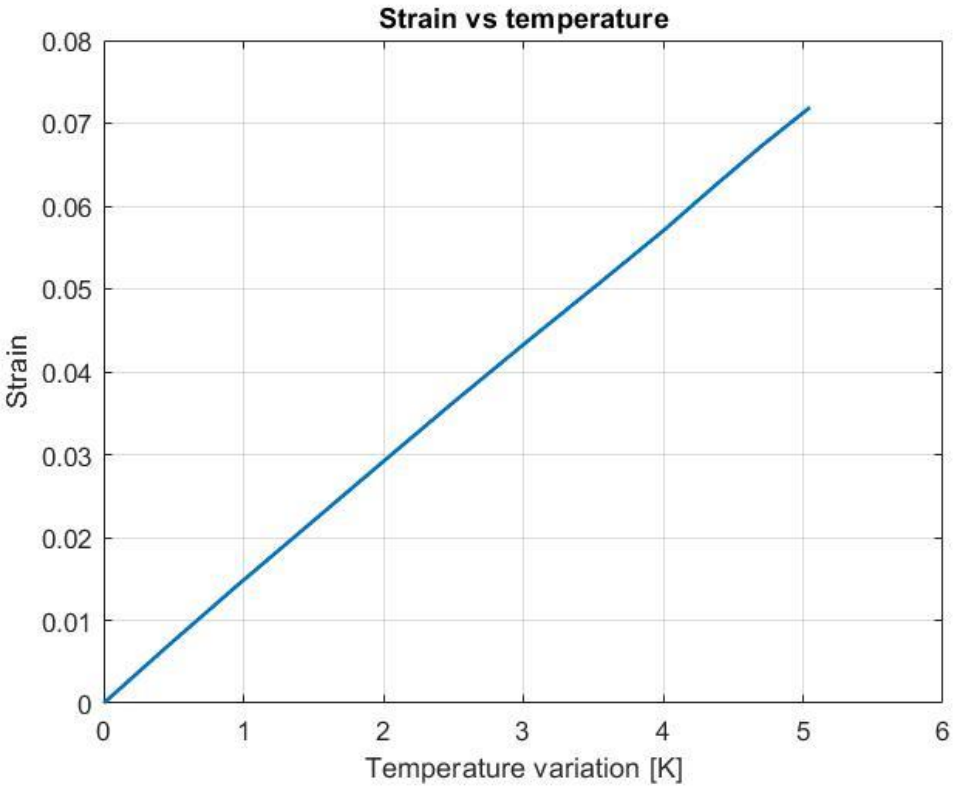

27 STRAIN VS ΔT SPECIMEN A POINT B

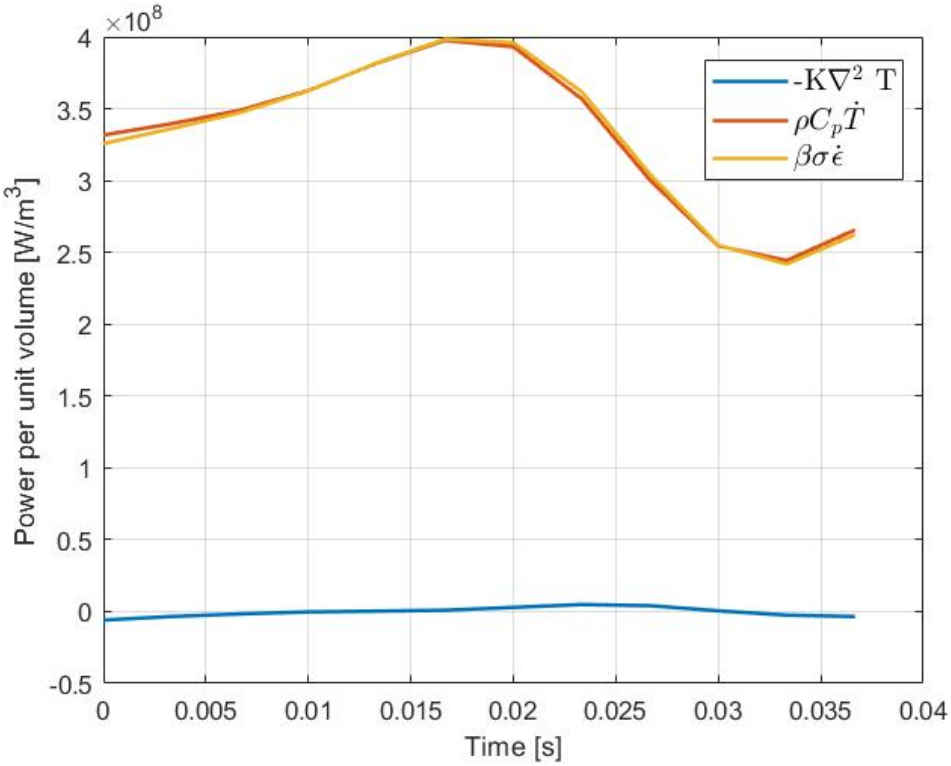

28 POWER COMPONENT SPECIMEN A POINT B

9.2.2 Specimen B

Point A

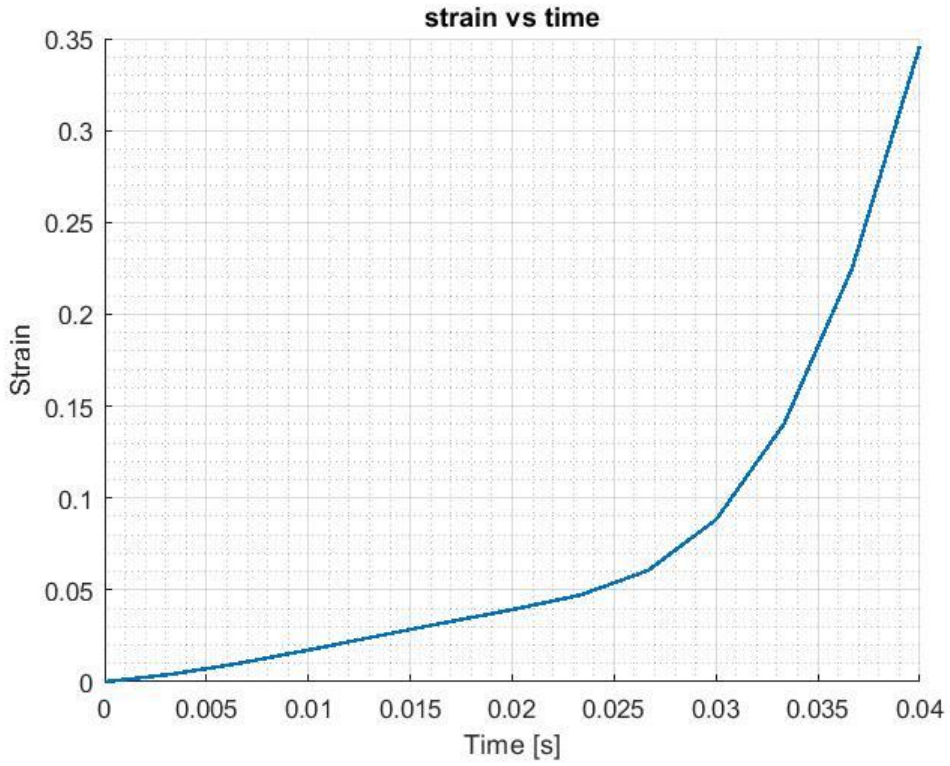

29 STRAIN SPECIMEN B POINT A

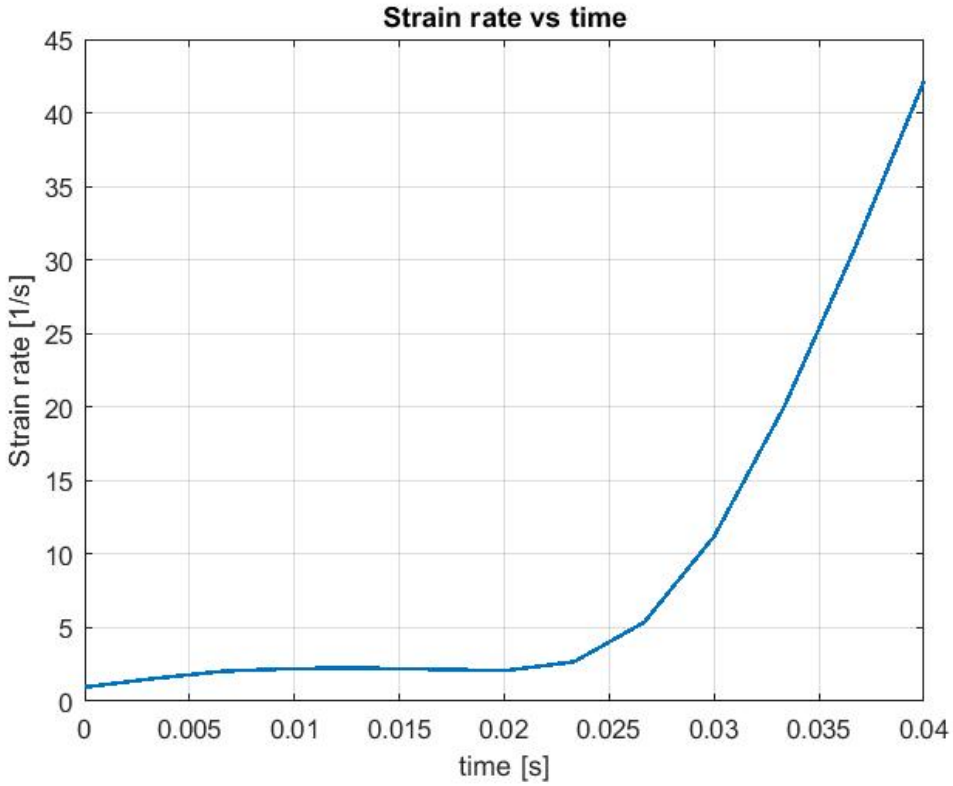

30 STRAIN RATE SPECIMEN B POINT A

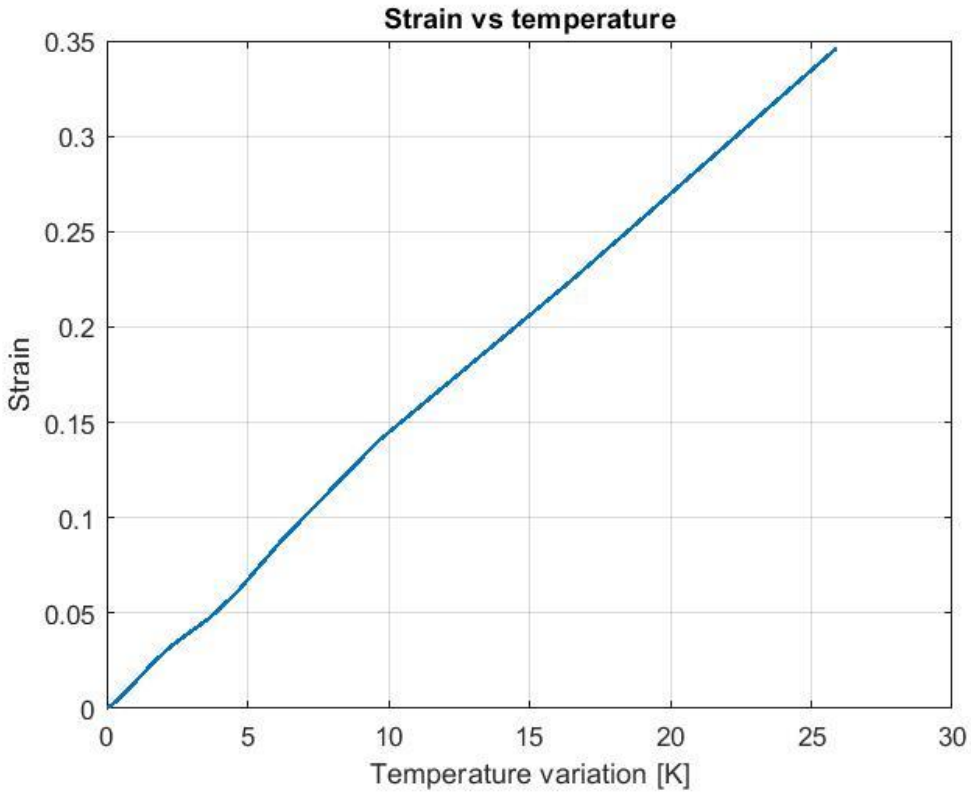

31 STRAIN VS ΔT SPECIMEN B POINT A

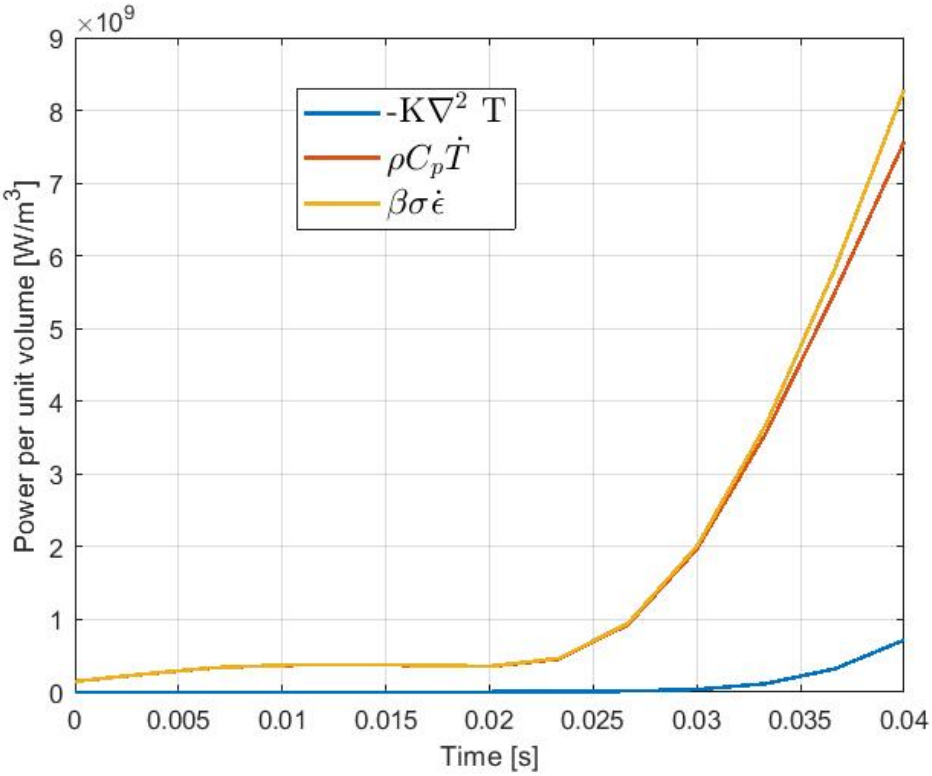

32 POWER COMPONENT SPECIMEN B POINT A

Point B

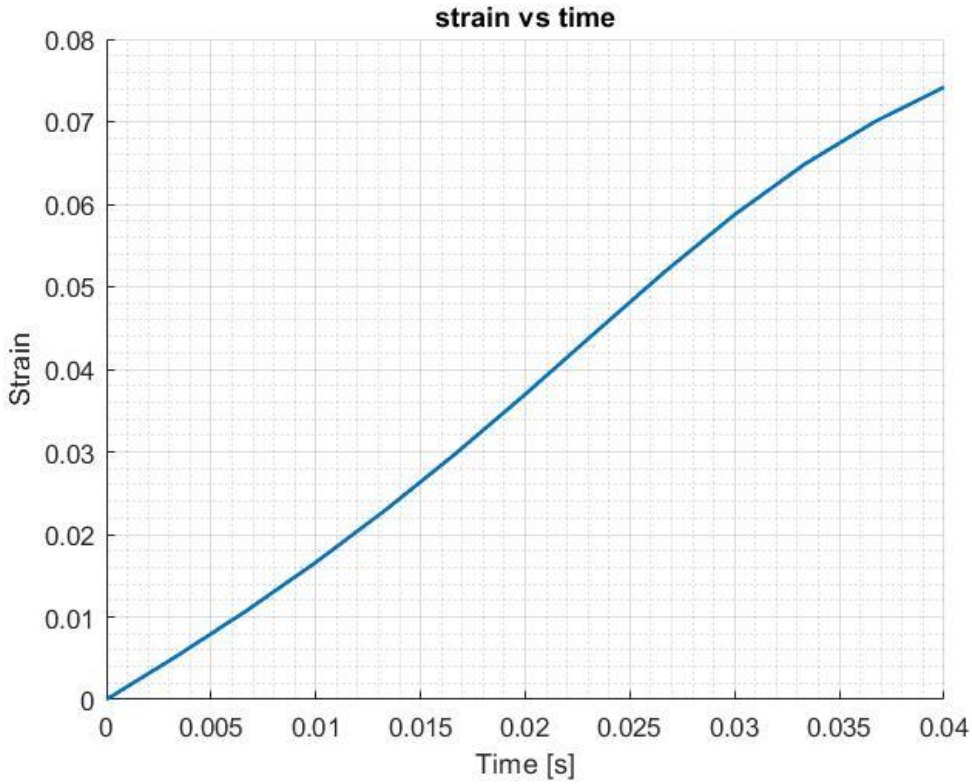

33 STRAIN SPECIMEN B POINT B

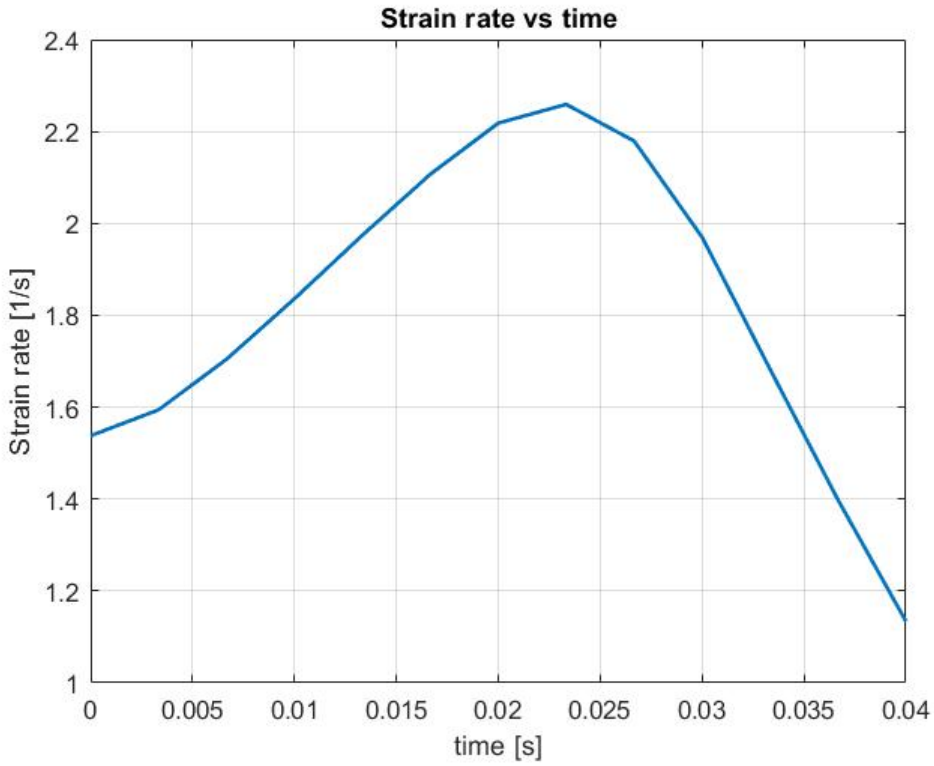

34 STRAIN RATE SPECIMEN B POINT B

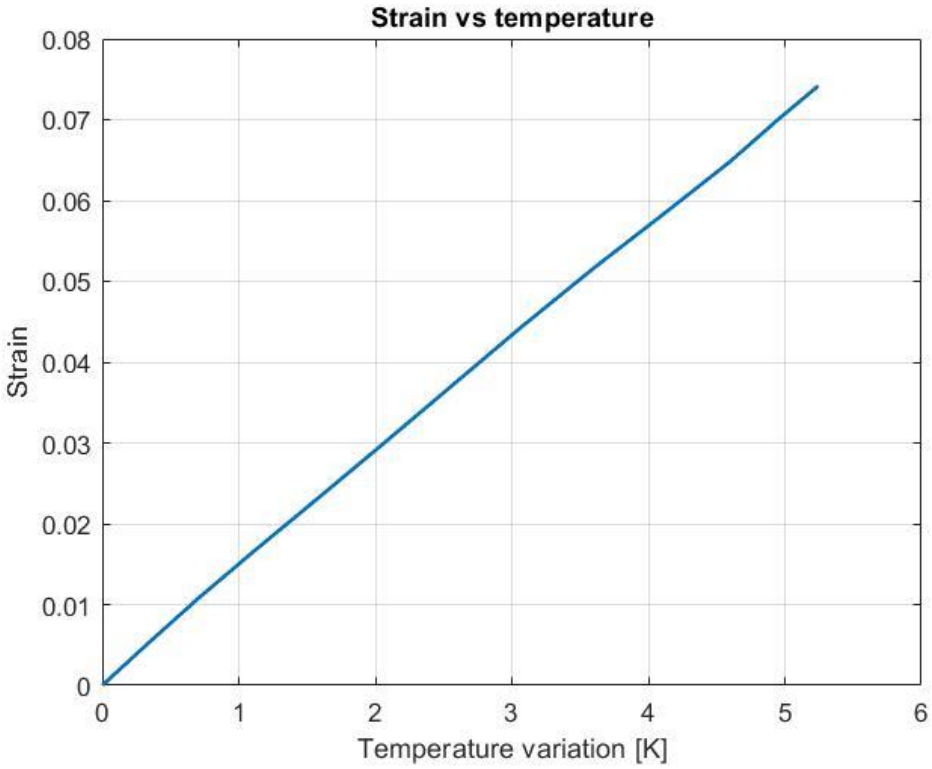

35 STRAIN VS ΔT SPECIMEN B POINT B

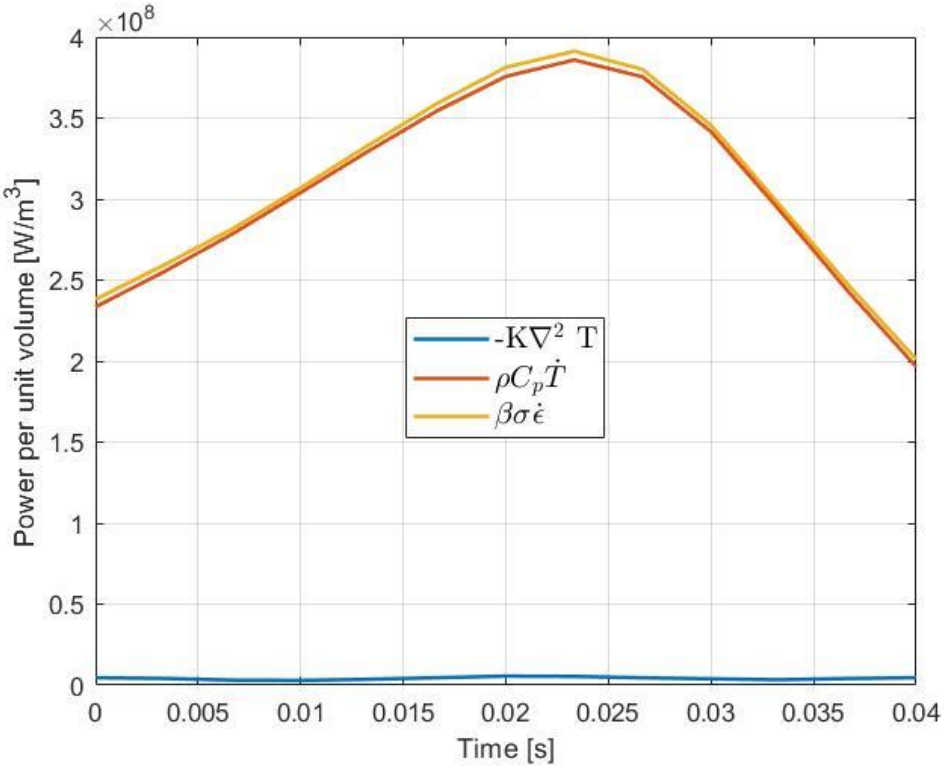

36 POWER COMPONENT SPECIMEN B POINT B

9.2.3 Specimen H

Point A

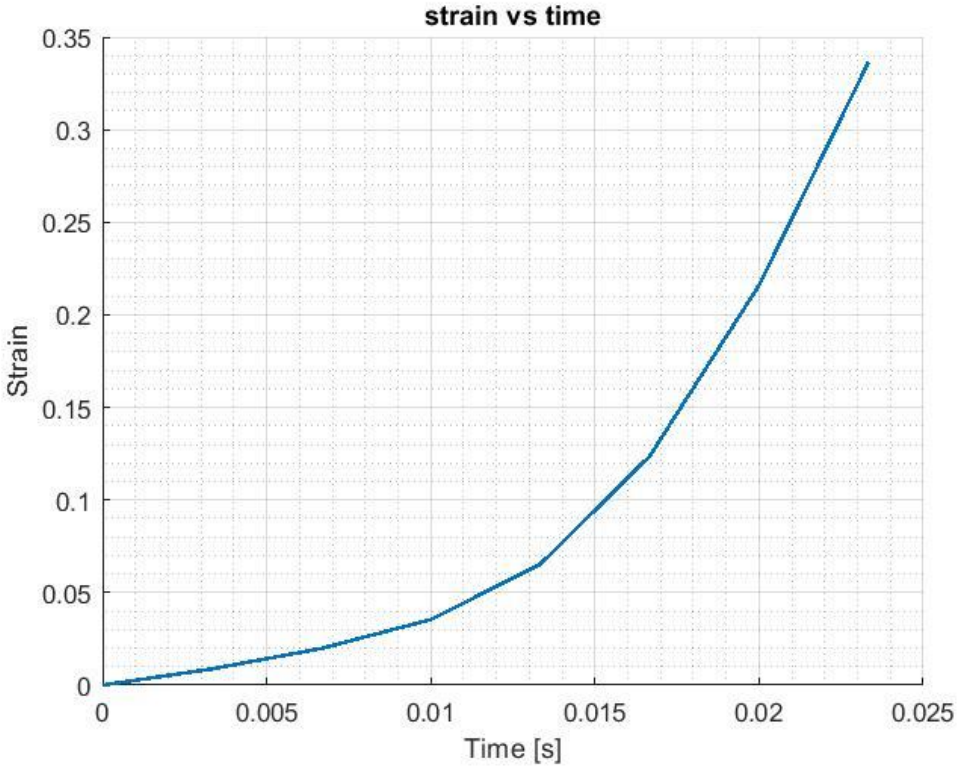

37 STRAIN SPECIMEN H POINT A

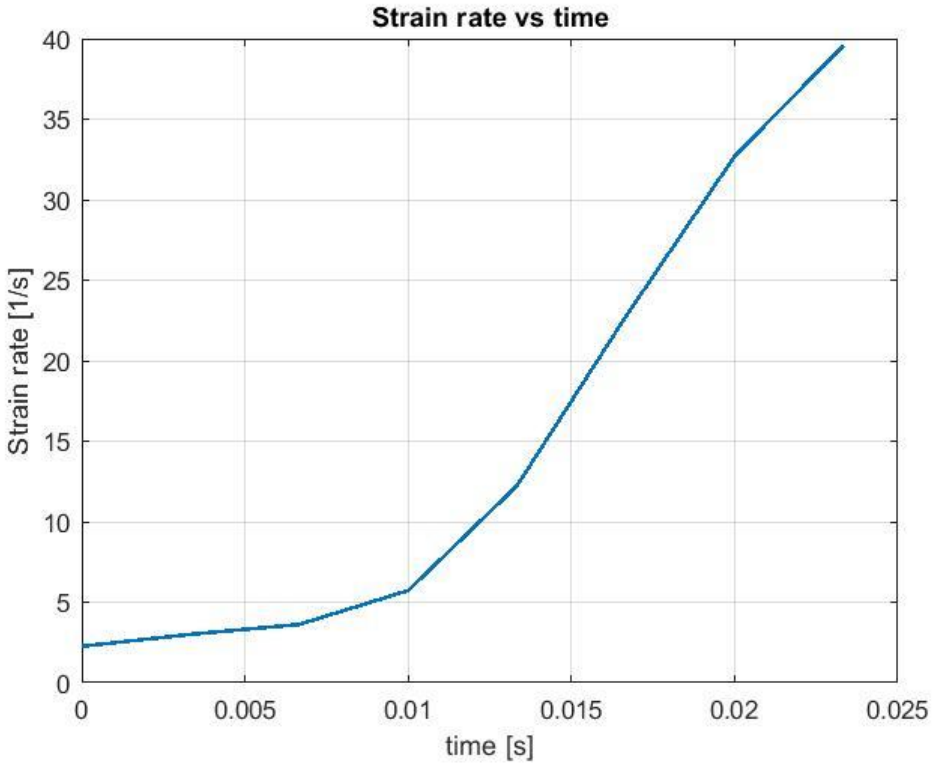

38 STRAIN RATE SPECIMEN H POINT A

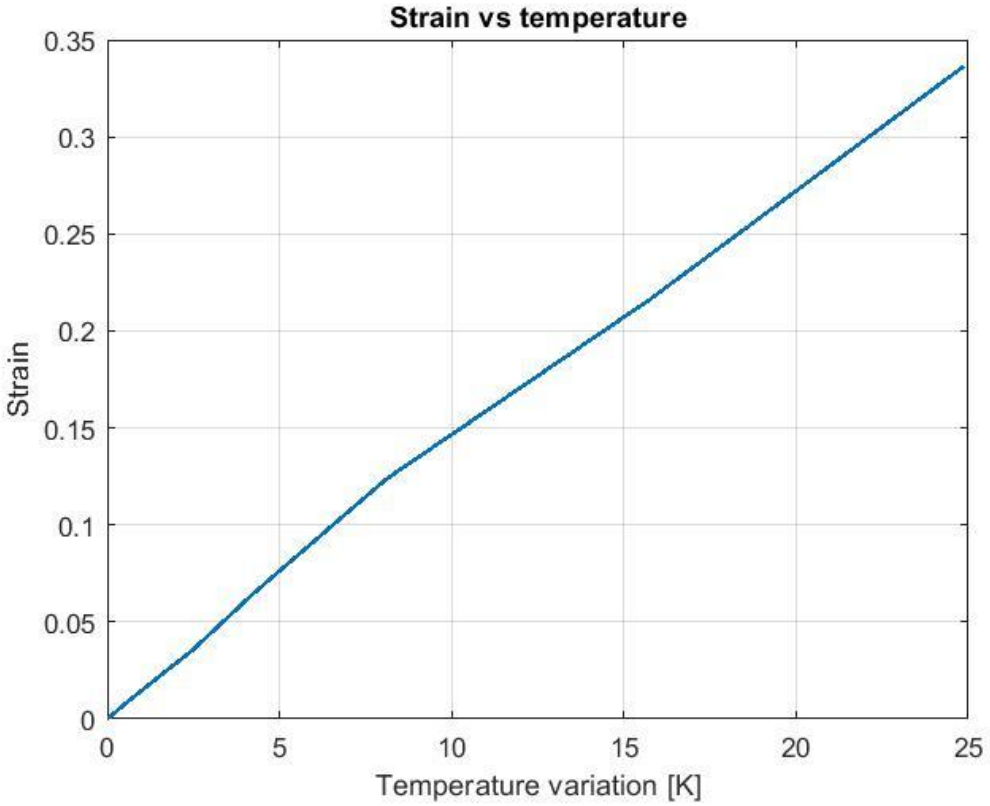

39 STRAIN VS ΔT SPECIMEN H POINT A

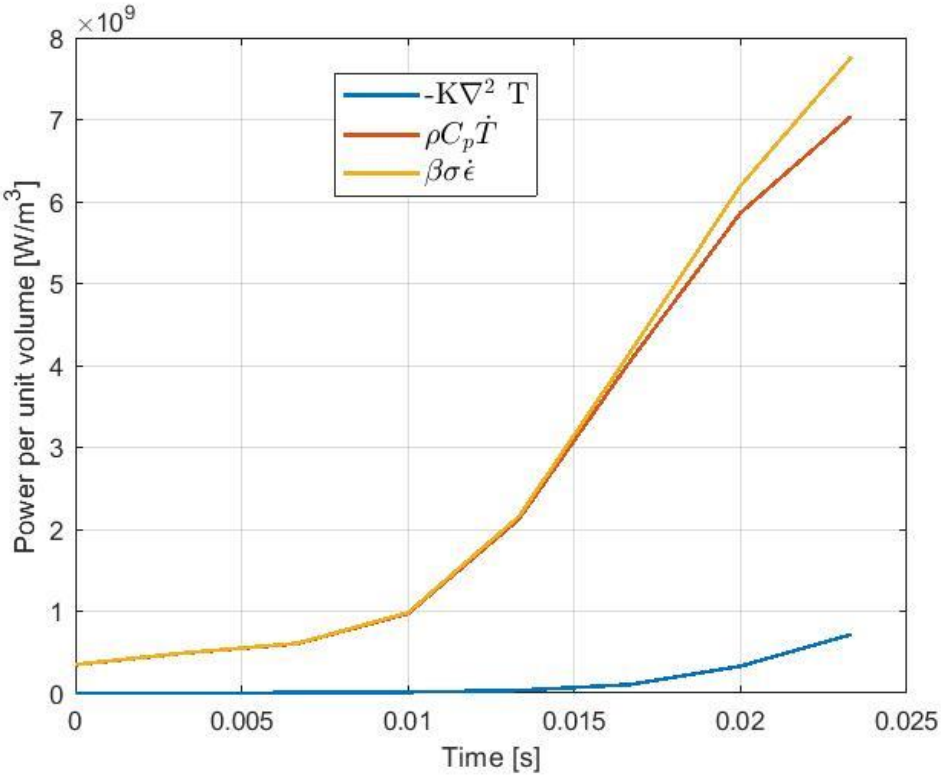

40 POWER COMPONENT SPECIMEN H POINT A

Point B

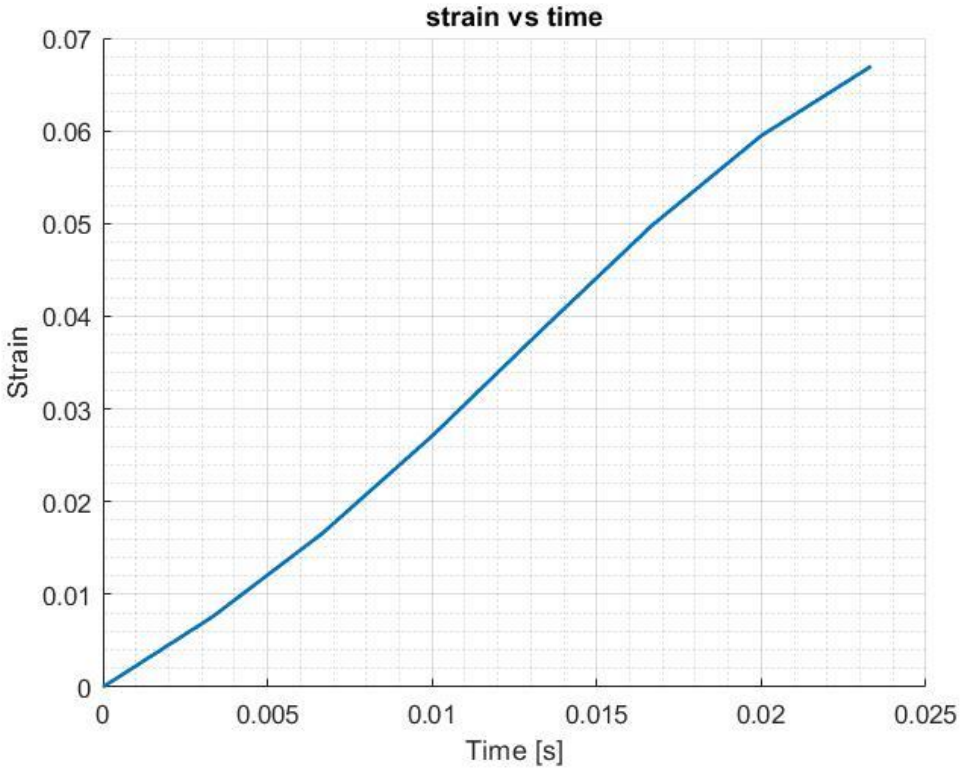

41 STRAIN SPECIMEN H POINT B

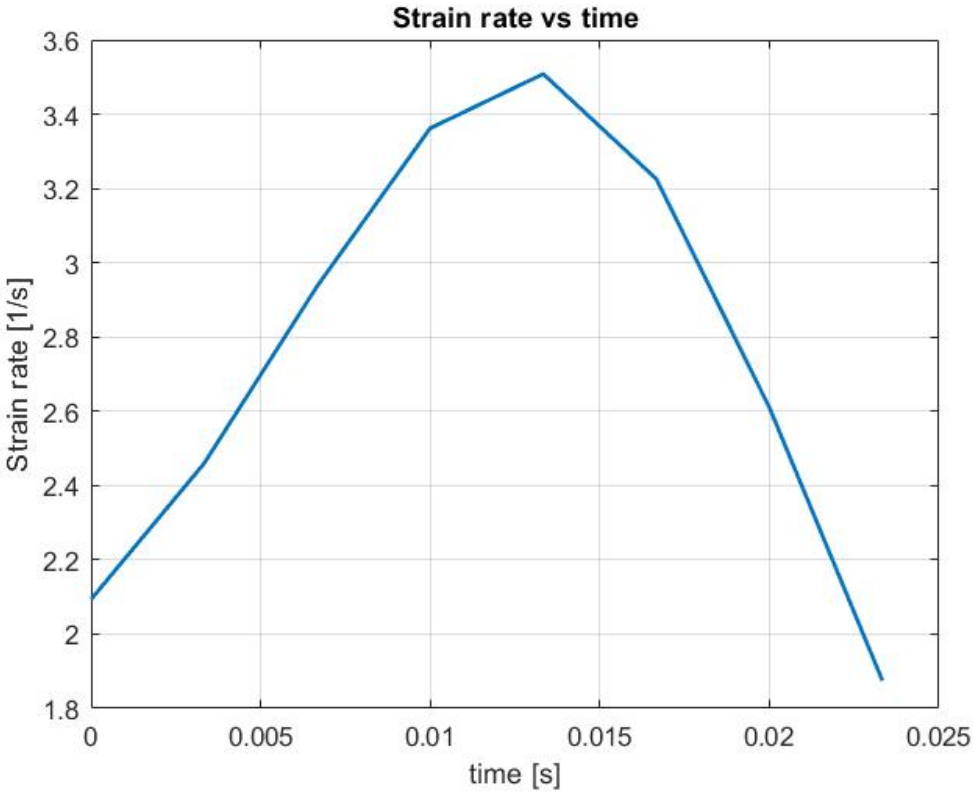

42 STRAIN RATE SPECIMEN H POINT B

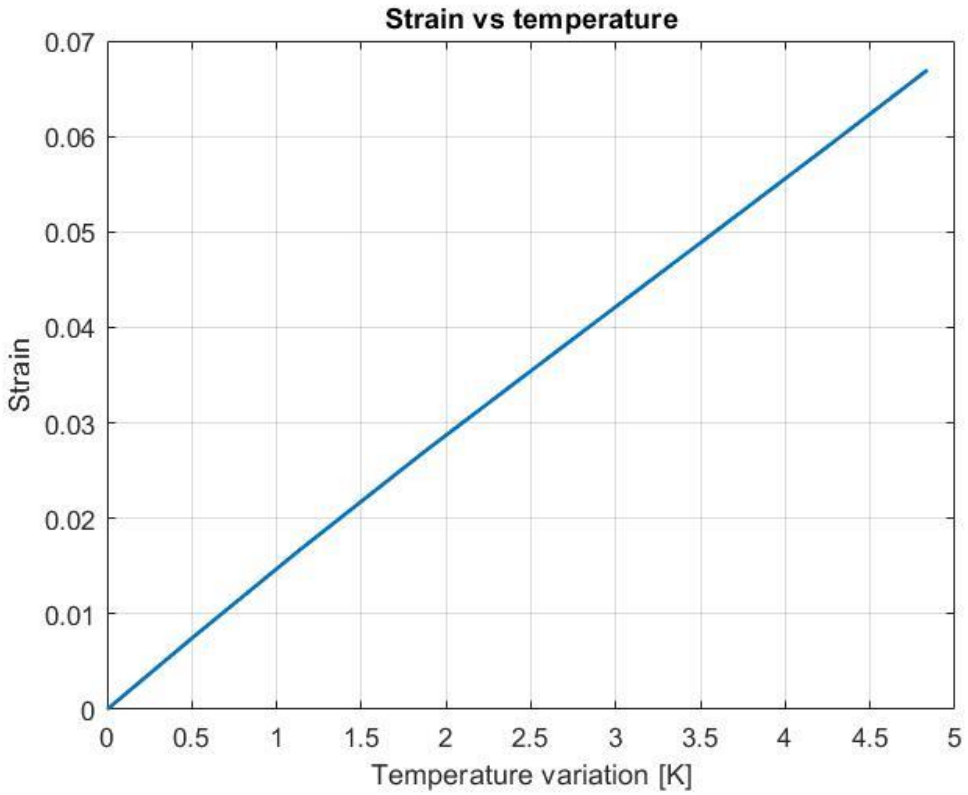

43 STRAIN VS ΔT SPECIMEN H POINT B

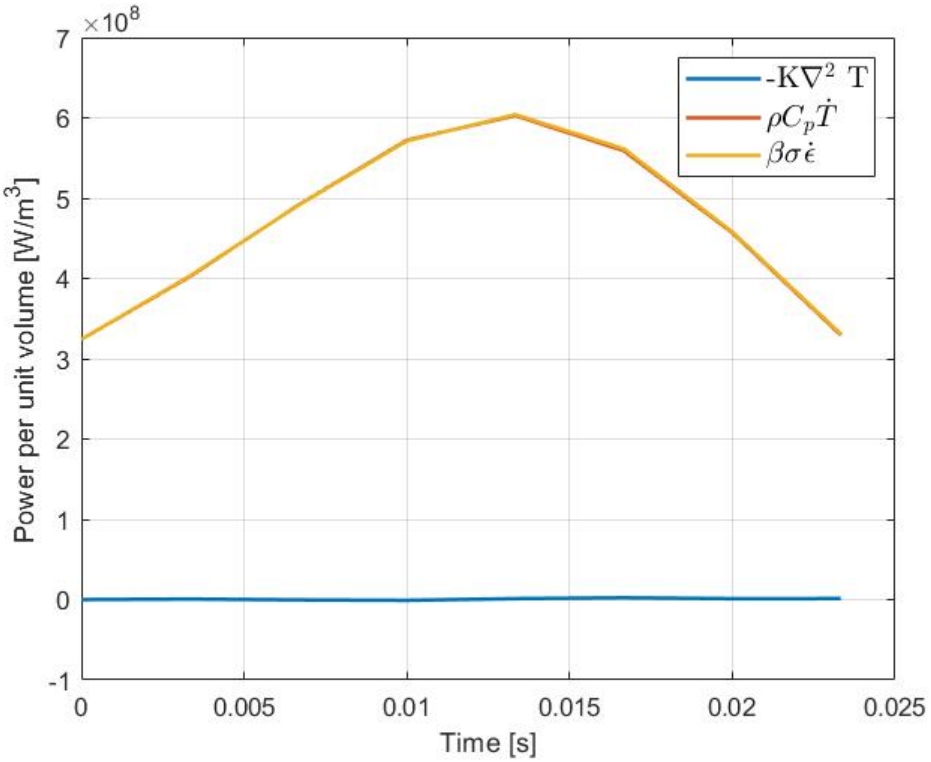

44 POWER COMPONENT SPECIMEN H POINT B

9.2.4 Specimen F

Point A

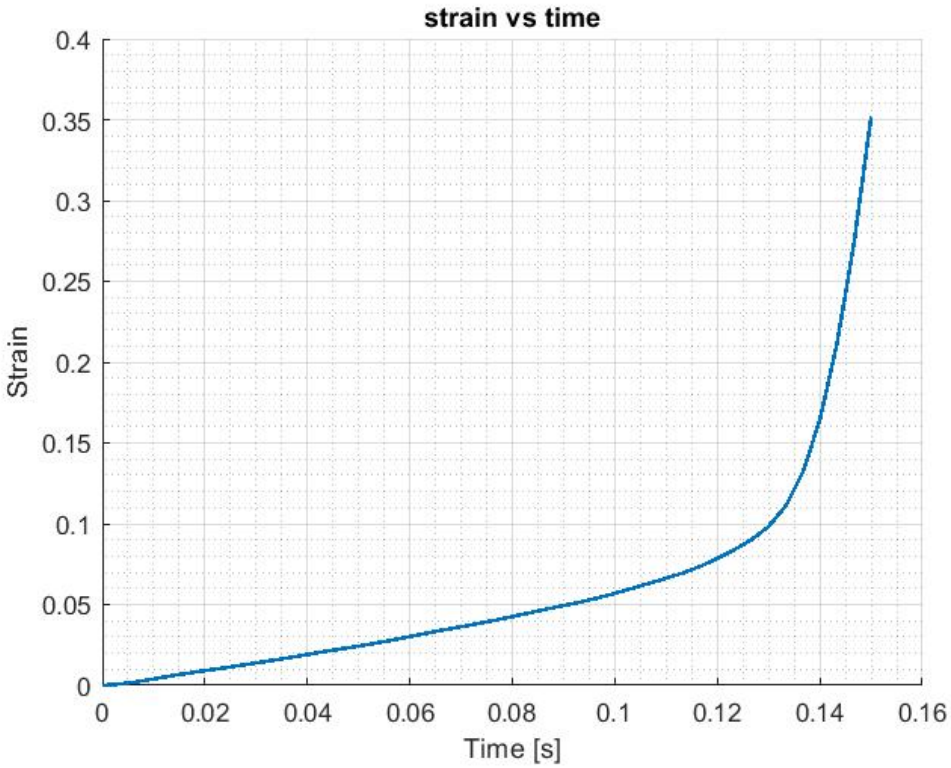

45 STRAIN SPECIMEN F POINT A

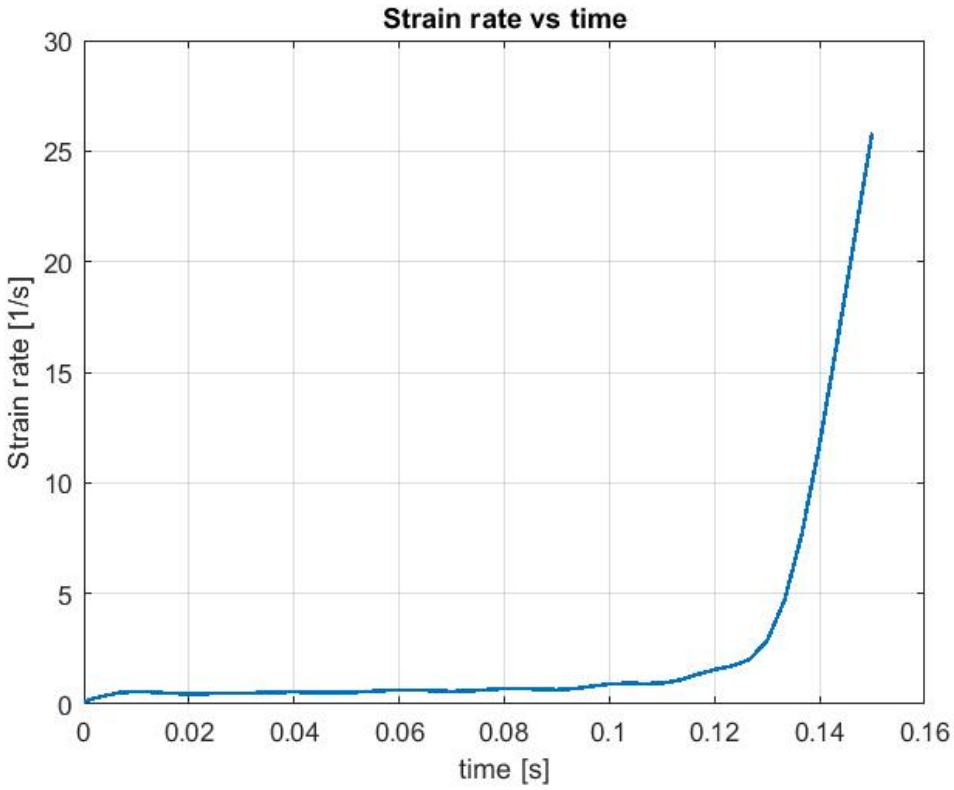

46 STRAIN RATE SPECIMEN F POINT A

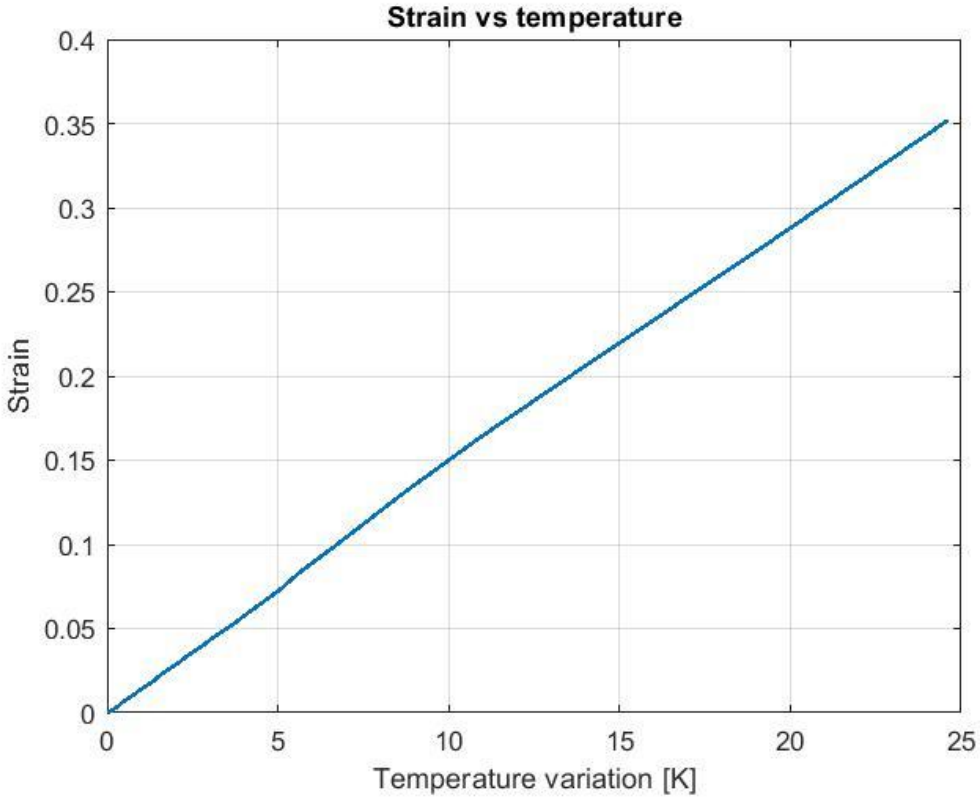

47 STRAIN VS ΔT SPECIMEN F POINT A

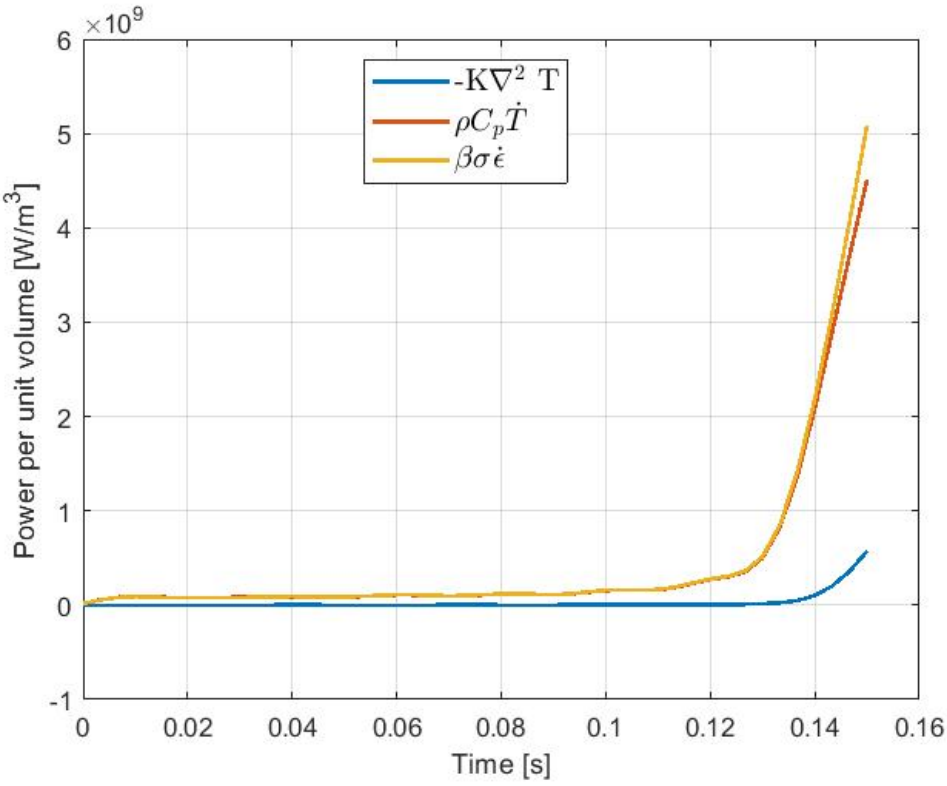

48 POWER COMPONENT SPECIMEN F POINT A

Punto B

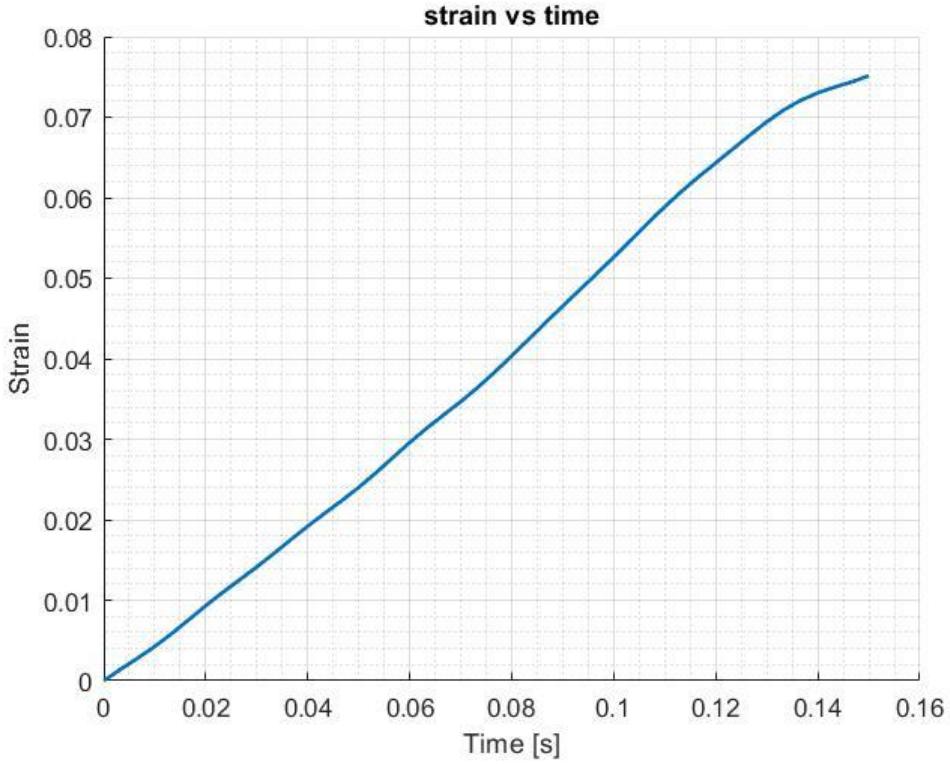

49 STRAIN SPECIMEN F POINT B

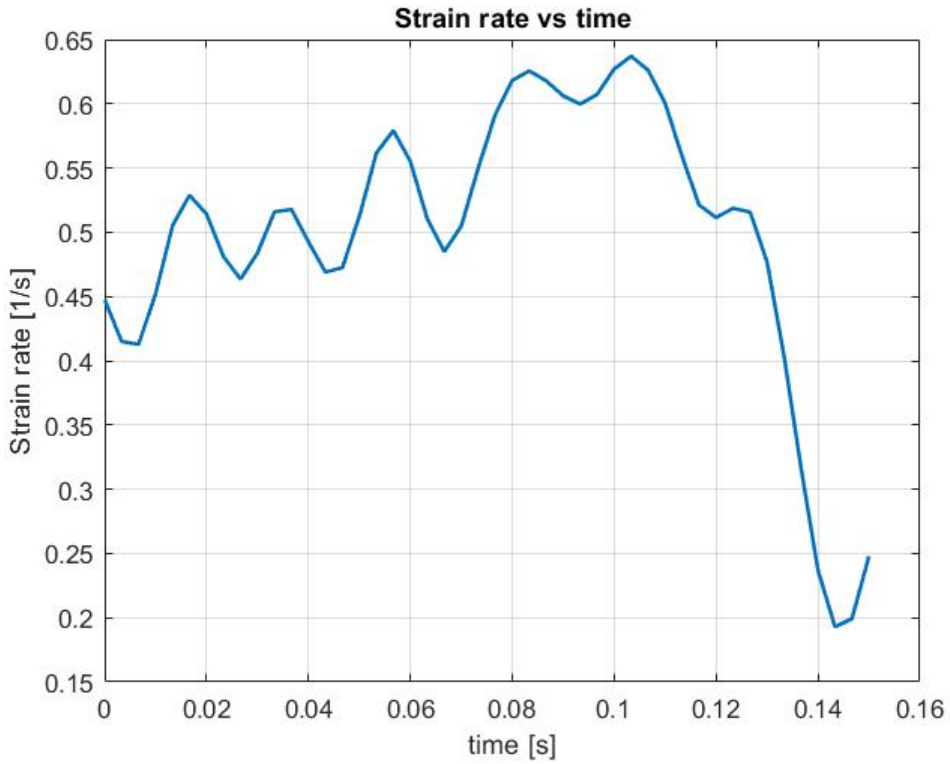

50 STRAIN RATE SPECIMEN F POINT B

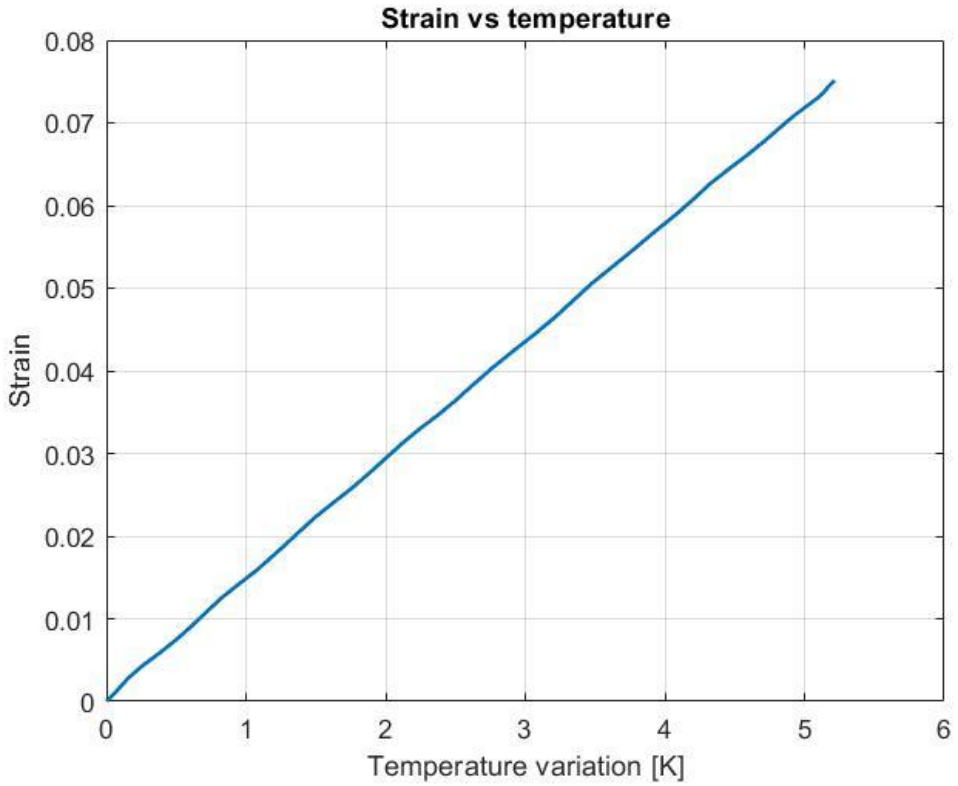

51 STRAIN VS ΔT SPECIMEN F POINT B

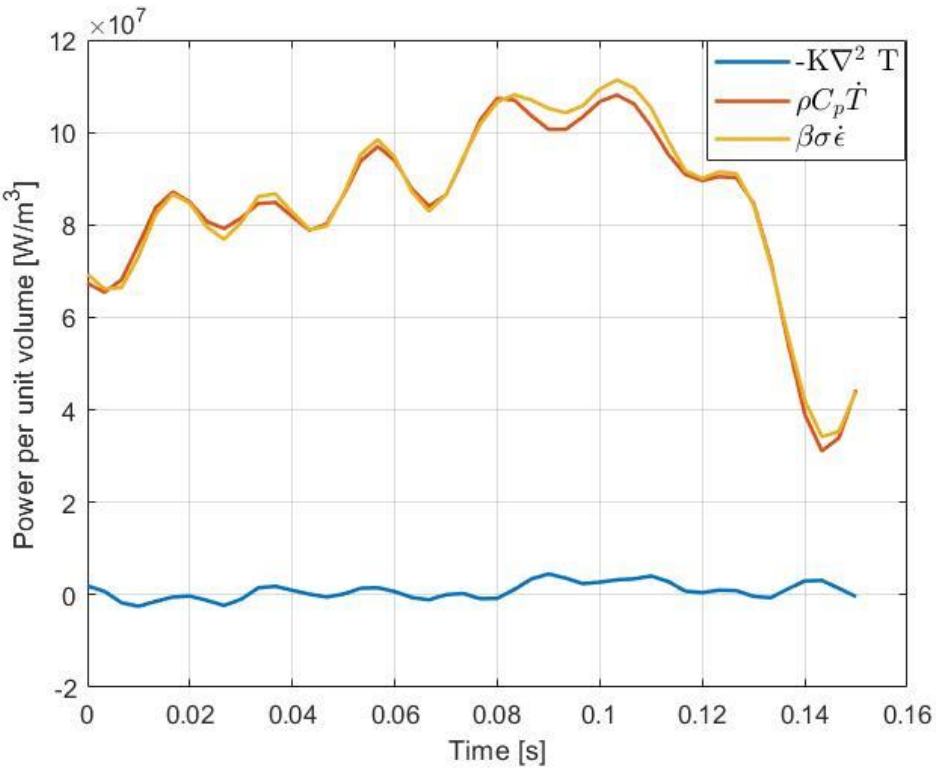

52 POWER COMPONENT SPECIMEN F POINT B

9.2.5 Specimen D

Point A

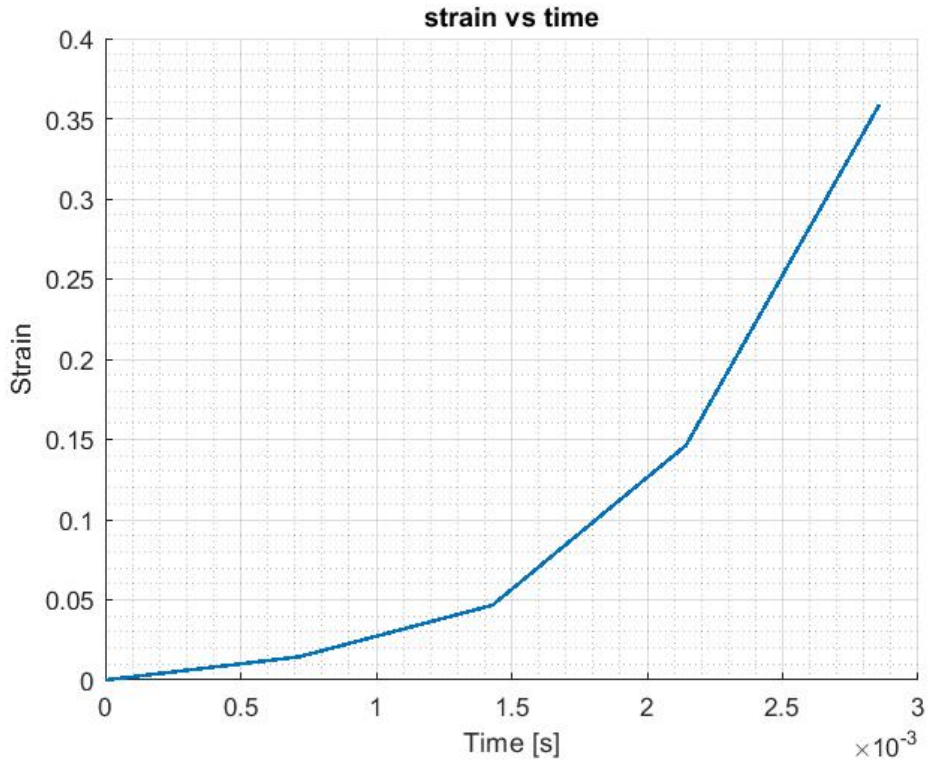

53 STRAIN SPECIMEN D POINT A

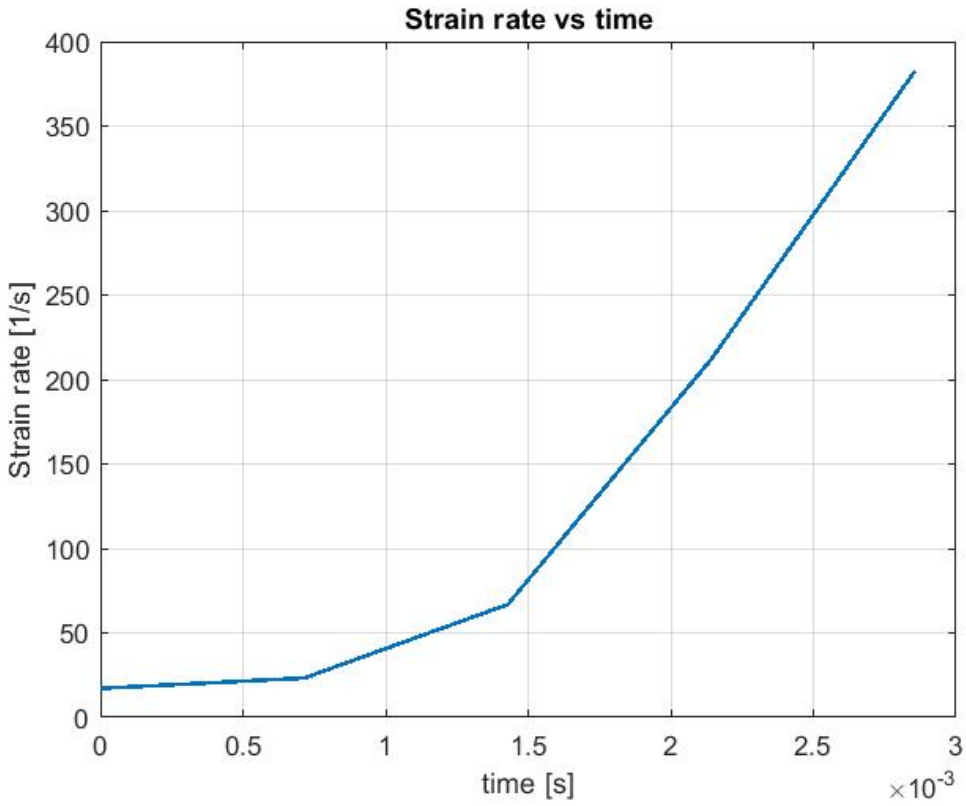

54 STRAIN RATE SPECIMEN D POINT A

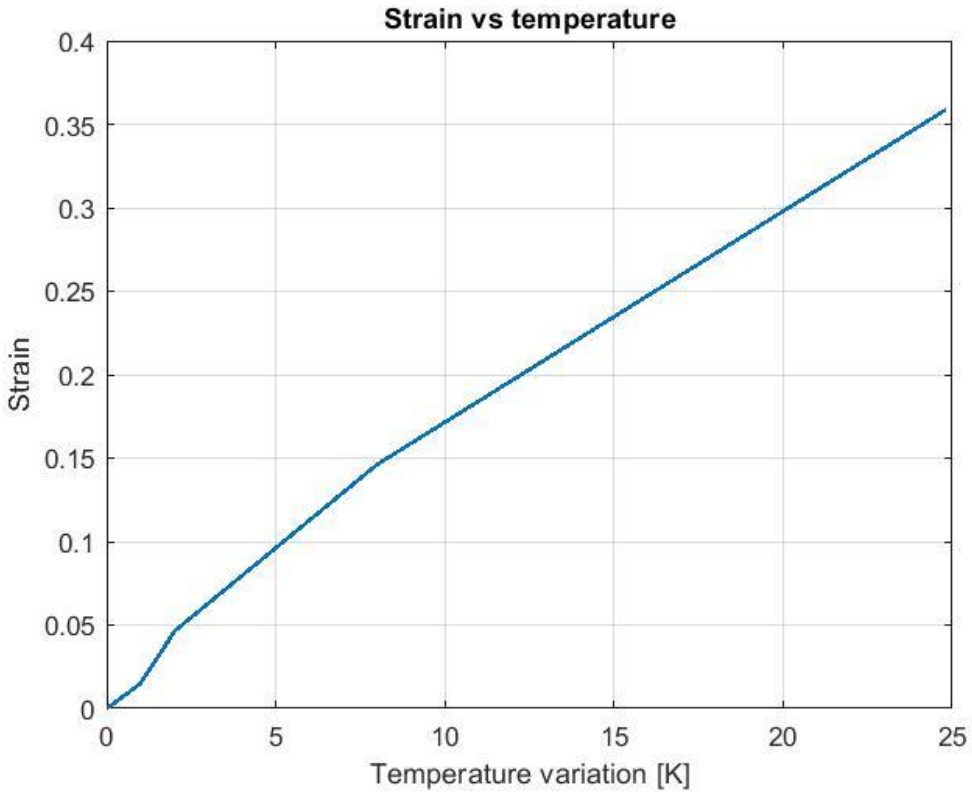

55 STRAIN VS ΔT SPECIMEN D POINT A

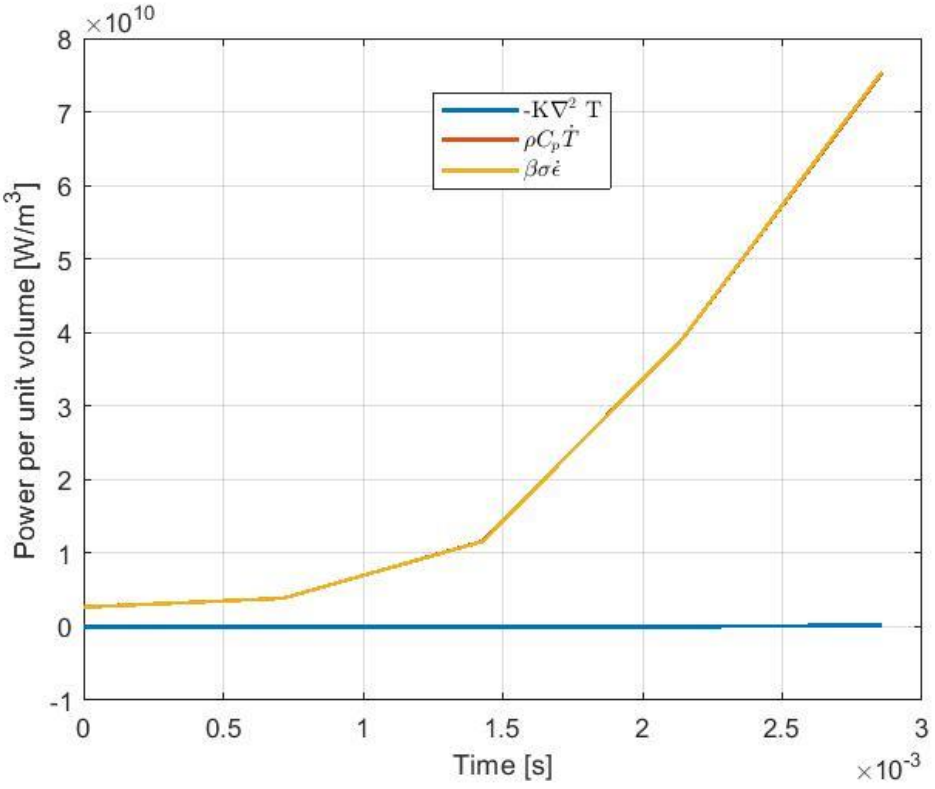

56 POWER COMPONENT SPECIMEN D POINT A

Point B

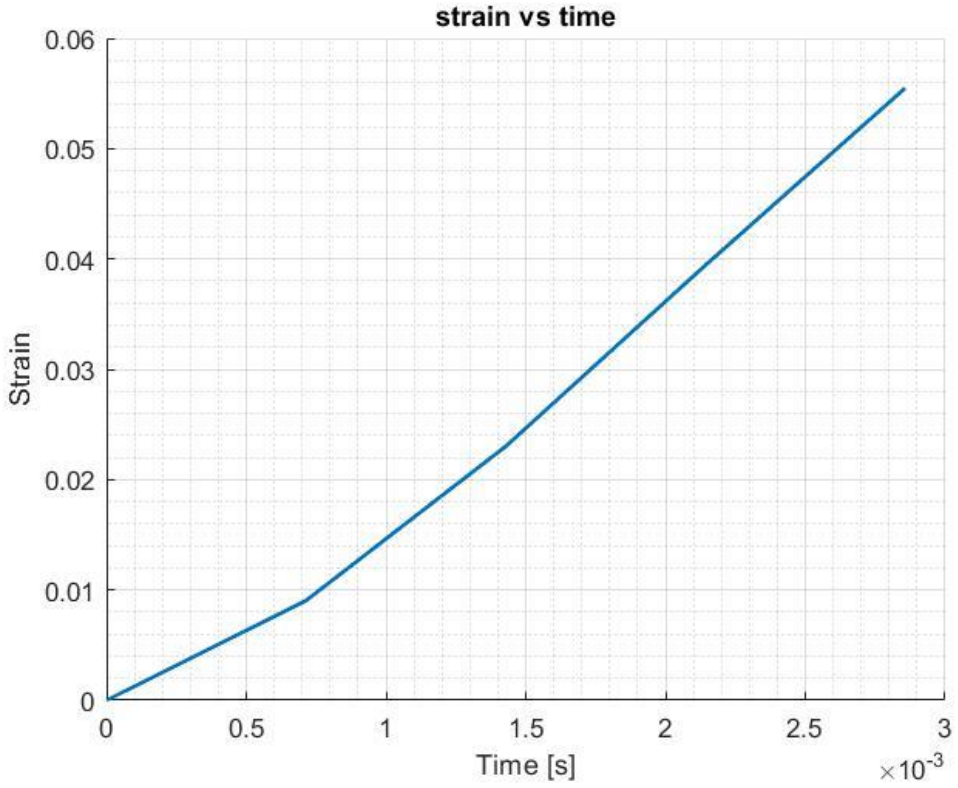

57 STRAIN SPECIMEN D POINT B

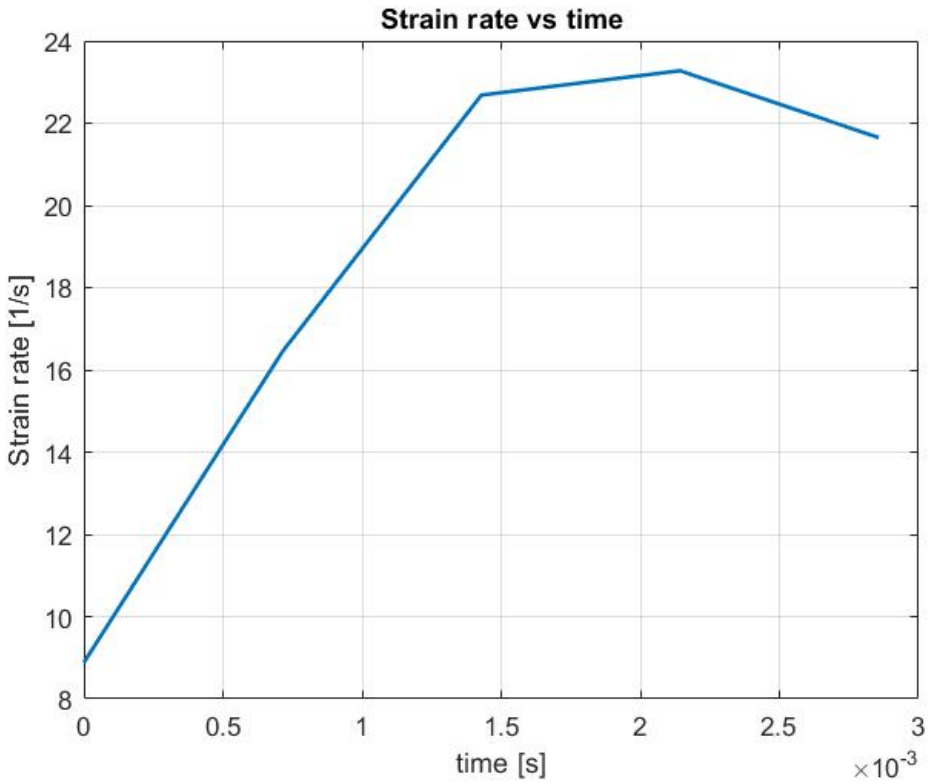

58 STRAIN RATE SPECIMEN D POINT B

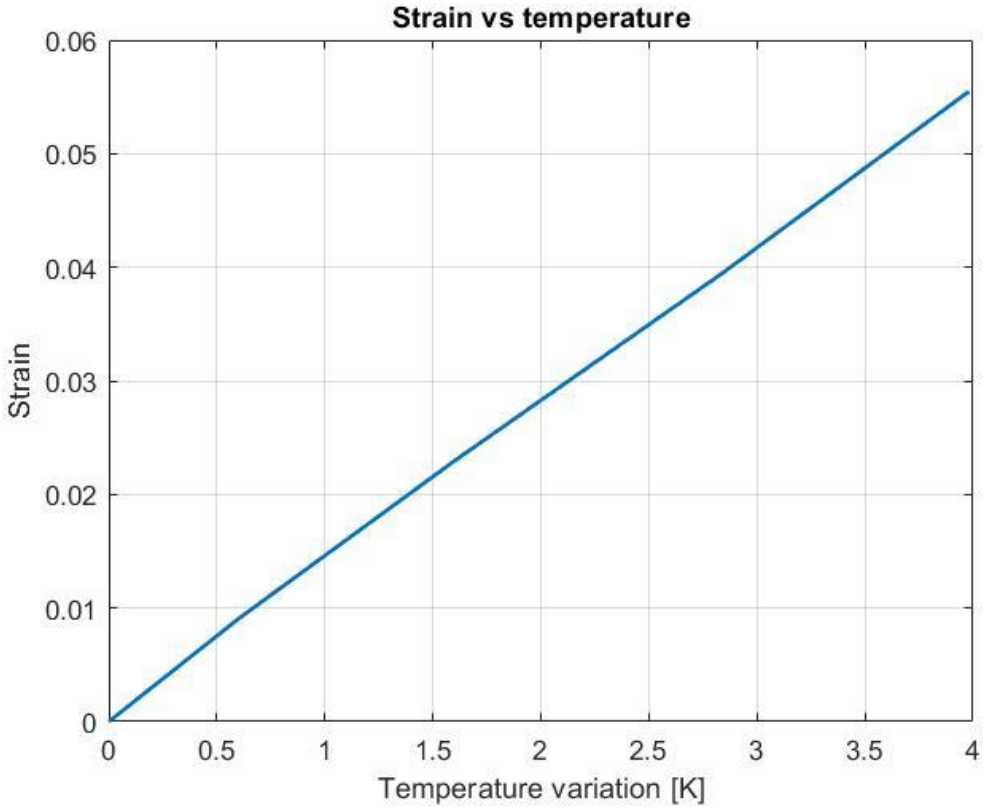

59 STRAIN VS ΔT SPECIMEN D POINT B

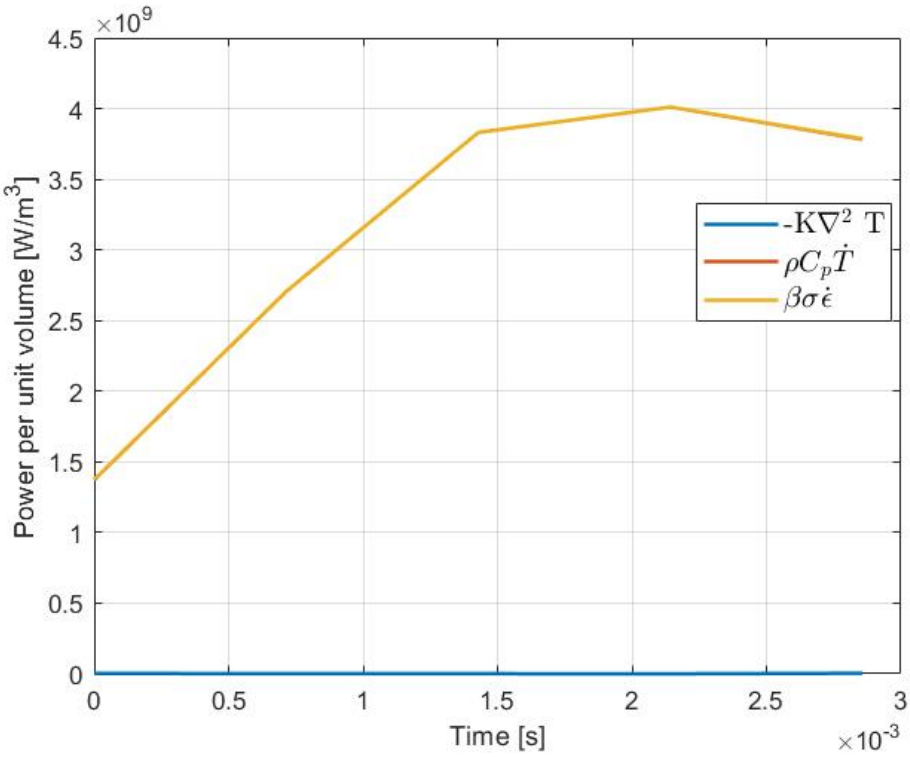

60 POWER COMPONENT SPECIMEN D POINT B

9.2.6 Specimen E

Point A

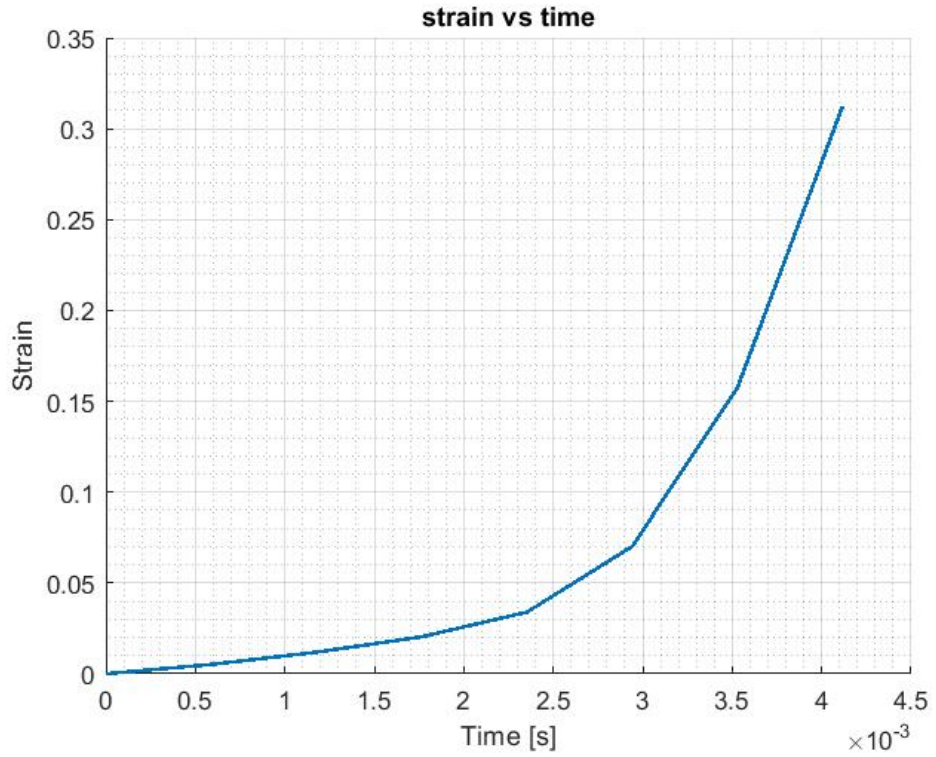

61 STRAIN SPECIMEN E POINT A

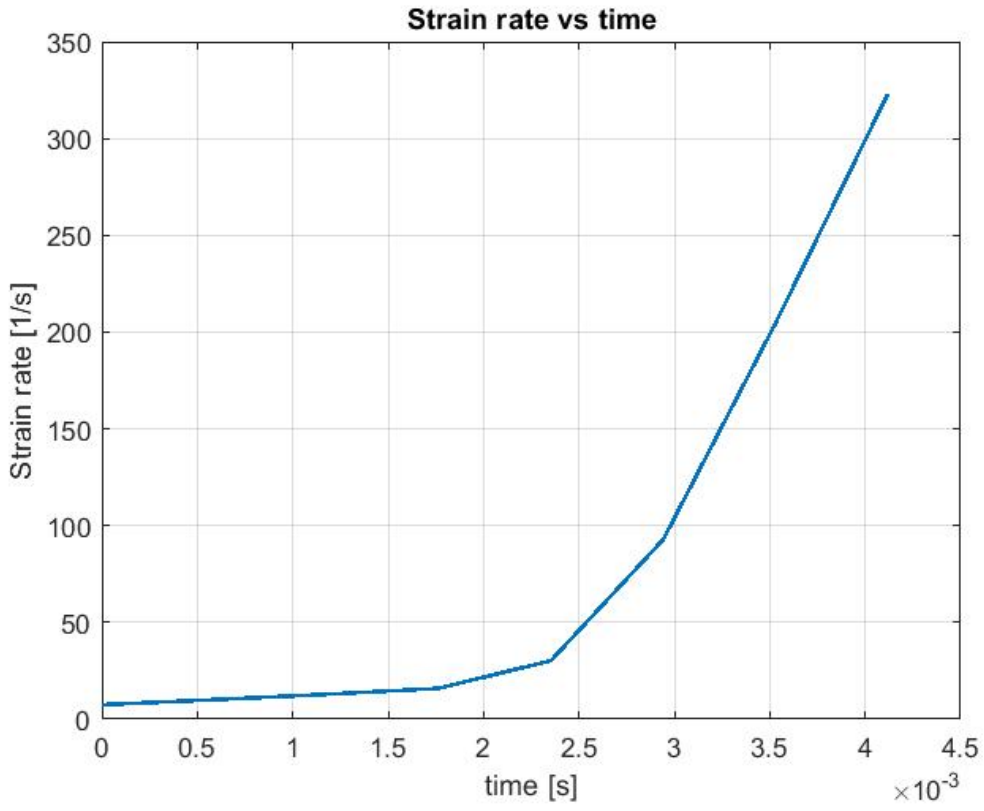

62 STRAIN RATE SPECIMEN E POINT A

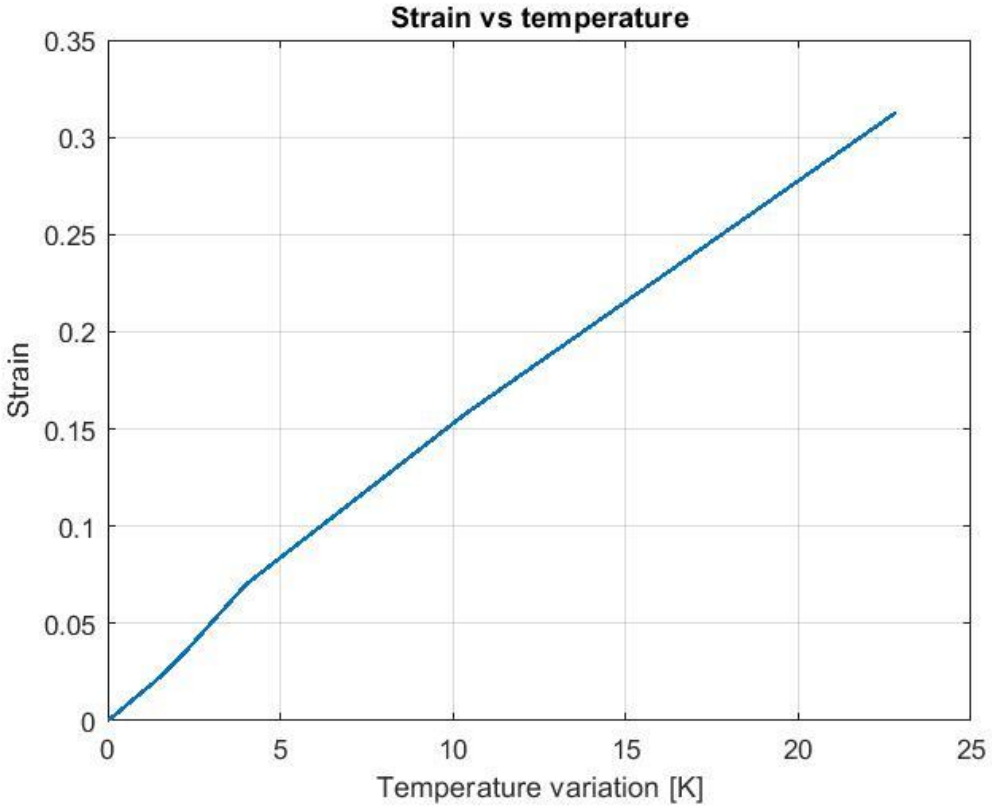

63 STRAIN VS ΔT SPECIMEN E POINT A

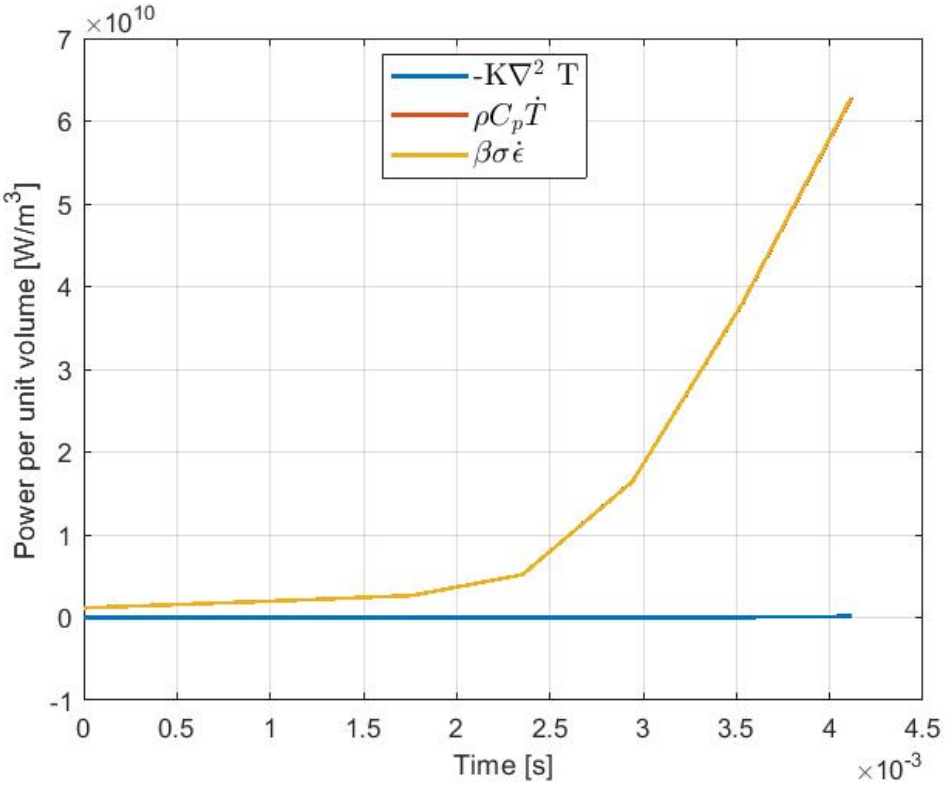

64 POWER COMPONENT SPECIMEN E POINT A

Point B

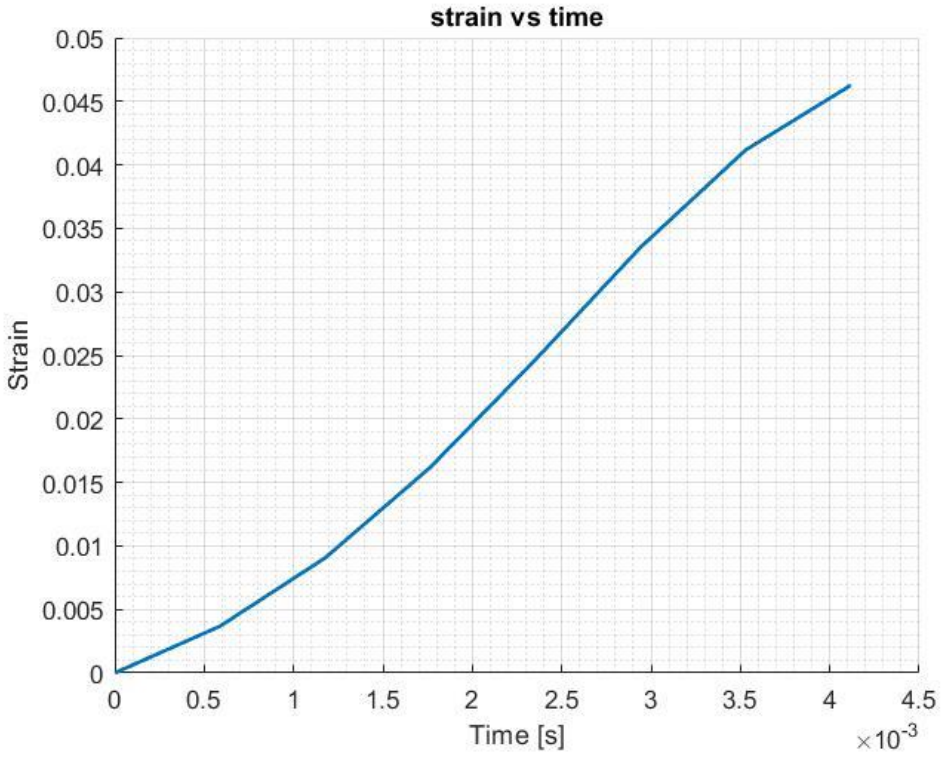

65 STRAIN SPECIMEN E POINT B

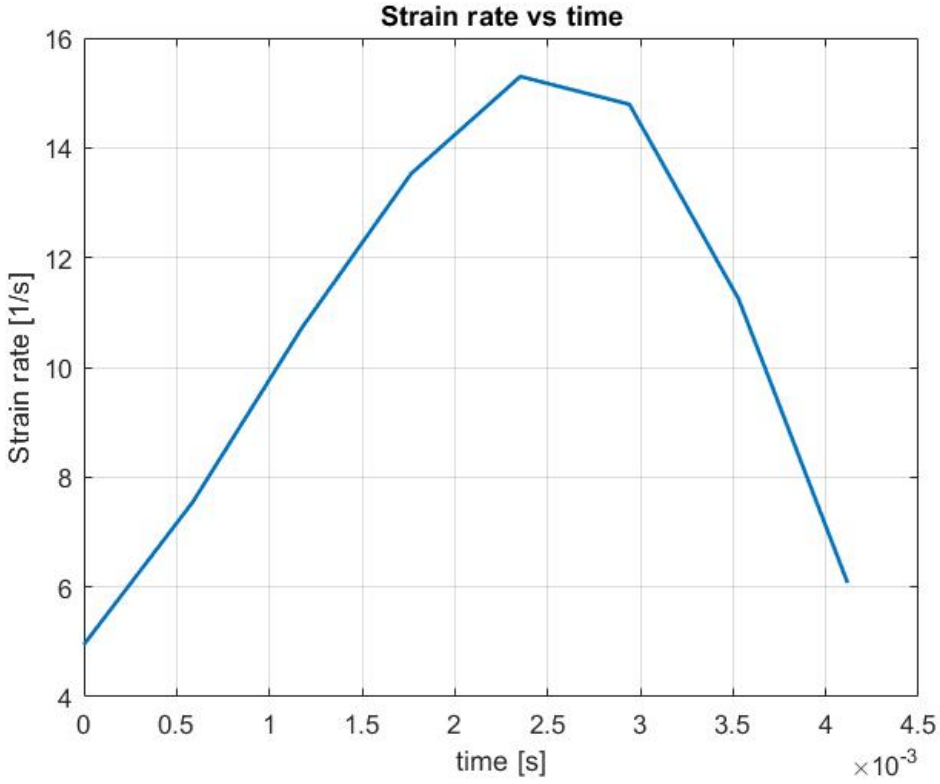

66 STRAIN RATE SPECIMEN E POINT B

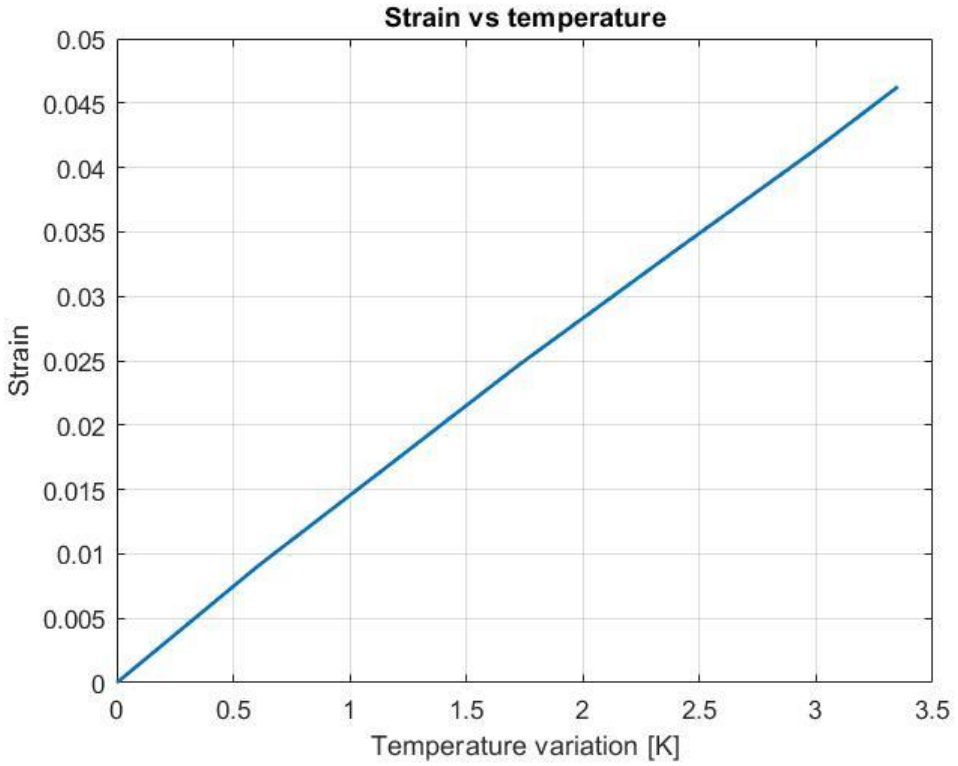

67 STRAIN VS ΔT SPECIMEN E POINT B

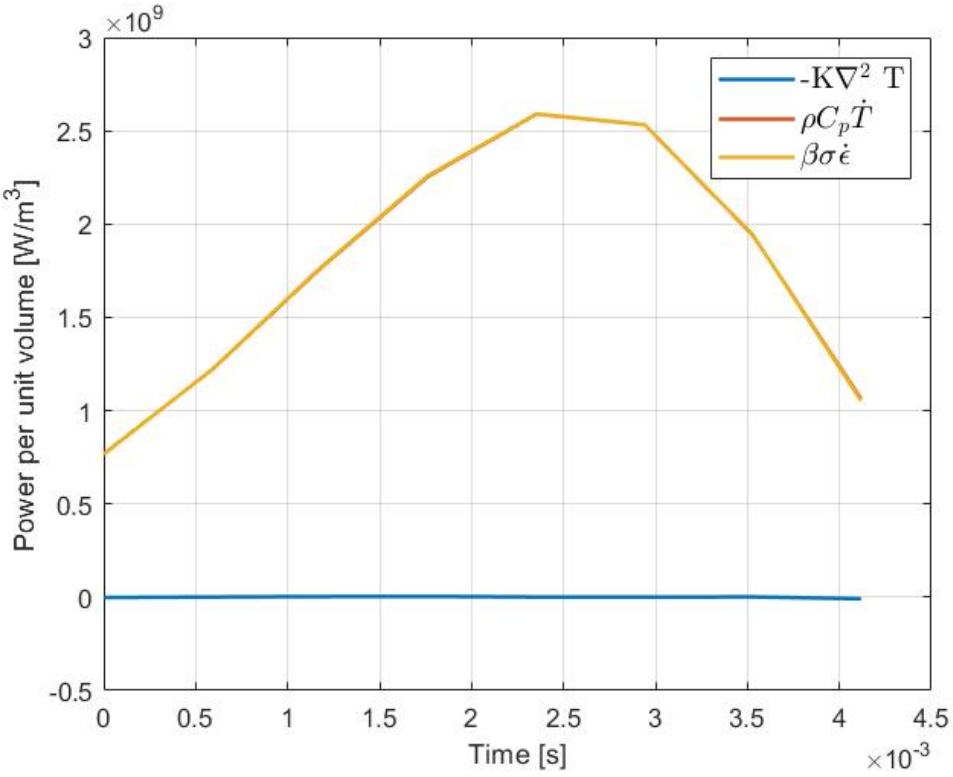

68 POWER COMPONENT SPECIMEN E POINT B

9.3 Comparison of the results

The results obtained were compared with data from DIC and strain gauge analysis. Each test has its own time scale, so visualizing the comparison may be difficult to understand.
A pseudo-time scale was chosen as a substitute for the real time scale so that each test is defined in the same interval. This pseudo-time should not be understood as real time, but as a time representing the position on the timeline relative to the total time of the test.
As can be seen, for both regions, the integration results agree with the measurements obtained with the DIC and strain gauge.
The strains of samples D and E, for the point B, are much lower than the other results. This is probably due to the rapid dynamics combined with limited temperature variation, which makes it more sensitive to measurement noise.

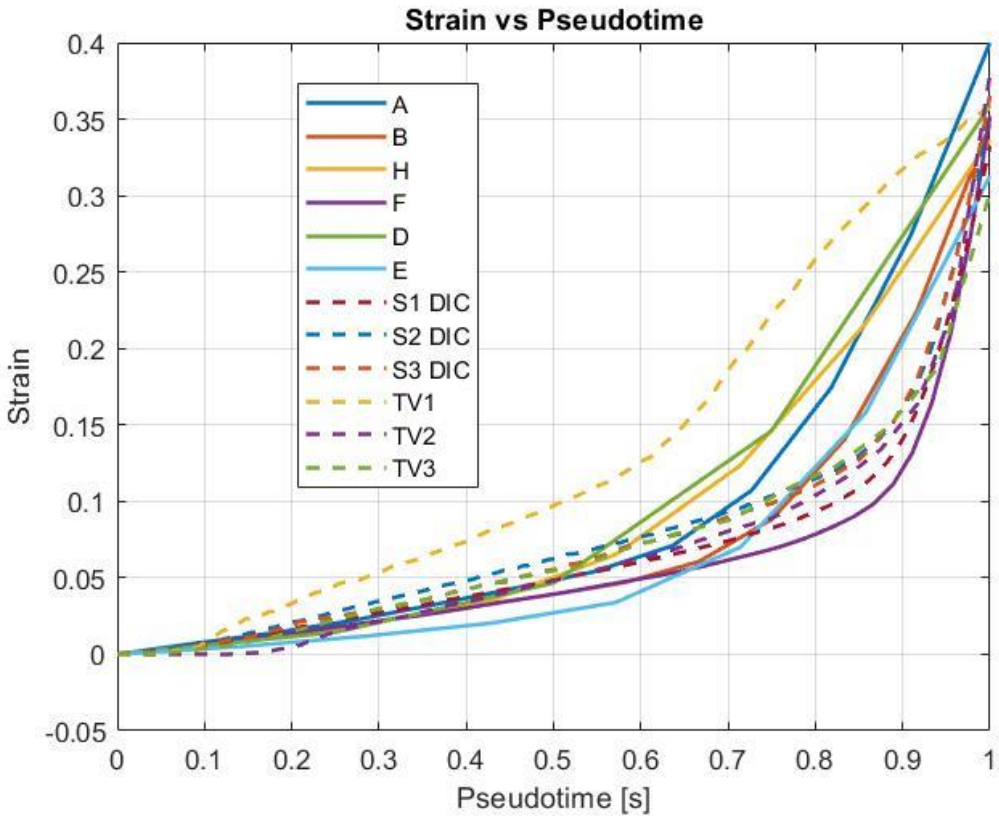

69 COMPARISON POINT A

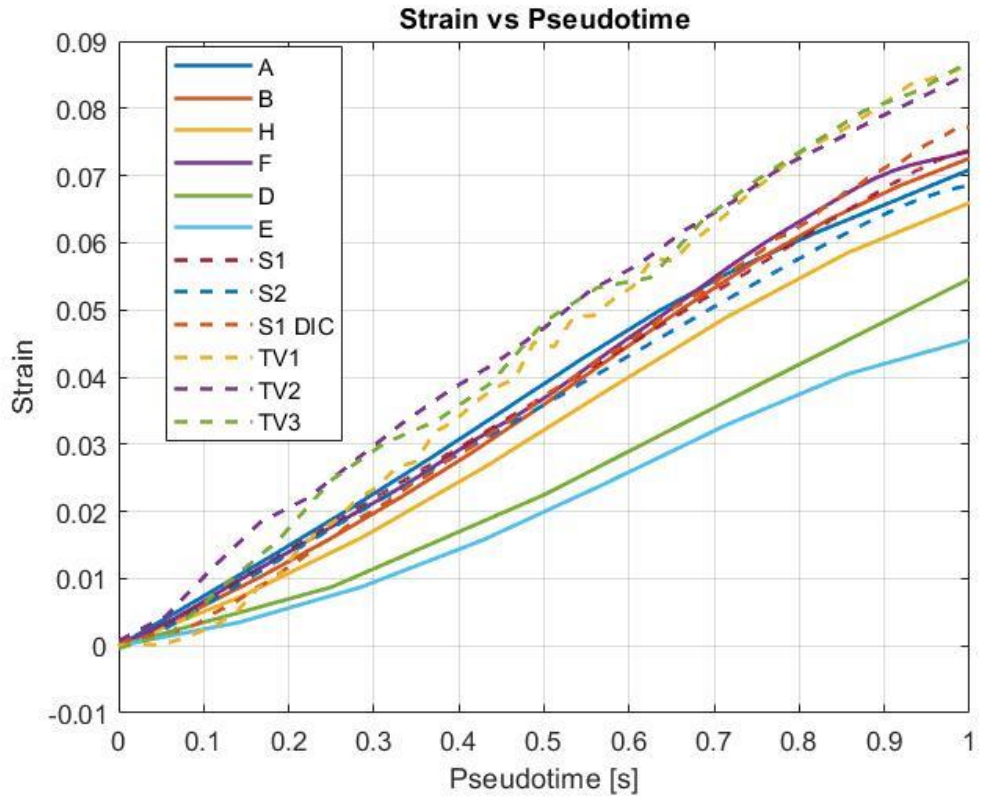

70 COMPARISON POINT B

9.4 Results Comments

The results are mostly in agreement with the DIC and extensometer results. The strain trend is as expected. The strains at the point near rupture grow uniformly to those at the rest of the specimen until the necking zone begins to form and there is the strain concentration

It can be seen that the conduction component within the energy equation is always much smaller than the other two components. As was expected the tests at higher velocities have practically no contribution from conduction, while the slower tests have a noticeable if relatively low contribution.

It can be seen that, in the case of having few integration steps and small temperature changes, the strain rate is definitely underestimated relative to the value that would be expected. This is particularly evident in the last two results where the deformations obtained do not follow the same trend as in the other tests.

A more detailed study will therefore be needed.

9.5 The link between temperature and strain

One of the advantages of measuring deformations through a thermal imaging camera is the possibility of obtaining data for a relatively large area compared with a simple local measurement.
For this reason, applying the integration scheme for all recorded points may be inadvisable because of the time and cost of calculation.
A very simple solution to this problem is to find an empirical curve that links plastic deformation to temperature change. This curve is found through polynomial regression on the data in the integration scheme. The curve found can then be used to estimate the strain on other points and for future tests.
In this particular case, the shape of the curves of the results of the integration method can be fitted using aa first order or second order regression.

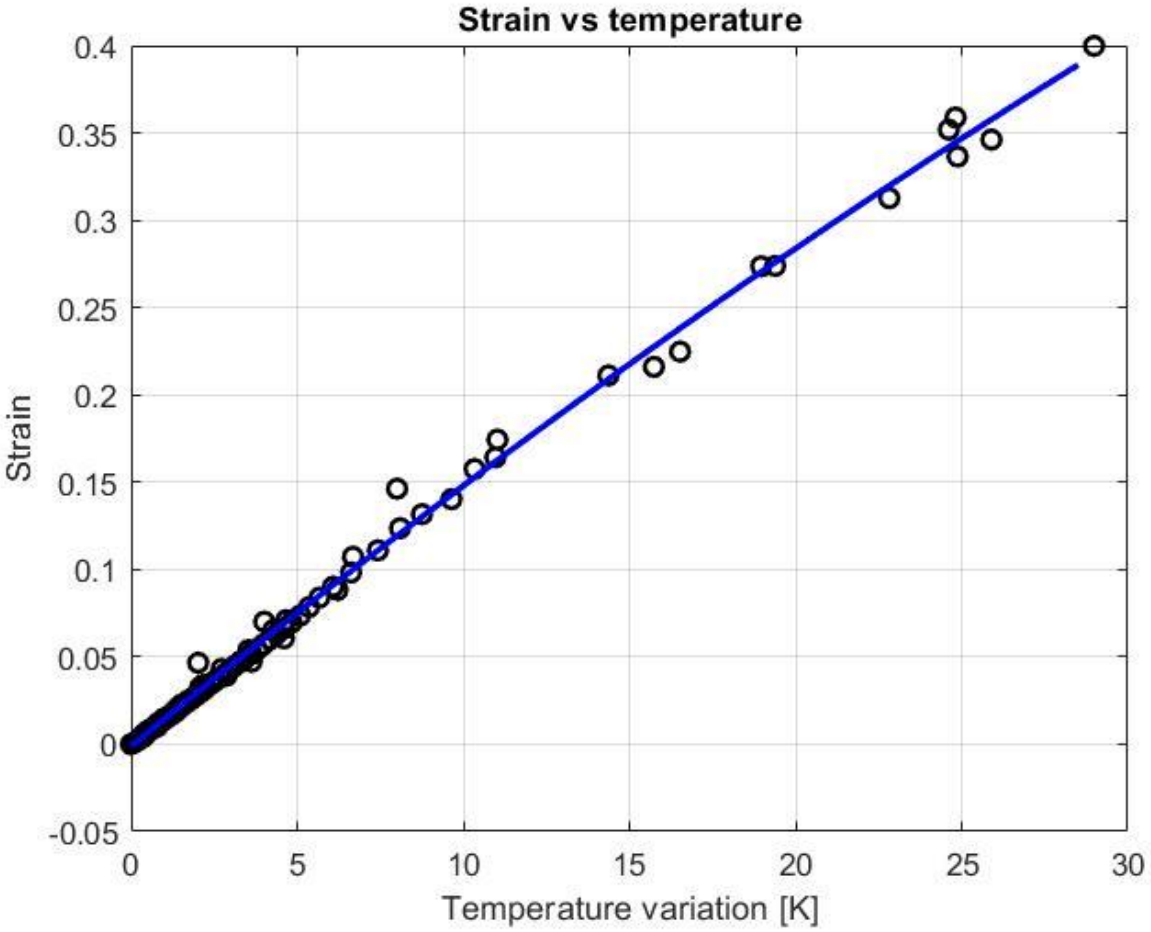

71 SECOND ORDER REGRESSION OF THE RESULTS

Applying second-order polynomial regression, we obtain the polynomial

$$\varepsilon_p = -6.64 \cdot 10^{-5}\Delta T^2 + 1.56 \cdot 10^{-2}\Delta T - 1.15 \cdot 10^{-3}$$

At this point one can easily estimate the entire strain range from the thermal camera videos for each frame. This generates a series of images representing the entire time evolution showing qualitatively and quantitatively the strain distribution.
The results are promising, but care must be taken.
As said before, near the point of failure, bare aluminum begins to reflect its surroundings, so the measurement at those points cannot be relied upon.
The result may still be valid near the breaking point, but the closer you get, the less reliable it becomes.

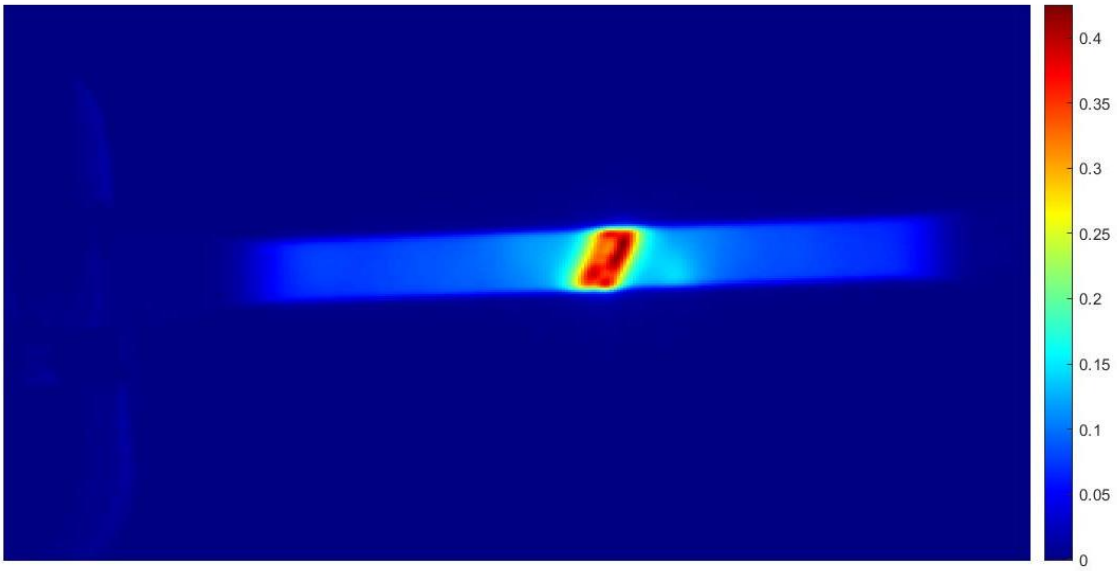

72 STRAIN FIELD SPECIMEN A

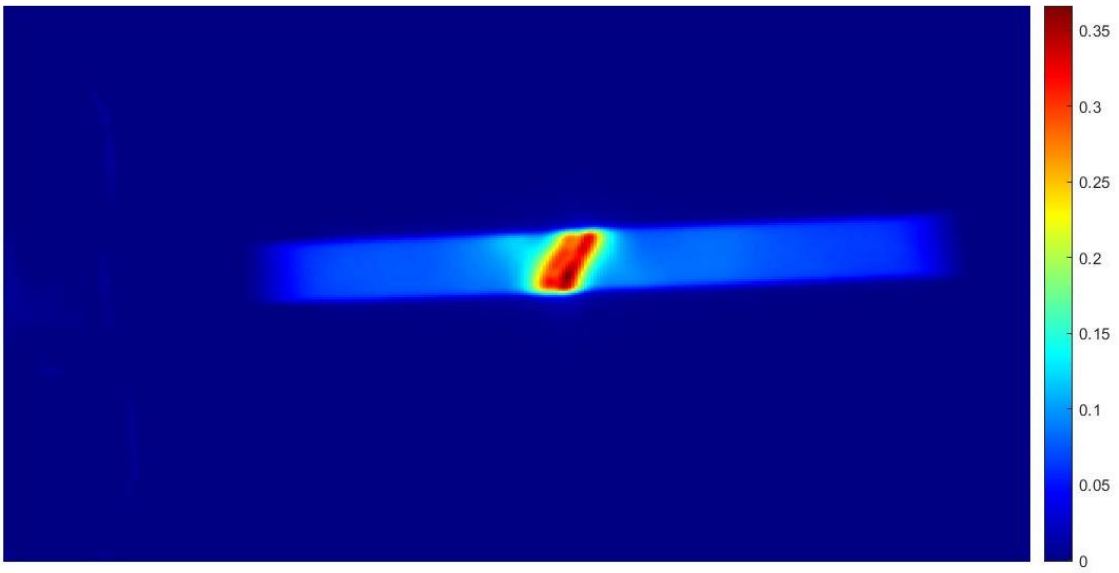

73 STRAIN FIELD SPECIMEN B

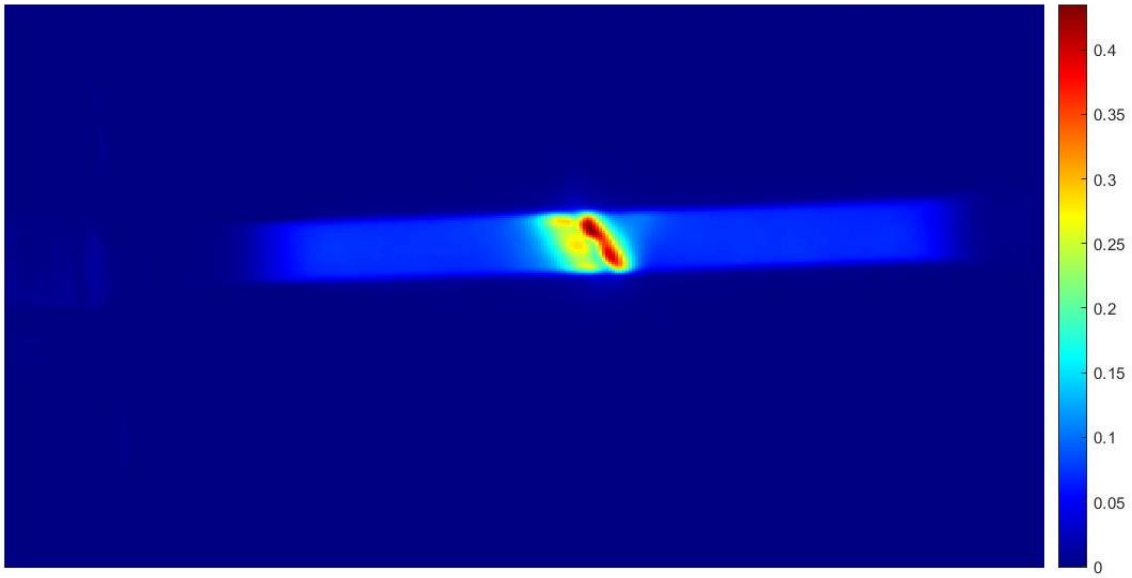

74 STRAIN FIELD SPECIMEN H

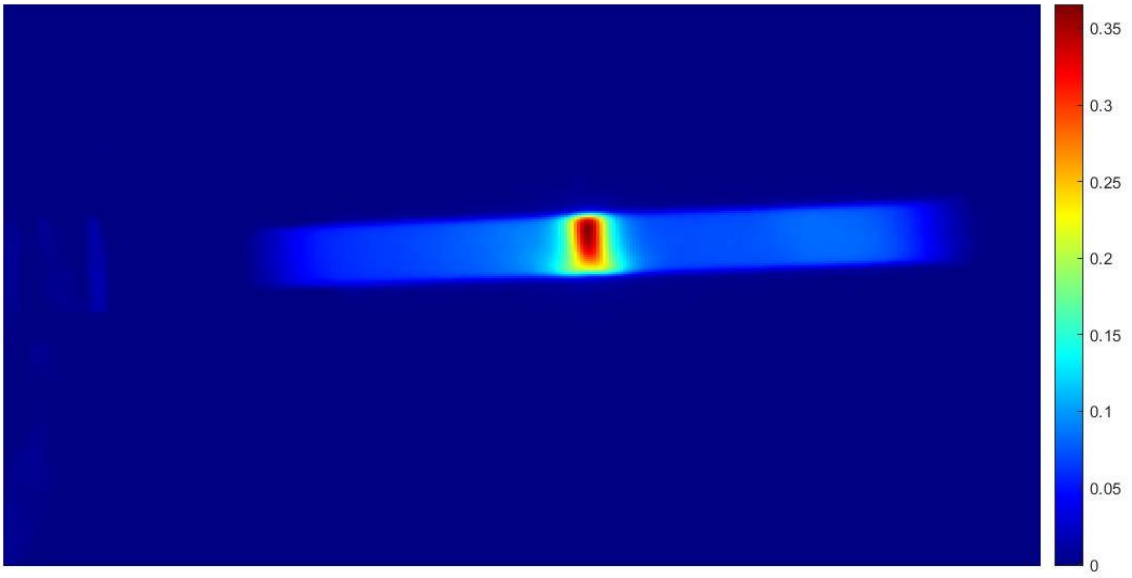

75 STRAIN FIELD SPECIMEN F

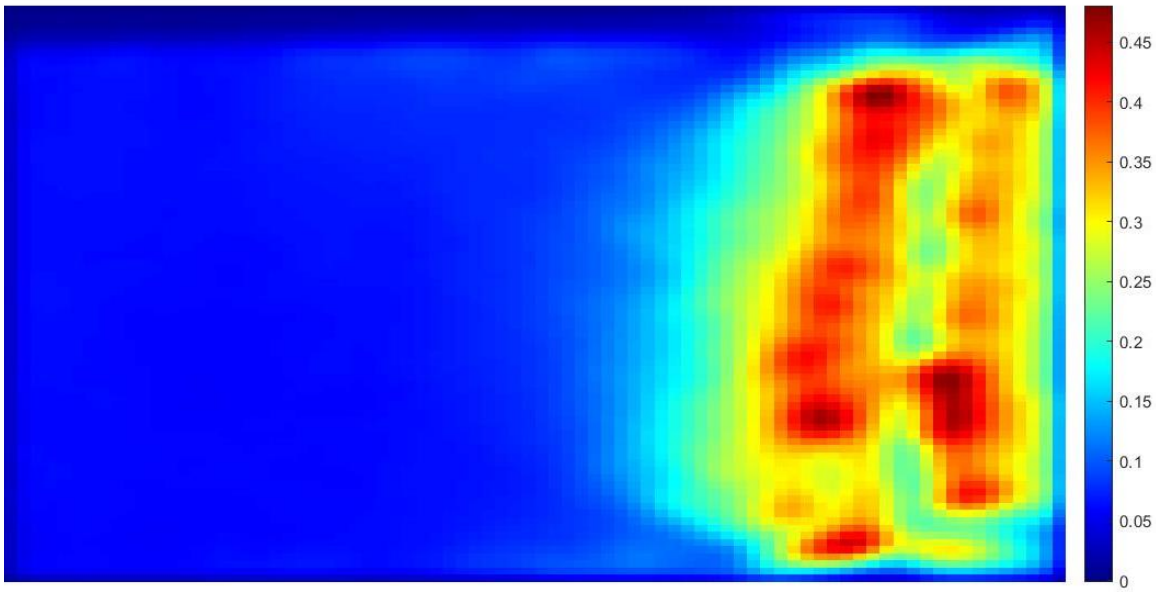

76 STRAIN FIELD SPECIMEN D

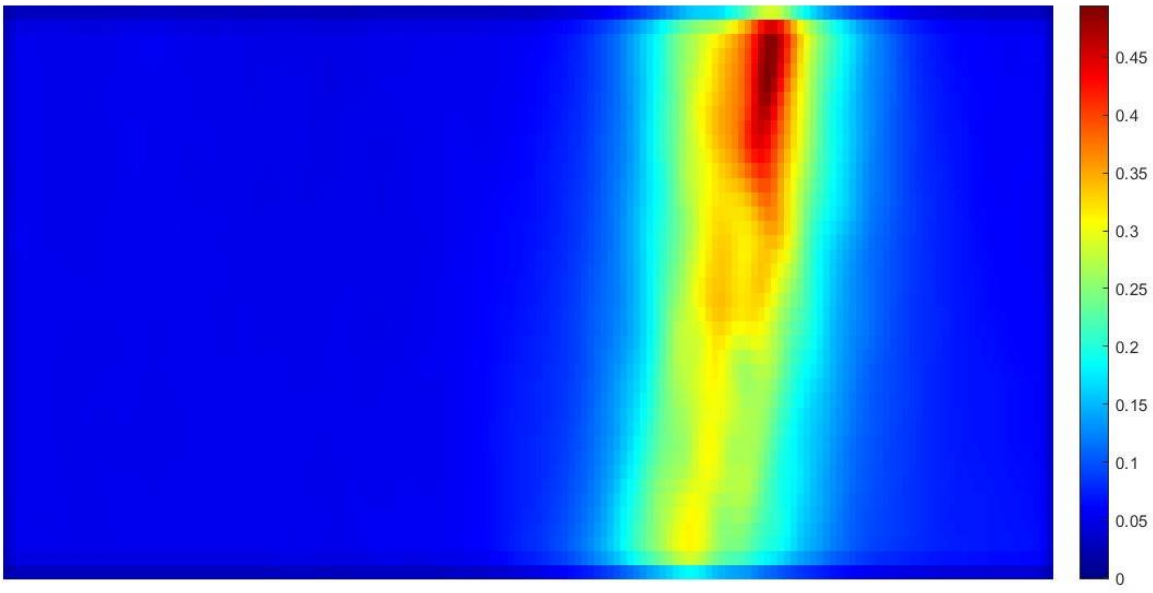

77 STRAIN FIELD SPECIMEN E

10 Dynamic tests applications

10.1 Considerations for material change

To test the application on dynamic tests presenting a more complex deformation, the method was applied to a compression tests for circular tubes.
Since these tests predate the beginning of this work, the material making up the cylinders is different from the one characterized in this study.
Even though the material is different, an alloy from aluminum is being considered in both cases, consequently similar behavior during deformation was assumed.
The characterisation curve can't be directly applied as it is because the yielding stress of the two materials is quite different, in particular the one of the cylinders is around 90 MPa greater.
A simple way to work around this issue is to exploit the almost linearity of the characterisation curve. First the strains are evaluated through the curve and then they are scaled to match the real plastic work.
For semplicity of notation the characterised material will be "called material 1" and the other "material 2".
Applying the linear curve with the temperature data, the strain obtained are calculated taking into account the plastic work of the material 1, so the curve should be expressed as $\varepsilon = K\Delta T_1$.
The objective is now to use ΔT_2 instead of ΔT_1, taking so in account the plastic work of the material 2.
First of all the energy equation is represented in its simplest form parting the plastic work in a linear term, linked to the base value of the yielding stress, and a non linear term. In this case the hardening rule for the two materials is supposed to be the same so the non linear term will have the same expression.

$$\begin{cases} \rho C_p \Delta T_1 = \sigma_{y1}\varepsilon + H(\varepsilon) \\ \rho C_p \Delta T_2 = \sigma_{y2}\varepsilon + H(\varepsilon) \\ \sigma_2 = \sigma_1 + \Delta\sigma_y \end{cases}$$

The ratio between the first two equation results in

$$\frac{\Delta T_2}{\Delta T_1} = \frac{\sigma_{y2}\varepsilon + H(\varepsilon)}{\sigma_{y1}\varepsilon + H(\varepsilon)} = \frac{\sigma_{y1}\varepsilon + H(\varepsilon) + \Delta\sigma_y\varepsilon}{\sigma_{y1}\varepsilon + H(\varepsilon)} = 1 + \frac{\Delta\sigma_y\varepsilon}{\sigma_{y1}\varepsilon + H(\varepsilon)} = \frac{1}{L(\varepsilon)}$$

In the case of the simplified Johnson-Cook model $H_{(\varepsilon)} = \frac{B}{N+1}\varepsilon^{N+1}$ so

$$\frac{1}{L(\varepsilon)} = 1 + \frac{\Delta\sigma_y}{\sigma_{y1} + \frac{B}{N+1}\varepsilon^N}$$

Fist of all the strain are calculated using the curve and then the result are scaled by a factor L(ε) calculated using the strains just found.

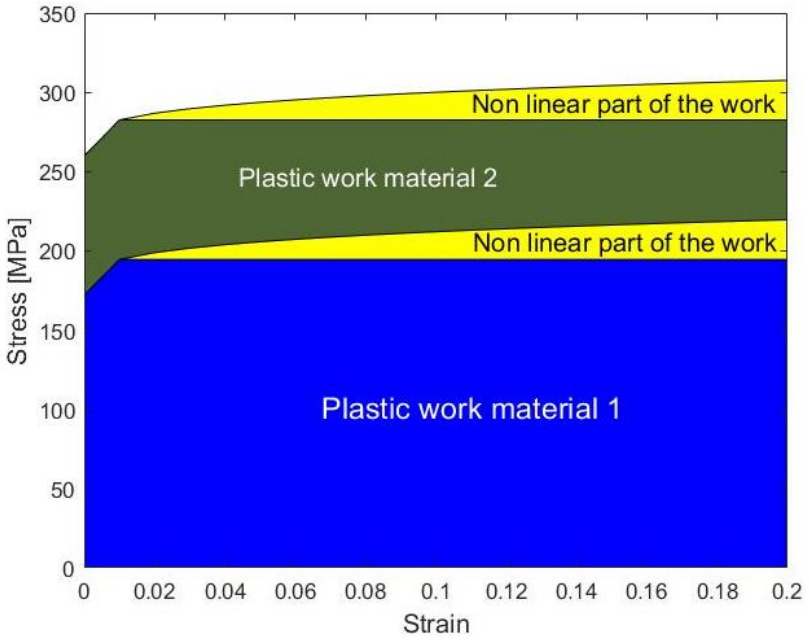

78 PLASTIC WORK PARTITION

10.2 Cylinder compression tests

Cylinder compression tests are carried out by impacting a mass in the longitudinal direction to the cylinder.
The cylinder starts to buckle under the compressing load, generally starting from one end and advancing toward the other, repeating specific deformation modes. The first is an axisymmetric mode composed of concentric folds while the second is a diamond mode with a more complex shape.

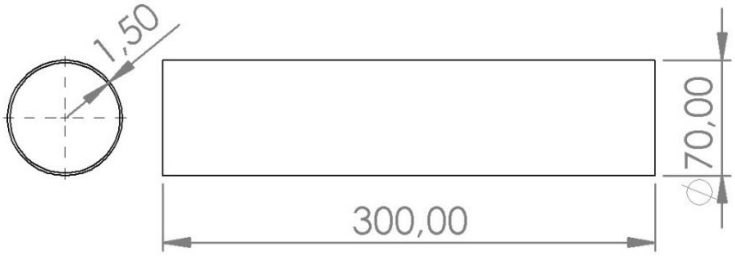

79 CYLINDER DIMENSIONS

Tube	Speed [m/s]	Recording speed [frame/s]
T01	8.11	505
T02	8.14	505
T03	8.16	505
T04	8.05	505

TABLE 3 CYLINDER COMPRESSION TESTS DATA

82 TUBE 01

80 TUBE 02

83 TUBE 03

81 TUBE 04

10.2.1 Tube 1

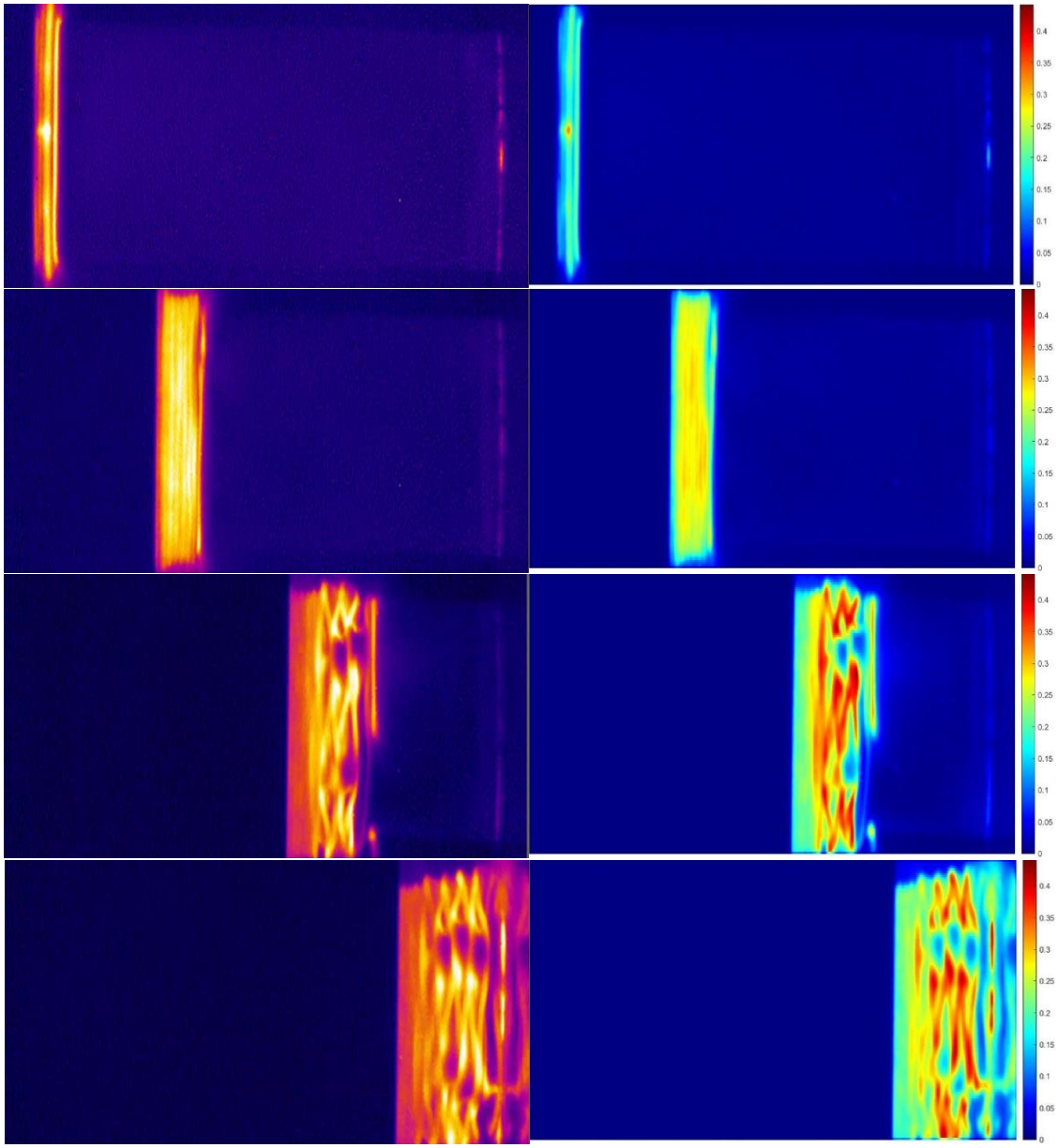

84 TEMPERATURE DISTRIBUTION T01

85 STRAIN DISTRIBUTION T01

10.2.2 Tube 2

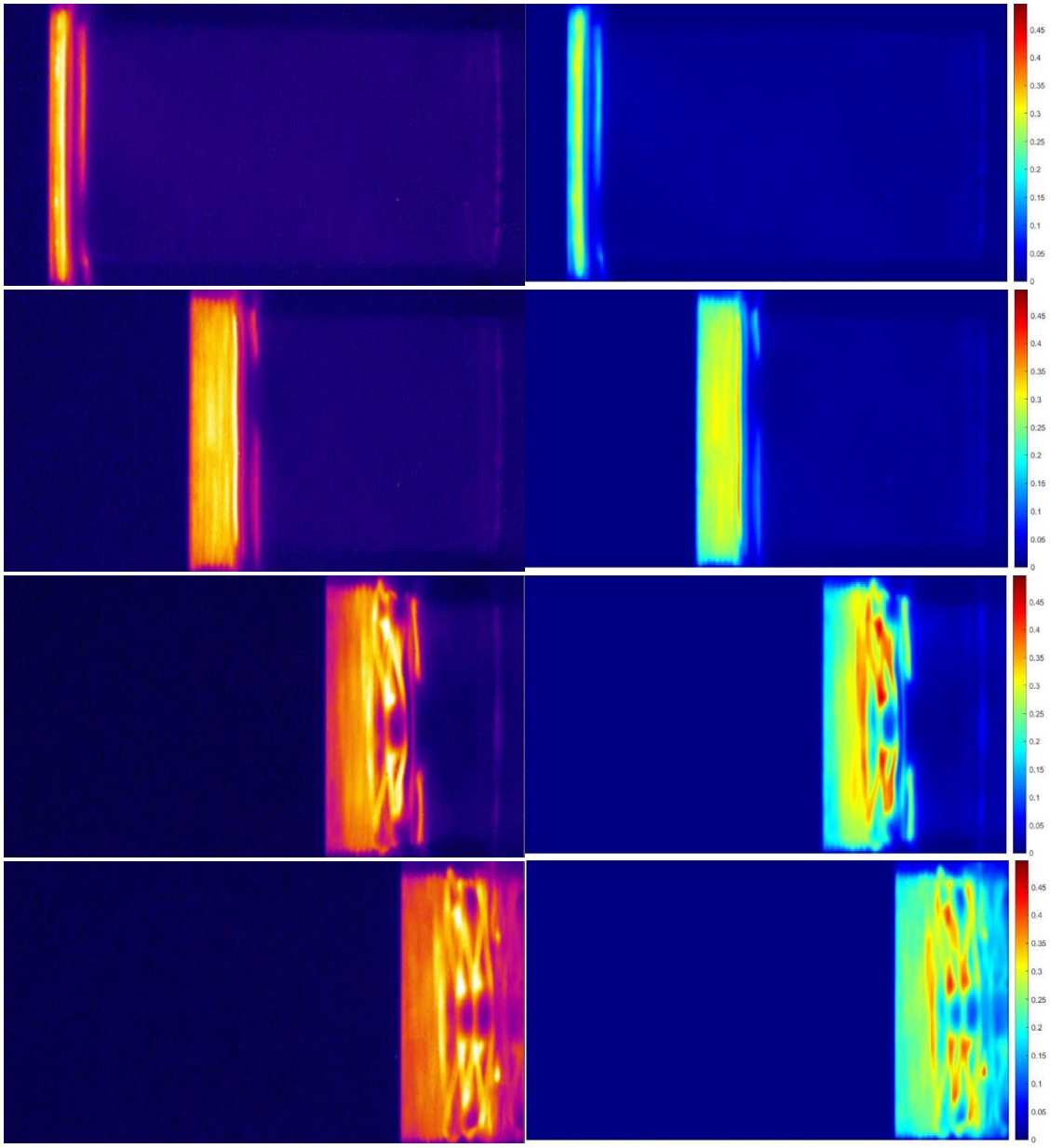

87 TEMPERATURE DISTRIBUTION 02

86 STRAIN DISTRIBUTION T02

10.2.3 Tube 3

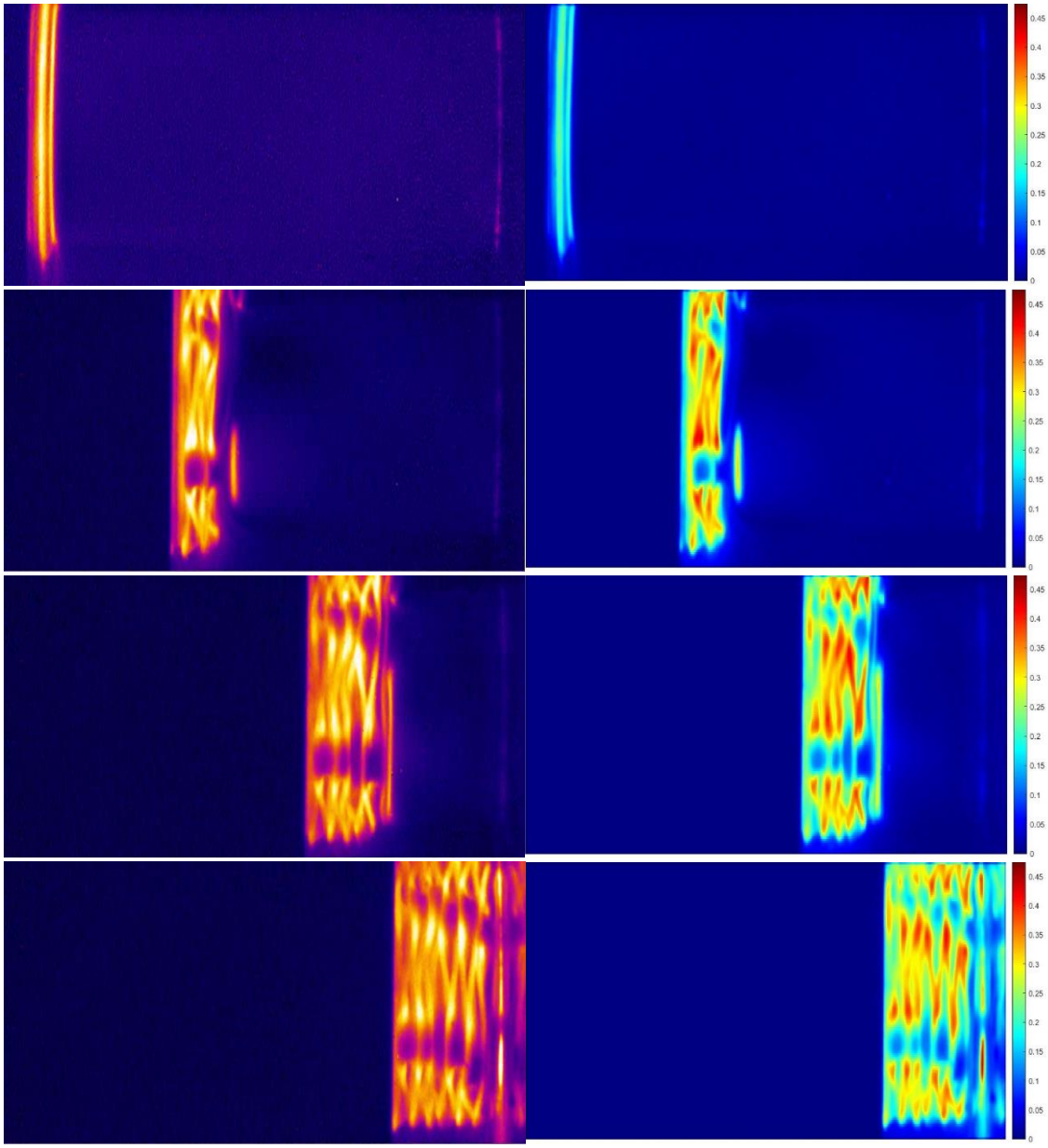

89 TEMPERATURE DISTRIBUTION T03

88 STRAIN DISTRIBUTION T03

10.2.4 Tube 4

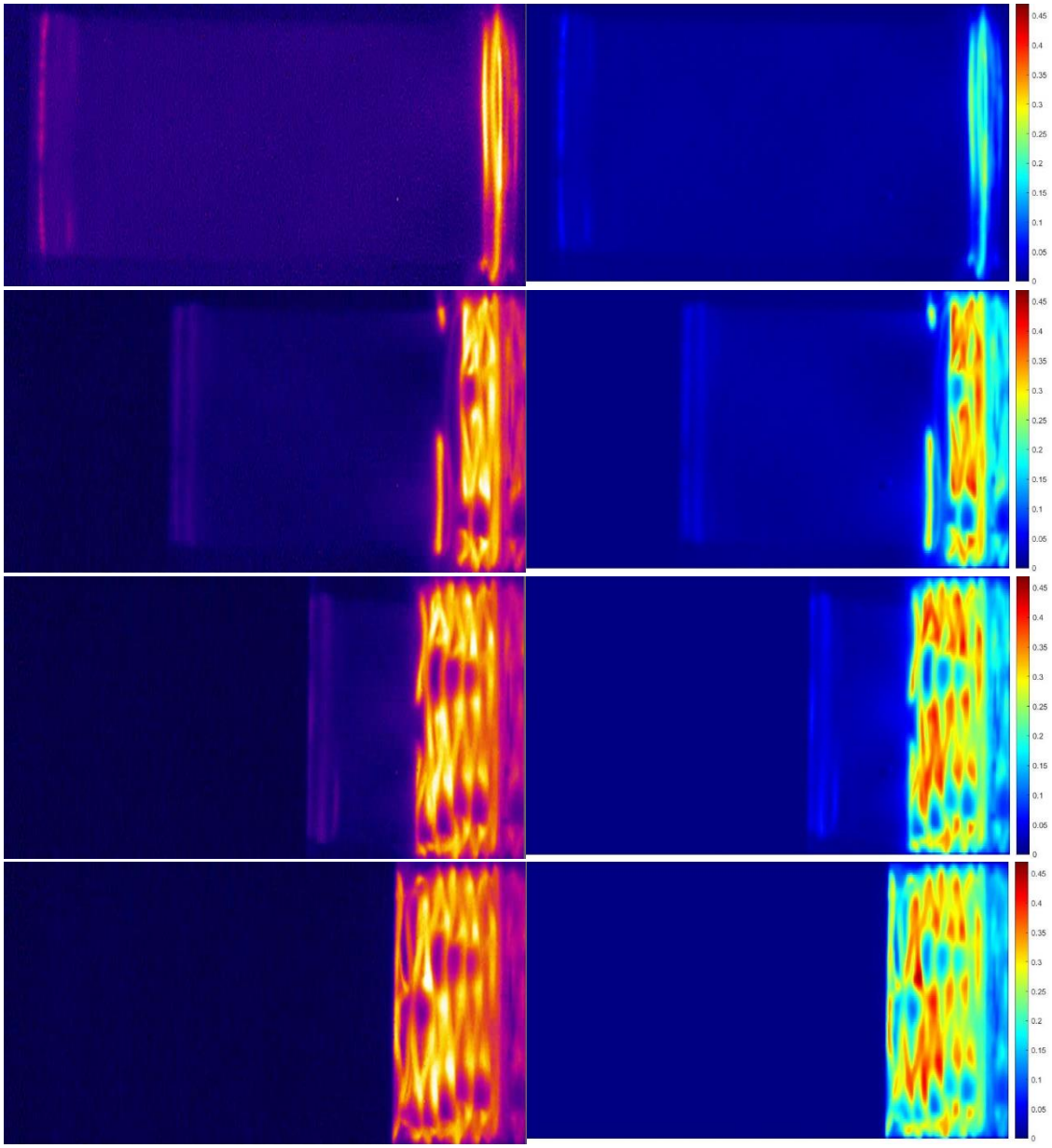

91 TEMPERATURE DISTRIBUTION T04

90 STRAIN DISTRIBUTION T04

Conclusions

The objective of the study was to derive an empirical relationship to link plastic deformation and the generated temperature change to use for measuring strains during dynamic tests.
Specifically, we focused on characterizing aluminum specimens through standard tensile tests.
Integration of the energy equation, through the temperature data from the thermal imaging camera, yielded results mostly in agreement with the reference results obtained from DIC and strain gauge analysis.
This made it possible to derive a material characterization curve, the application of which gave very satisfactory results that could generate the strain field directly from the thermal camera measurement.
The application of the curve on the dogbone specimens show results in agreement with other measuring methods.
The application on the cylinders, with the results derived from the scaled curve, show the capabilities of this method for measurements during dynamic tests.
As the application on the dynamic tests has been performed through a scaled curve, the objective is now to apply it in a test with the same material studied in this work.

Bibliografy

1. *A review on Johnson Cook material model.* **Vasu, Sirigiri, et al.** s.l. : Materials Today: Proceedings, 2022, Vol. 62.
2. *ASM Handbook Vol.8.* **Howard, Kuhn e Dana, Medlin.** 2000.
3. *On the high strain rate behavior of 63-37 Sn-Pb eutectic solders with temperature effects.* **Naveed, Iqbala, et al.** s.l. : International Journal of Impact Engineering, 2014, Vol. 74.
4. *Thermal Image Analysis for Evaluating Plastic Deformation.* **Hidetoshi, Sakamoto, Mituharu, Yamamoto e Eiji, Nakamachi.** s.l. : METALS AND MATERIALS, 1998, Vol. 4.
5. *Multibody system dynamics Notes.* **Pierangelo, Masarati.** 2022.
6. *A Good Practices Guide for DIC.* **Jones, E.M.C., Ladicola.** s.l. : International Digital Image Correlation Society, 2018.
7. *Image Correlation for Shape, Motion and Deformation Measurements.* **Hubert, Schreier, Jean-José, Orteu e Michael A., Sutton.** s.l. : Springer, 2009.
8. *Strain Measurement by Digital Image Correlation: Influence of Two Types of Speckle Patterns Made from Rigid or Deformable Marks.* **Y., Barranger, et al.** s.l. : Wiley Publishing Ltd, 2012.
9. *Optimum Paint Sequence for Speckle Patterns in Digital Image Correlation.* **W.S., LePage, J.A., Shaw e S.H., Daly.** s.l. : Experimental Techniques, 2017, Vol. 41.
10. *An effective procedure to create a speckle pattern on biological soft tissue for digital image correlation measurements.* **Giacomo, Lionello, Camille, Sirieix e Massimiliano, Baleani,.** s.l. : Journal of the Mechanical Behavior of Biomedical Materials, 2014, Vol. 39.
11. *Experimental Investigation of Strain Rate Dependence of Nanocrystalline Pt Films.* **Jonnalagadda, K.N., Chasiotis e I., Yagnamurthy.** s.l. : Experimental Mechanics, 2010, Vol. 50.
12. *A New Method of Creating High-Temperature Speckle Patterns and Its Application in the Determination of the High-Temperature Mechanical Properties of Metals.* **Hu Y., Wang e Y., Chen.** s.l. : Experimental Techniques, 2018, Vol. 42.
13. *Self-Assembled Nanoparticle Surface Patterning for Improved Digital Image Correlation in a Scanning Electron Microscope.* **Kammers, A.D. e Daly, S.** s.l. : Experimental Mechanics, 2013, Vol. 53.
14. *Determination of temperature rise during high strain rate.* **Rajeev, Kapoor e Sia, Nemat-Nasser.** s.l. : Mechanics of Materials, 1998, Vol. 27.
15. *TEMPERATURE INCREASE ASSOCIATED WITH PLASTIC DEFORMATION UNDER DYNAMIC COMPRESSION: APPLICATION TO ALUMINIUM ALLOY AL 6082.* **José-Luis, Pérez-Castellanos e Alexis, Rusinek.** s.l. : JOURNAL OF THEORETICAL, 2012, Vol. 50.
16. *Full-Field Measurement of Strain and Temperature in Quasi-Static and Dynamic Tensile Tests on Stainless Steel 316L.* **Amos, Gilata, et al.** s.l. : Procedia Engineering, Vol. 207.
17. *Conversion of Plastic Work to Heat: A full-field study of thermomechanical coupling.* **Amanda, Jones, et al.** 2018.
18. *Measurement of local strain and heat propagation during high-temperature testing in a split-Hopkinson tension bar system.* **V., Vilamosa, et al.** s.l. : The European Physical Journal Conferences, 2012.
19. *A thermodynamic internal variable model for the partition of plastic work into heat and stored energy in metals.* **P., Rosakisa, A.J., Rosakisb e G., Ravichandranb.** s.l. : Journal of the Mechanics and Physics of Solids, 2000, Vol. 48.

20. *Experimental and numerical analysis of the heat generated by plasticdeformation in quasi-static uniaxial tensile tests.* **D.M., Netoa, et al.** s.l. : Mechanics of Materials, 2020, Vol. 146.
21. *On the Calculations of the Stored Energy of Cold Work.* **N, Aravas, K-S., Kim e F. A., Leckie.** s.l. : Journal of Engineering Materials and Technology, 1990.
22. *Analysis of heat generation under plastic deformation, crack initiation and propagation*. **H., Sakamoto, J., Shi e D., Kumagai.** s.l. : WIT Press, 2001.
23. *Evaluation of local plastic deformation by detecting heat generation in orthotropic material.* **H., Sakamoto, et al.** s.l. : WIT Press, 2004.
24. *Experiments on heat generated during plastic deformation and stored energy for TRIP steels.* **A., Rusinek e J.R., Klepaczko.** s.l. : Materials and Design, 2009, Vol. 30.
25. *Partition of Plastic Work into Heat and Stored Energy in Metals.* **J., Hodowany, et al.** s.l. : Experimental Mechanics, 2000, Vol. 40.
26. *Thermal image analysis of plastic deformation and fracture behavior by a thermo-video measurement system.* **Yoshifumi, Ohbuchi, Hidetoshi, Sakamoto e Nobuaki, Nagatomo.** s.l. : Measurement Science and Technology, 2016, Vol. 27.
27. *ON THE CONVERSION OF PLASTIC WORK INTO HEAT DURING HIGH-STRAIN-RATE DEFORMATION.* **Guruswami, Ravichandran, et al.** s.l. : Shock Compression of Condensed Matter, 2001.
28. *Crushing modes of aluminium tubes under axial compression using finite element analysis.* **N.D., Ghazali e M.R., Said.** 2017.
29. *ISO-6892-1-2019.* **s.l. : International Organization for Standardization.**

List of figures

List of tables